Investigation of the thermal effects in nanofluidic transport and their application in gating

THÈSE N^{O} 6825 (2015)

PRÉSENTÉE LE 11 NOVEMBRE 2015

À LA FACULTÉ DES SCIENCES ET TECHNIQUES DE L'INGÉNIEUR

LABORATOIRE DE MICROSYSTÈMES 4

PROGRAMME DOCTORAL EN MICROSYSTÈMES ET MICROÉLECTRONIQUE

ÉCOLE POLYTECHNIQUE FÉDÉRALE DE LAUSANNE

POUR L'OBTENTION DU GRADE DE DOCTEUR ÈS SCIENCES

PAR

Mojtaba TAGHIPOOR

acceptée sur proposition du jury:

Prof. H. Shea, président du jury
Prof. Ph. Renaud, directeur de thèse
Prof. J. Eijkel, rapporteur
Prof. R. Kamali, rapporteur
Prof. J. Brugger, rapporteur

ÉCOLE POLYTECHNIQUE
FÉDÉRALE DE LAUSANNE

Suisse
2015

To my wife and two fruits of my heart…
MohammReza and Hossein

Abstract

Scaling down to nanometer size fluidic conduits has opened a new window into the world of sensing and manipulation of nanoscale species. Thousands of publications and hundreds of patents in this field are only a starting point for exploring and manipulating at the small-scale. Even these starting studies have offered promising applications in sensing and manipulation of molecules of different types such as DNAs, proteins and viruses as well as small ions. The present thesis focuses on the study and control of the ionic transport through nanometer-size channels, as one of the main applications of nanofluidic features inspired from the protein ion channels present in cell membranes.

In the first part of this thesis, the latest developments in the field of nanofluidics are surveyed and a particular attention is given to the methods allowing gating of nanofluidic transport. Different methods of gating the nanofluidic transport are compared and some possible directions for future developments are suggested.

Then, a pH-regulated multi-ion model for the electric conductance of nanochannels is introduced. The electrical conductance measurement is a widely used technique for the characterization of nanofluidic devices. Many research groups measured or modeled the electric conductance of nanochannels. Theoretical analysis and experimental investigations imply that the nanochannel conductance does not follow the macro-scale models. It is generally accepted that the conductance of nanochannels deviates from the bulk and tends to a constant value at low ionic concentrations. a new model is presented, which takes into account the surface chemistry of the nanochannel wall and describes the nanochannel conductance at low ionic concentrations in a more realistic way.

The electrical conductivity of electrolytes is known to be dependent on temperature. However, the similarity of the temperature sensitivity of the electrical conductivity for bulk and nanochannels has not been validated. In order to examine this dependency, the ionic transport inside the nanochannel was studied. The results from the experimental measurements as well as the analytical modeling show the significant difference between the bulk and the nanoscale. The temperature sensitivity of the electrical conductance of nanochannels is higher at low ionic concentrations where the nanofluidic transport is governed by the electrostatic effects from the wall. Neglecting this effect can result in significant errors for high temperature measurements.

Based on the results from temperature sensitivity measurements of the electric conductance of nanochannels, a new nanofluidic gating mechanism is introduced that uses the thermal effect for modulating the ionic transport inside nanofluidic channels. The thermal gate controls the ionic transport more effectively than most other gating mechanisms previously described in scientific literature. Gating in both bulk and overlapping electric double layer regimes is obtained. The response time of the thermal gate is stud-

ied and compared with the one of other gating methods. The relatively short time response of the opening and closing processes makes it a good candidate for manipulating small molecules in micro- and nanoscale devices.

Keywords

Nanofluidics, ionic transport, nanofluidic transport, temperature sensitivity, surface charge density, wall electric potential, zeta potential, nanofluidic platforms, sacrificial layer, pH regulated model, multi-ion model, enthalpy of reaction, Thermal gate, gate effectiveness, response time, electric conductance.

Résumé

Réduire les dimensions de canaux fluidiques jusqu'à l'échelle nanométrique a ouvert un nouvel espace de possibilités pour la détection et la manipulation d'objets nanoscopique. Les milliers de publications et les centaines de brevets dans ce domaine ne sont considérés que comme le commencement de l'exploration et la manipulation du monde nanoscopique. Ces études fondatrices ont offert de prometteuses applications dans la détection et la manipulation de molécules telles que l'ADN, les protéines et les virus ainsi que les ions. La présente thèse doctorale se concentre sur l'étude et le contrôle du transport ionique à travers des canaux nanométriques : une des nombreuses applications de la nanofluidique inspirée du transport de protéines dans les canaux membranaires.
La première partie de cette thèse présente les derniers développements dans le domaine de la nanofluidique et en particulier la modulation du transport nanofluidique. Différentes méthodes de modulation du transport sont comparées et des possibilités de futurs développements sont suggérées.
Ensuite, un modèle multi-ions et sensible au pH pour la conductance électrique des nanocanaux est présenté. La mesure de la conductance électrique est une technique répandue pour la caractérisation de systèmes nanofluidiques. De nombreux groupes de recherche ont mesuré et modélisé la conductance électrique de nanocanaux. Les considérations théoriques et les observations analytiques montrent que cette conductance ne suit pas les modèles macroscopiques. Il est généralement reconnu que la conductance des nanocanaux s'écarte de celle rencontrée dans le volume pour tendre vers une valeur constante à faible concentration ionique. Le modèle présenté prend en compte la chimie de surface des parois du nanocanal. Il montre que la conductance des nanocanaux n'est pas constante à faible concentration ionique.
La conductivité électrique des électrolytes est généralement considérée dépendante de la température. Toutefois, la similarité de la sensibilité en température de la conductivité électrique entre le volume et le nanocanal n'a pas été validée. Dans le but d'examiner cette dépendance, le transport ionique au sein du nanocanal a été étudié. Tant les mesures expérimentales que les modèles analytiques montrent une différence significative entre le volume et les régimes nanoscopiques. La sensibilité en température de la conductance électrique des nanocanaux est supérieure à faible concentration ionique où les phénomènes de transports nanofluidiques sont gouvernés par les effets électrostatiques dus aux parois. En ne considérant pas cet effet, on peut rencontrer des erreurs significatives lors de mesures à haute température.
Basé sur ces résultats de sensibilité en température de la conductance électrique des nanocanaux, un nouveau mécanisme de modulation du transport nanofluidique est proposé qui utilise les effets thermiques pour moduler le transport ionique étudié. La mo-

dulation thermique contrôle le transport ionique plus efficacement que la plupart des autres méthodes de modulation précédemment présente dans la littérature scientifique. Une modulation est obtenue autant dans le régime « bulk » que dans le régime de superposition des double couches électriques. Le temps de réponse de la modulation thermique est étudié et comparé aux temps de réponse d'autres mécanismes de modulation. Le temps de réponse rapide pour l'enclenchement et l'arrêt du transport nanofluidique en fait un candidat de choix pour la manipulation de petites molécules dans les micro et nano systèmes.

Mots-clés

Nanofluidique, transport ionique, transport nanofluidique, sensibilité en température, densité de charge de surface, potentiel de surface des parois, potentiel zeta, platforme nanofluidique, couche sacrificielle, modèle sensible au pH, modèle multi-ion, enthalpé de reaction, modulation thermique, efficacité de la modulation, temps de réponse, conductance electrique.

Acknowledgments

This work would not have been possible without the support of many people, which are too far many to list here. However, among them, first, I would like to express my sincere gratitude to my thesis director, Professor Philippe Renaud for his continuing support during the past four years. I remember the moments when I was stuck in a problem and was able to move forward only because he was there to help, and I remember the moments when he gave me the freedom and encouragement that I needed to move on. These memories, however, show only a small portion of what made my PhD work with Professor Philippe Renaud a unique and pleasant experience.

I am also thankful to the jury members Prof. Kamali, Prof. Eijkel, Prof. Brugger and Prof. Shea who provided fruitful discussions and valuable feedbacks on my dissertation.

Many thanks to Dr. Arnaud Bertsch for the numerous discussions we had during my PhD. I am also thankful to him for proofreading of this thesis.

I would like to express my special gratitude to Sylvie Clavel, Marie Halm, Lucie Auberson and Melody Meyer for all their kindness and administrative advices.

I would like to thank all the present and former members of microsystems laboratory (LMIS4). My deepest gratitude goes to all my office-mates Yufei, David, Robert and Willyan for the memorable time and myriad discussions. Many thanks to Harald for being available and always open to answering any technical question, Fabien and Sophie for microscopy and lab trainings, Songmei for fruitful discussions on nanofluidics, Robert for impedance analyzer training, Nicolas for Generous helps on my experimental setup and LabVIEW interface, David B. for his comments on my electric circuit, Guillaume for fabrication of the aluminum adaptor for my mini-hot-plate and Damien for the helpful discussions on thermodynamics of surface reactions. Stefano and Loudovic, Elodie and Sébastien, Mark and Nader, Lynda and Jules, Nina and Ludovica, Pietro and Carolin, Pierre and Amélie, Thomas and Niccolo, Chris and Jonathan and you …… (I may have forgotten), Thank you for all happy moments we had together.

I would like to thank all the staffs of center of micronanotechnology (CMI) for their continuously supports. Many thanks to Cyrille Hibert, Philippe Langlet, Joffrey Pernollet, Anthony Guillet, Jullien Dorsaz , Jean-Marie Voirol, Patrick Madliger, Giancarlo Corradini, Adin Ferhatovic and Gatera Kumuntu for their non-stop supports.

I would like to acknowledge the master students who have contributed to this work, Kunal Sharma and Mourad Chouacki.

My very special thanks to my family for all their everlasting love and pray. I would like to express my deepest and sincere appreciation and gratitude to my parents and my

parents in law, my brothers and my brother and sisters in law and their warm-hearted spouses.
Particularly, I would like to thank my wife for her patience and support during the past four years and for taking care of our sons when I was busy with my thesis work. Without her support, this work would never have been possible; words cannot express how grateful I am to her. Many thanks to our beautiful sons, MohammadReza and Hossein whose smiles always pump bless and happiness into our life.

Mojtaba Taghipoor
10 Oct 2015

Contents

List of Figures

List of Tables

Chapter 1
Introduction

Hundreds of scientific articles focusing on the field of nanofluidics are published every year. Different nanofluidic platforms and applications have been reported. This first chapter introduces the latest developments and applications in the field of nanofluidic transport. Firstly, it describes the nanofluidic transport, its history and the diversity of its applications. Then, the word ‘‘gating’’ is defined which clarifies the title of this thesis. Later, four nanofluidic platforms are presented and compared. After, the important reported applications of nanofluidic are reviewed and finally, the objectives and structure of the thesis are described.

1.1 Nanofluidic transport

1.1.1 Definition

‘‘*Nanofluidics*’’ has been defined as the study of phenomena that involve fluid flow inside conduits with less than 100 nm in at least one direction (Schoch et al., 2008). In comparison to fluid flow at the macroscale, there are some major differences mainly due to the higher surface to volume ratio at nanoscale. The dominant surface forces and effects cause novel phenomenon at the nanoscale, which are imperceptible at the macroscale. The body forces that have major effects at the macroscale are usually negligible at the nanoscale. On the other hand, the forces that are normally neglected at the macroscale are sometimes the dominant force at the nanoscale. For example, the inertial force is smaller than the viscous terms and is not considered in fluid dynamic studies at the nanoscale.

In addition, the term ‘‘*nanofluidic transport’’* is a general term that is used to express fluidic, molecular, ionic and particle transport inside nanoscale conduits. Accordingly, there will be some additional forces due to the electrostatic field, fluctuation, solvation and Van der Waals force that influence the species transport at the nanometer scale (Durand, 2010; Eijkel and Berg, 2005). The strength of each of the mentioned forces depends on the distance and is comparable in magnitude with viscous and gravitational force at nanometer scale.

The term ‘‘*nanofluidic conduit*’’ corresponds to a nanometer size conduit with any geometrical shape, in which a liquid can flow. It can be a solid state nanochannel with rectangular cross section, a nanopore in a solid state membrane or graphite sheet, a nanopipet, a solid state or carbon nanotube or even an ionic channel in a cell membrane. The size of a nanofluidic conduit varies from less than 10 nm up to 100 nm, which will generate different flow conditions according to their size and material.

1.1.2 Why nanofluidics

Recent development of nanofluidics has mainly been driven by the following three factors. According to the recent reviews (Duan et al., 2013; Sparreboom et al., 2009), advances in micro/nanofabrication technologies and the possibility of fabricating nanometer size features can be mentioned as the most important factor that boosted the nanofluidic research. Standard photolithography that has recently reached a resolution better than one micrometer and other high resolution nanolithography techniques like Focused ion beam (FIB) and electron beam lithography (EBL) provide the possibility of manufacturing accurate well-defined nano structures.

The curiosity of researchers looking for new phenomena at the nanometer scale can be mentioned as the second factor. Speedy successes of microfluidic platforms in multidisciplinary studies encouraged the research institutions to explore the smaller world for new phenomena. Moreover, incitements from the

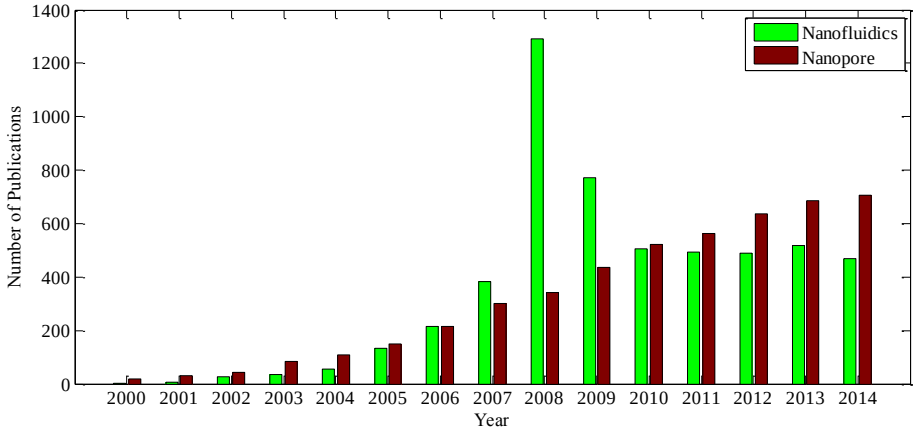

Figure 1-1. Evolution with time of the number of publications with the subject of ‘‘*nanofluidics*’’ and ‘‘*nanopore*’’ according to Elsevier Scopus. It shows that the number of publication in nanofluidics decreases after its boost in 2008 while nanopore continued its progress with a uniform rate. The green bars correspond to a search for ‘‘Nanofluidics’’ without the terms ‘‘nanofluid’’ and ‘‘ nanopore’’ while the red bars are the number of publications that have the term ‘‘Nanopore’’ in their title, abstract or keywords.

funding agencies for multidisciplinary subjects acted like a catalyzer for the curiosity of scientists.

Technology as a powerful impetus has motivated science to make use of new phenomena. Nanofluidics was not an exception, but also attracted more attention due to its original characteristics. Developments in nanofluidics could open new windows into unknowns in different fields and provide new concepts for addressing technological problems.

1.1.3 Progress of nanofluidics

The presence of the term ‘‘nanofluidics’’ in academic studies dates back to the late 1990s. Fabrication of nanofluidic media for DNA electrophoresis (Turner and Craighead, 1998) and using the nanofluidic channels for trapping long DNA (Han and Craighead, 1999) were among the first works that used nanoscale channels. According to Elsevier Scopus (Figure 1-1), nanofluidics could attract many attentions in less than a decade. In 2008, the number of publications exceeded 1000. After, the number of publications decreased and stayed almost constant. The search was performed to find all publications that have the term ‘‘Nanofluidics’’ in their title, abstract or keywords and does not involve ‘‘Nanofluid’’ or ‘‘Nanopore’’.

Analyzing the reasons behind this trend is out of the scope of this study. However, at first glance, two facts can be mentioned as the most influential causes. Firstly, the inclination of research groups to explore the original fields on the one hand and the excessive exhortative incitements from the funding agencies in micro-nanofluidics on the other hand, generated a bubble in number of publications at 2008. A comparison to the results for the term ‘‘Nanopore’’ demonstrates this bubble.

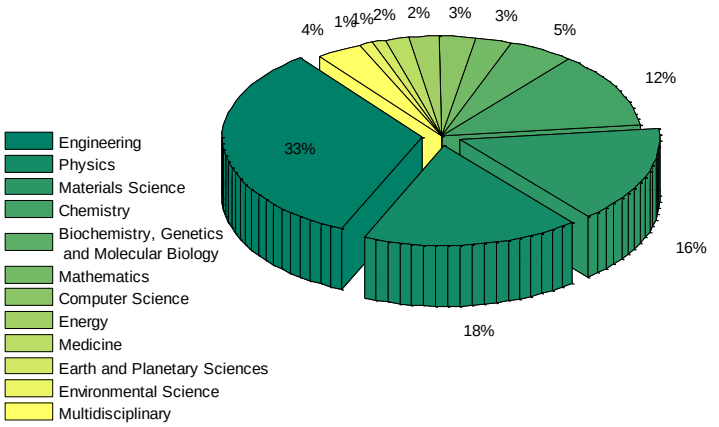

Figure 1-2. The proportion of the number of scientific publications in in the field of nanofluidics published since 2000. It shows that a considerable part of the studies has focused on the basic study of fluid and species transport at the nanoscale. The results are based on Elsevier Scopus.

Secondly, a large number of review articles were published in 2008 pretending that no room was left for original academic research in this field. About 30 percent of all reviews in this field were published in 2008-2009. This fact might have discouraged the funding agencies to take the risk of granting further projects in this field after 2009.

Nevertheless, the new findings and discovered potentials of nanofluidics in manipulation and sensing of tiny particles and small volumes will attract more attention in the next few years. To date, a considerable proportion of the works in nanofluidics have studied the basics and working principles of fluid and species transport at the nanoscale. In comparison to an older field like microfluidics, it is expected to have more application-based studies in the next few years, specially, in biochemistry and molecular biology. Figure 1-2 shows the pie diagram of the proportion of different fields in nanofluidic research. It looks that there is still a lot of room for real applications of nanofluidics at the small scale.

1.2 Gating phenomenon

Similar to its general application, the word ‘‘*Gating*’’ can be defined as the property of opening and closing in response to an external stimuli (Tian et al., 2012). This property can be considered either as a binary status valve, that provides the possibility of opening and closing or as a continuous valve, which manipulates the rate of entrance and exit.

For the case of nanofluidic transport, there has been considerable interest to develop features that mimic the gating property of biological ionic channels. The biological ion channels are composed of proteins and peptides, control the ionic transport across lipid cellular membranes. Their three characteristics, selectivi-

ty, rectification and gating (Hille, 1978), can potentially be implemented by solid state nanofluidic features (Hou et al., 2011).
Apart from the interest in mimicking nature, various designated applications in nanofluidics require the fluidic transport to be sensitive to external stimuli. Temperature, pH and electrostatic field are some of the factors that can cause the stimulation. The possibility of manipulation of fluid and species inside nanofluidic apertures may lead to smart nano-devices that can be used in nano-bio-sensing, remote controlled delivery, nano-tweezers, etc.

1.3 Nanofluidic platforms

Since the beginning of nanofluidic studies, different platforms have been introduced by research groups, which are similar in terms of their nanoscale characteristic lengths but different in terms of geometrical configuration. Nanopores, nanochannels, nanocapilaries, nanotubes and nanoslits have been used and characterized for different applications in nanofluidics. In this section, the properties of these platforms are briefly introduced and compared.

1.3.1 Nanopores

The study of the ionic transport in nanoporous membranes has been the subject of many studies in membrane and colloid science for decades. However, the developments in Focused ion beam (FIB) and the improvement of resolution of electron beam lithography (EBL) have made it possible to fabricate high precision, reproducible nanometer size pores and nanopore arrays. Different nanofabrication techniques such as ion beam drilling (Ivanov et al., 2011), ion beam sculpting (Li et al., 2001), selective ion track etching in thin membranes (Sanz et al., 2006; Wu et al., 2012), heating Au particles on cermic substrate (de Vreede et al., 2015), *etc* have been employed to fabricate nanopore membranes. More recently, nanofabrication techniques were used to improve the nanopore fabrication in terms of accuracy, reproducibility, production time and smaller size of nanopores.
Simpler integration of nanopore membranes to the macroscale, its similar configuration to the ion channels in cell membranes and a long-standing experience of membrane science have guided the nanopore membrane to be one of the best options in nanofluidic applications. This platform has been used in many nanofluidic applications like rectification (Vlassiouk and Siwy, 2007), gating (Jiang and Stein, 2011), DNA sensing and sequencing (Ivanov et al., 2011), *etc*. Figure 1-1 shows the increasing rate of use of nanopores whereas the subject ‘‘nanofluidic’’ without ‘‘nanopore’’ does not follow a similar trend.
Although the nanopore membrane is easy to fabricate and it can simply be integrated to macroscale, it has the drawback of the limited length of the nanopore. A lower nanopore length results in a lower nanofluidic electrostatic effect. Additionally, the observation of fluidic transport inside nanopores is challenging.

1.3.2 Nanochannels

One-dimensional solid-state nanochannels are one of the first platforms that was used to investigate the ionic and molecular transport at the nanoscale (R. Karnik et al., 2005; R. B. Schoch and Renaud, 2005). The possibility of optical observations and measurements due to the in-plane configuration of the nanochannels makes it the best option for fundamental studies as well as biomolecular sensing. It might even be possible to observe a nanoscale chemical reaction inside this kind of nano-apertures. The well-defined and controllable size of nanochannels in all three dimensions due to simple and controllable MEMS based nanofabrication processes is another advantage of this platform. In contrast to the nanopore membranes, there is almost no limitation for the length of the nanochannels.

Three main approaches have been introduced for the fabrication of one and two-dimensional nanochannels. The ‘‘etching and bonding’’ method that uses a controlled etching process to pattern the nanochannel shape on a substrate followed by a bonding step to another substrate has been used in some of the nanofluidic studies (Duan and Majumdar, 2010; R. B. Schoch and Renaud, 2005). The nanochannel can also be fabricated by defining the nanochannel geometry using a sacrificial layer, that will be released at the end of fabrication in order to open the nanochannel (R. Karnik et al., 2005; Stern et al., 1997). This approach is called ‘‘Sacrificial layer releasing (SLR)’’. The third approach that is called ‘‘Etching and deposition’’ replaces the bonding step of the first approach by a deposition step that closes the channel (Wong et al., 2007). All these approaches have been recently discussed and compared in a detailed review article (Duan et al., 2013). Figure 1-3 shows the micrographs of some of the fabricated nanochannels using the mentioned approaches.

The nanochannels have been used in a wide range of applications from fundamental studies of molecular and ionic transport at the nanoscale (R. Karnik et al., 2005; R. B. Schoch and Renaud, 2005) to power generation (van der Heyden et al., 2007) and sensing biomolecules (Durand et al., 2008).

1.3.3 Nanotubes

Solid-state nanotubes and carbon nanotubes (CNT) as pathways in nanofluidic transport have also attracted attention. They allow the possibility of studying long singular two-dimensional nanochannels. We categorize them as a separate platform due to their considerable difference from the nanochannels. Not only their fabrication process is different from the nanochannels, but also their range of nanochannel size, applications and possibilities are not similar to the ones of the nanochannels. As an example, the possibility of fabricating gate-surrounded features for the case of nanofluidic field effect transistors (FET) increases the gating performance dramatically in comparison to one-dimensional nanochannels (Fan et al., 2005).

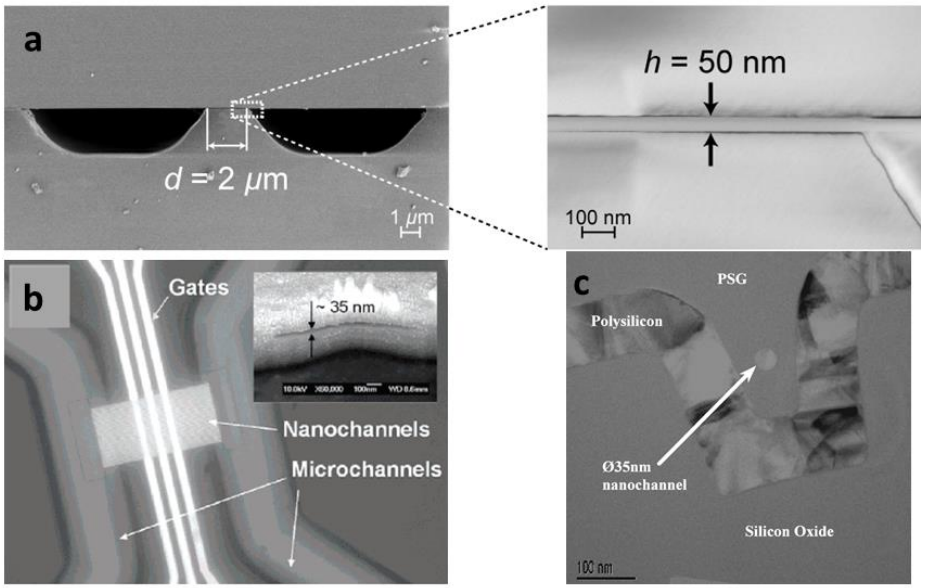

Figure 1-3. a) A 50 nm in height 2 μm in length nanochannel fabricated using ‘‘Etching and bonding’’ method. Two Pyrex wafers were bonded together having an a-Si in between. Reprinted from (Schoch, 2006). b) A 35 nm in height 120 μm in length nanochannel fabricated using SLR method. The sacrificial layer was polysilicon. Reprinted with permission from (Karnik et al. 2005). Copyright American Chemical Society. c) A 35 nm channel fabricated using ‘‘Etching and deposition’’ method. Reprinted from (Wong et al., 2007) with permission.

The conventional way of fabricating solid state nanotubes is to oxidize the surface of silicon nanowires (Figure 1-4.h) and then release the middle silicon part (Figure 1-4.g) as it was introduced by Goldberger et al. (Goldberger et al., 2006). Although the dimensions of the solid state nanotubes can be up to 100 nm, the inner diameter of carbon nanotubes is limited to less than 2 nm (Duan et al., 2013) which can be an advantage while mimicking very tiny ion channels. Ionic diffusion, gas and liquid transport through CNT membrane have been studied and the effect of hydrophilicity on the slip regime have been investigated (Majumder et al., 2011). Single walled CNTs were reported to increase the electrophoretic mobility of the ions passing through it. Figure 1-4.f shows a transmission electron micrograph (TEM) of a single-walled CNT.

1.3.4 Nanocapillary/pipet

In contrast to the previous solid-state platforms, nanocapillaries are easy to fabricate, cost effective and can be fabricated without using cleanroom facilities. Nanocapillaries are made out of glass-like materials such as quartz or borosilicate glass. They can be fabricated using a laser pipette puller, which heats the cylindrical hollow capillary and stretches it at the same time (Steinbock et al., 2010). This causes the diameter of the capillary to decrease at the heated spot and finally break into two conical tips. Controlling the pulling parameters provides the possibility of tuning the diameter of the capillary. Diameters of 30 nm can be reached reliably using laser pullers. Moreover, it has been shown

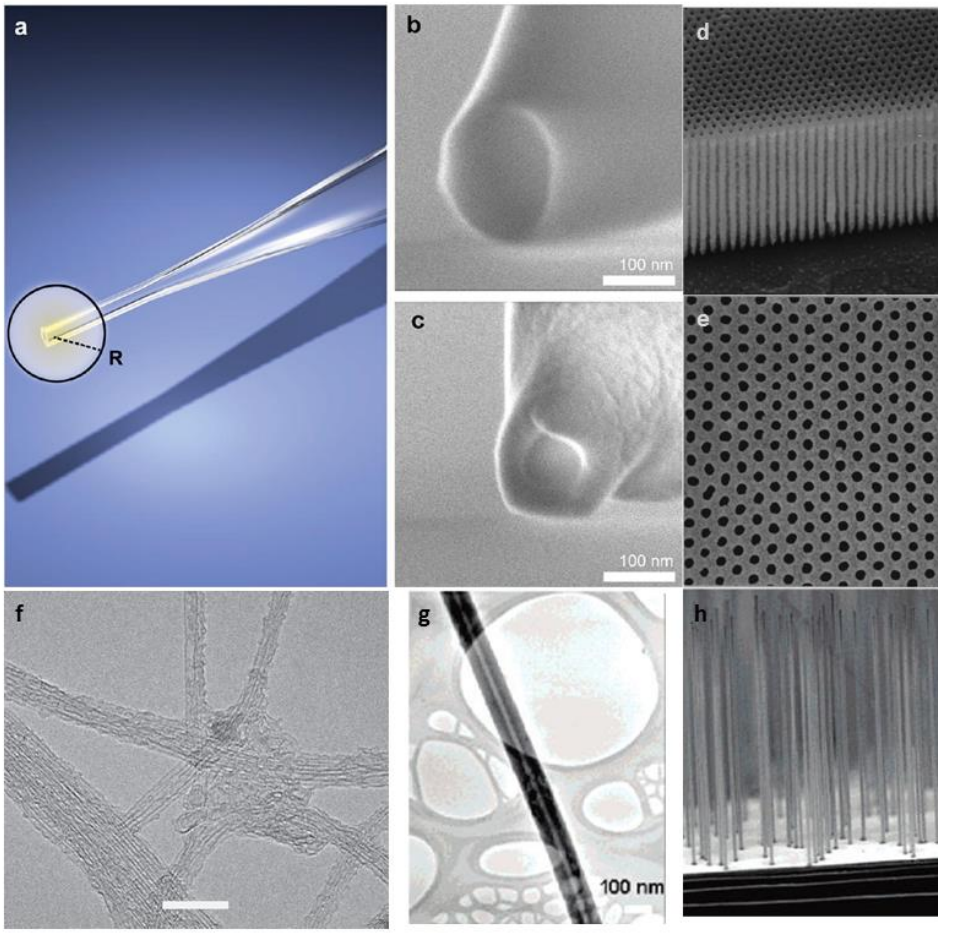

Figure 1-4. **a**) Scheme of the conical end of a nanocapillary. **b**) SEM in-lens image of a quartz nanocapillary. **c**) Shrunken nanocapillary after 14 min of electron beam irradiation under constant angle and beam parameters. Reprinted from (Steinbock et al., 2013). Copyright 2013 American Chemical Society. **d** and **e**) Ordered array of nanopores in an alumina membrane fabricated using electron beam lithography (EBL). Reprinted from (Asoh et al., 2001) with permission. **f**) TEM image of single-walled carbon nanotubes. Scale bar is 10 nm. Reprinted from (J. Wu et al., 2012) with permission. **g**) TEM image a silica nanotube made of silicon nanowire (**h**). Reprinted with permission from (Goldberger et al., 2006). Copyright 2006 American Chemical Society.

that under scanning electron microscope (SEM), the diameter of the tip can be shrunk more. The tip diameter can be tuned by thermal heating while exposed to the electron beam from the SEM (L. J. Steinbock et al., 2013). Figure 1-4.a-c demonstrate the nanocapilaries fabricated by this method.

In addition to the advantage of simple fabrication process, the nanocapillaries can be integrated to normal lab pipettes, which allow more handy applications. Decreasing the tip diameter using electron beam results in various applications like in the resistive pulse technique, where small diameters increase the sensing sensitivity (L. J. Steinbock et al., 2013).

1.3.5 Platform selection

Table 1-1 compares the characteristics of different nanofluidic platforms. Every nanofluidic platform has its own advantages and drawbacks. The objectives and limitations of the applications will define which platform is suitable. For example, nanopore membranes can be used in molecular sieving while the nanochannel is perfect for fundamental studies, optical observation and sensing of particles. The advantages of nanocapillaries in their integration to normal pipettes and their simple and cheap fabrication cause them to be an ideal platform for controlled molecular dispensers and sensors.
In addition to the mentioned platforms, nanoporous membranes and specially, emerging graphene membranes have attracted some attention in the past few years. Although these types of platforms might be categorized in the membrane science field of study, it has been studied by the people in nanofluidics since the word ‘‘nanofluidics’’ appeared in academic research. For example, graphene membranes were used for different nanofluidic applications like desalination of water (Wang and Karnik, 2012), power generation (Guo et al., 2013), DNA translocation detection (Traversi et al., 2013) and nanofiltration (O’Hern et al., 2015) mainly by nanofluidic research groups.

Table 1-1. Comparison of different nanofluidic platforms

	Nanopore	**Nanochannel**	**Nanotube**	**Nanocapillary**
Macroscale integration	✓	○	✗	✓
Optical observation	✗	✓	○	✗
Possible length	✗	✓	✓	✗
Fabrication Process	○	✓	✗	✓
Fabrication cost	○	○	○	✓
Reproducibility	○	✓	○	○
	✓ :Superior	○ :Ordinary	✗:Inferior	

1.4 New availabilities at the nanoscale

The phenomena that occur at the nanometer scale provide new tools and possibilities to manipulate, control and observe tiny species, which were impossible before. Beside many studies that focused on discovering and interpreting fundamental phenomena at the nanoscale fluidic transport, some applications have also been introduced in different fields. Biotechnology, point of care (POC) applications, lab on a chip (LOC) systems, nano electromechanical systems (NEMS) and even membrane science have been reported to benefit from nanofluidics. Here, some of the promising applications are briefly reviewed.

1.4.1 Controlling the ionic and molecular transport

The term ‘‘*nanofluidics*’’ was introduced for the first time by the possibility of *controlling the ionic and molecular transport*. The electrostatic properties of nanofluidic conduits beside their high surface to volume ratio result in a unique phenomenon that allows controlling the ionic transport across them. In contrast to the microscale, as it is depicted in Figure 1-5.a and b, the electric double layer (EDL) due to the charged walls is as thick as the characteristic length of the nanofluidic conduit. In this situation, the fluidic transport is strongly dependent on the electrostatic effects of the walls.

Different configurations have been used to rectify the ionic current through nanofluidic pores and channels. The pure electrostatic effect was utilized by coating the two sides of the nanochannel wall with asymmetric charged molecules in order to mimic the semiconductor diode configuration in nanofluidics

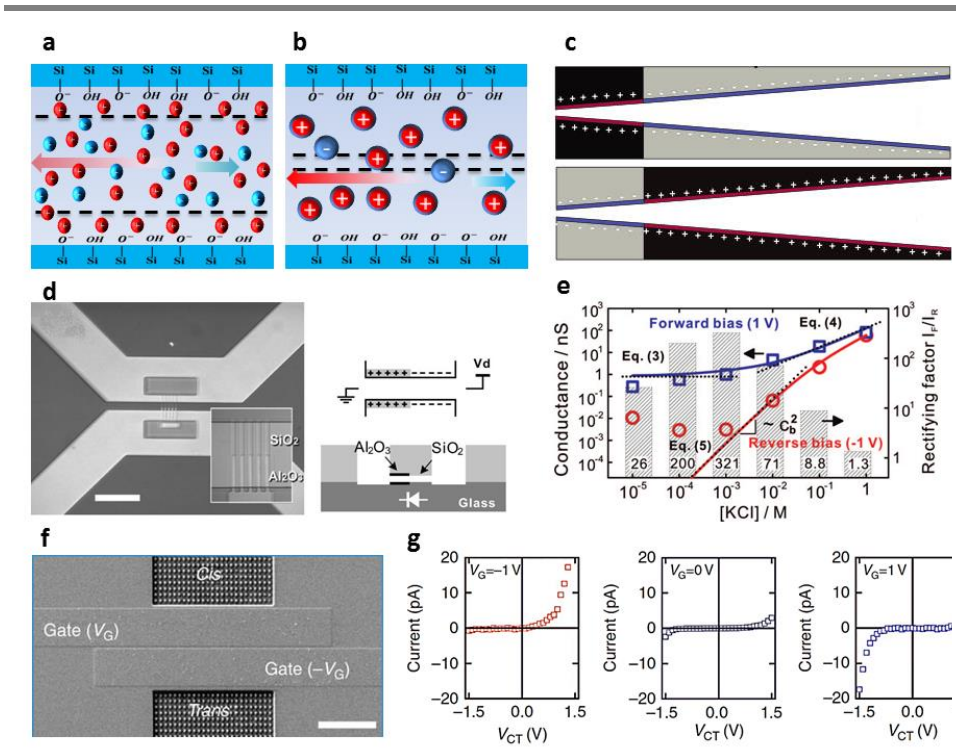

Figure 1-5. Schematic of the ionic transport at **a**) microscale and **b**) nanoscale. The electric double layer (EDL) may overlap in nanochannels and cause them to be selective to counter ions. **c**) Schematic of a conical nanopore with patterns of surface charge that lead to formation of a nanofluidic diode. **d**) microscope image (left) and schematic (right) of a nanofluidic diode composed of aluminum oxide in one side and silicon dioxide on the other side in order to rectify the current. The scale bar is 100 µm. The result is shown in (**e**). The rectification factor is more than 2 orders of magnitude. The blue and red data points show the forward and reverse biased conductance of a nanochannel at different ionic concentrations. Reprinted from (Cheng and Guo, 2009). Copyright 2009 American Chemical Society. **f**) SEM image of a two side gated nanofluidic diode. The scale bar is 100µm. applying asymmetric voltages to the gates results in a diode effect that rectifies the ionic current as depicted in **g**. Reprinted from (Guan et al., 2011) with permission.

(Karnik et al., 2007) . This approach was also followed by using different oxides (Figure 1-5.d) (Cheng and Guo, 2009). Integrating two electrodes on top of the nanochannel (Figure 1-5.f) was also studied in ionic transport rectification and reported to reach a rectification degree of up to 100 (Guan et al., 2011). The field effect modulated nanofluidic diode was also fabricated in nanoporous membrane (Wu et al., 2013). Using a conical nanopipet as an asymmetric geometry can bring about a rectification property (Wei et al., 1997). The rectification degree was reported to increase by surface modification (Vlassiouk and Siwy, 2007). The surface were also modified by pH tunable polymer brushes in order to provide the pH tunable rectifying characteristics (Yameen et al., 2009a). Apart from the electrostatic rectification of the ionic transport, the electroosmotic flow rectification was also reported recently (Laohakunakorn et al., 2013).

In addition to making use of selectivity and rectifying properties, many studies focused on controlling the nanofluidic transport. Different mechanisms for the manipulation of nanofluidic transport such as using electrostatic field (Fan et al., 2005; R. Karnik et al., 2005; Reto B. Schoch and Renaud, 2005), liquid reconfiguration (Powell et al., 2011; Smirnov et al., 2011) and steric volume exclusion (Xia et al., 2008; Yameen et al., 2009b) have been introduced. Recent advances related to the gating phenomenon will be discussed in detail in the next chapter.

1.4.2 Single molecule sensing

Scaling down the dimension of a nanofluidic device to a size comparable to the one of a particle provides the possibility of detecting the particle when it passes through the device. The high sensitivity and resolution of the nanofluidic sensors in addition to the possibility of extracting detailed particle properties such as size, charge and shape (Kozak et al., 2012; Storm et al., 2005) have made them undisputed sensors at the molecular level. Monitoring the DNA translocation across gated nanofluidic conduits have provided the possibility of ultrafast DNA sequencing while using tunneling technique (Ivanov et al., 2011). The possibility of DNA sequencing using Graphene nanopores, as the next generation of DNA sequencing technique, were illustrated by means of molecular dynamics (MD) simulations (Wells et al., 2012). Graphene nano ribbons (GNRs) were integrated to a nanoporous membrane as a single base pair DNA sensor due to their small length (Traversi et al., 2013). It was also reported that DNA-graphene interactions slow down the DNA translocation across the graphene (Banerjee et al., 2015).

Different methods have been introduced for sensing small particles inside nanofluidic channels. Resistive pulse sensing (RPS) is a widely used one. It was first employed in nanofluidics to detect a 500 base pairs (bp) double-strand DNA (dsDNA) in a 5 nm solid state nanopore (Li et al., 2001). Different lengths and shapes of DNAs can be detected by inspecting the translocation time and pulse type (Storm et al., 2005). Not only it reveals the important information about the particle geometry, but also it screens the wall-molecule in-

teractions. These interactions have been used for detecting smaller molecules like proteins (Freedman et al., 2011). Serial configurations of nanochannels have been utilized to detect viruses *via* measuring their electrophoretic mobility (Figure 1-6.b) (Harms et al., 2011). High resolution detection was reported that was capable of detecting a single protein on a DNA molecule and its orientation while translocating through the nanopore (Raillon et al., 2012). The RPS was exploited in a GNR integrated nanoporous membrane to sense two different DNA molecules in a solution (Figure 1-6.c) (Traversi et al., 2013).
Beside the resistive pulse sensing (RPS), other methods have been used for detecting particles in nanofluidic apertures. Monitoring the I-V curve to detect proteins that have interaction with the surface binded counterparts (Siwy et al., 2005) is one of the examples that utilized a different approach. Based on the change in rectification degree of a nanofluidic diode, one can detect a molecule

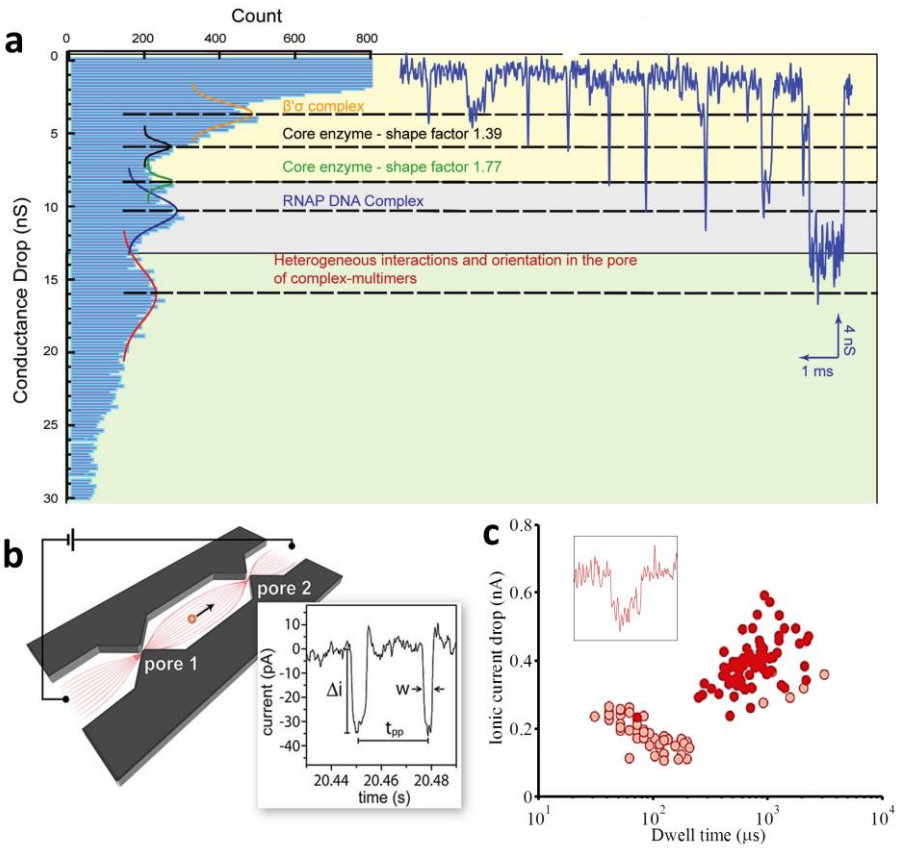

Figure 1-6. a) Identification of different molecules based on their specific conductance translocation signature. Reprinted from (Raillon et al., 2012). Copyright 2012 American Chemical Society. b) Resistive pulse sensing of hepatitis B virus (HBV) capsids based on their electrophoretic mobility which is defined by measuring pore to pore transit time. Reprinted from (Harms et al., 2011). Copyright 2011 American Chemical Society. c) Scatter plot of the translocation of pNEB DNA and λDNA through a solid state nanopore drilled in graphene integrated to silicon nitride membrane. The inset shows a detected translocation event. Adapted from (Traversi et al., 2013) with permission.

of interest since the wall-molecule interactions varies the rectification degree (Ali et al., 2010). A protein complex formation was detected based on the enhanced protein diffusion in nanofluidic channels (Durand et al., 2008). Recently, the impedance analyzing method was used to distinguish ssDNA and dsDNA in a nanoporous membrane (Wu et al., 2015).
It looks that progresses in nanofluidic sensing will revolutionize the developing POC systems *via* changing the paradigms for diagnosing the diseases.

1.4.3 Miscellaneous applications

Apart from the two previously mentioned important applications, some other applications have been presented in different fields such as POC systems, engineering, molecular biology, *etc.* Power generation at the nanoscale using the streaming current (van der Heyden et al., 2005) of a pressure driven flow inside a nanochannels was reported to be efficient at EDL overlapped conditions (van der Heyden et al., 2007). Making use of the concept of concentration polarization made it possible to desalinate water (Kim et al., 2010). Manipulation of molecules inside the nanochannel was studied. Stretching a DNA using an electric field (Heng et al., 2005), controlling its translocation (Belkin et al., 2013) or slowing down its motion while passing through a nanopore (Kowalczyk et al., 2012) and trapping nanoscale particles (Eijkel and van den Berg, 2010) were among the studies focused on the manipulation of species at the nanoscale.
Many other applications have been presented and reviewed. Resistive pulse sensing, separation and sieving, small volume delivery, electrospray ionization, flow detection, pumping and energy conversion are the applications that have been reviewed by some research groups (Eijkel and Berg, 2010; Haywood et al., 2015; Schoch et al., 2008; Sparreboom et al., 2010). There are also some reviews that focused on specified nanofluidics application such as POC systems (Segerink and Eijkel, 2014), single DNA sequencing (Marie and Kristensen, 2012), sensing (Tian et al., 2012) and active and passive control of molecular transport in nanopores (Keyser, 2011).

1.4.4 Future developments

The unique properties of nanometer-size conduits make them an ideal candidate to facilitate the research in biotechnology and molecular biology. Additionally, the incitements from funding agencies and impetus from technology have made the multidisciplinary filed of bioengineering a hot topic in the past decade. Many research groups have focused on these applications, as discussed in previous sections, and made considerable progresses. However, there is still a lot of room in both academia and technology in order to produce the actual products.
Some characteristics of nanofluidic features such as nanofluidic sensing of biological molecules and ultrafast DNA sequencing are expected to have a main role in not-too-far future of POC products. Some others like controlled drug delivery and genome analysis need more developments in both science and tech-

nology. Specially, the ability of nanofluidics to control the ionic and molecular transport needs more enhancements in order to be used in smart medicine. Smart medicine can make use of the ability of controlling the fluidic transport for controlled drug delivery inside the body.
Apart from the applications in biotechnology, there are still some unknowns, which have been neglected in fundamental studies for the sake of simplicity. The basic concepts of nanofluidic transport needs to be investigated more accurately.
Moreover, focusing on biotechnological applications does not mean that it is impossible to use the nanofluidic devices for other needs. The few applications in engineering, like power generation and water desalination are the examples, which emphasize that the nanofluidics can be useful in other fields as well. There are also some known and less-attended subjects like nanofluidics for energy and nanofluidics for environment. Fuel cells performance increases by using ion selective membranes and can benefit from nanofluidics. Molecular detection can also be used for improving the environmental sensors. Many new applications can be designed base on the technological demands in different fields. In one word, nanofluidic is still quite young.

1.5 Thesis objectives

As it was mentioned in the previous section, one of the important properties of nanofluidics is the possibility of controlling the fluidic transport, which can have important applications such as controlled drug delivery. According to the state of the art discussed in 1.4.1, *gating* the nanofluidic transport is the right paradigm for continuous bi-directional control of the ionic transport. The main goal of the present thesis is to study the latest advances in gating the nanofluidic transport and introduce methods and mechanisms to improve the performance and effectiveness of the gating in nanofluidic transport.
To this aim, some intermediate objectives were defined and achieved during my studies:

- To study the latest progresses in gating the nanofluidic transport.
- To select a proper fabrication method, design and fabricate the nanofluidic devices accordingly.
- To characterize the nanofluidic devices and check the conformity with the theory.
- To develop a theoretical model that is validated by the experiments.
- To study the influence of temperature on nanofluidic transport[1].

[1] This objective was defined after I noticed the influence of temperature on electrical conductance of nanochannel while studying the effect of electrostatic field.

- To introduce and characterize a new gating mechanism, called ‘‘thermal gating’’, based on the effects of temperature on nanofluidic transport.

1.6 Thesis structure

The thesis has been organized in a way that the reader becomes familiar, step by step, with the aspects of nanofluidic transport. Every chapter is written based on the preceding information provided in the previous ones.

As the first chapter discussed the general aspects of the nanofluidic transport such as nanofluidic platforms and applications, the second chapter, focuses on the latest advances in gating the nanofluidic transport. Different gating mechanisms are presented and compared.

Chapter 3 explains the materials and methods that are common in all the experimental studies that will be discussed in future chapters. Design, fabrication process and the integration of the fabricated nanofluidic devices to macroscale are the subjects of the microfabrication discussions in this chapter. Additionally, the procedure of measuring the electrical conductance of nanochannel using the AC impedance measurements will be described in detail.

In Chapter 4, the analytical modeling of the nanochannel conductance is discussed; a new analytical modeling approach is introduced and finally, the model predictions are compared with the experimental measurements.

Based on the theoretical aspects of chapter 4, the influence of temperature on the electric conductance of nanochannels is discussed in Chapter 5. Moreover, the analytical predictions will be confronted with the results from the experimental measurements. The temperature sensitivity of the electrical conductance of nanochannel is higher at low ionic concentration where the nanofluidic transport is governed by the electrostatic effects from the wall.

Finally, a new gating mechanism, called ‘‘thermal gate’’ that uses the thermal effect for modulating the ionic transport inside nanofluidic channels is introduced in Chapter 6. The ‘‘thermal gate’’ controls the ionic transport more effectively than most other gating mechanisms previously described in scientific literature.

The thesis is summarized in Chapter 7 where an outlook on future possible subjects of studies continuing this work is presented.

Chapter 2

Gating in nanofluidic transport

Opening and closing the nanofluidic apertures has been among the subjects of nanofluidic studies, as discussed in the previous chapter . In this chapter, the state of the art of the gating phenomenon in nanofluidic transport is presented. Using the steric volume exclusion effect of macro-molecules to occlude the channel, employing the effect of the electrostatic field to influence the fluidic transport and modulating the surface wettability, have been reported as gating mechanisms in nanofluidic studies. In addition to presenting these mechanisms, their advantages and drawbacks are compared.

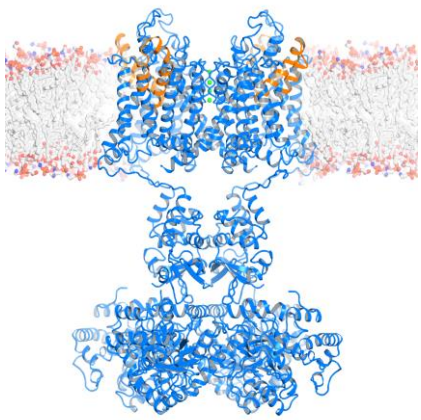

''Among their many functions, ion channels control the pace of the heart, regulate the secretion of hormones into the bloodstream, and generate the electrical impulses underlying information transfer in the nervous system.''

Prof. ***Roderick MacKinnon, Nobel Prize 2003***

2.1 Ion channel, the utmost ionic gate

The ionic and molecular transport is performed regularly through biological membranes in all living organisms. Controlling the ionic and molecular transport through any cell membrane is vital. Cells can actively control the inward and outward transport of ions and molecules through special nanopores in their membrane called ‘‘ion channels’’. There are hundreds of types of ion channels in a cell membrane whose gating mechanism varies according to their gating role (Yellen, 2002). The pore can be opened or closed by different types of stimulations, such as electric or chemical signal, temperature, etc. They can be selective to an ion of interest like chloride, potassium, sodium, etc. The ion channels are made of proteins of complex shapes with a diameter of around 1-2 nanometer. Using different types of proteins allows the cells to define different functions for their ion channels.

Figure 2-1 shows a schematic of a potassium ion channel in open and close mode. The channel uses a combination of electrostatic effect and steric exclusion and maybe some other effects to perform the role of gating.

The realization that nature produces these kinds of nanopores that can selectively gate the ionic transport, inspired the development of solid-state nano-confined features of similar properties.

Moreover, fabrication of optically observable nanochannels, although their aspect ratio and surface chemistry is different from the protein ion channels, allows the investigation of biomolecular transport at nano-confined geometries. Additionally, the electrical measurement, as a powerful label-free method, brings unique properties for both nanochannel characterization and particle detection. These properties offered by solid-state nanofluidic devices can give rise to new ways of manipulating and sensing single biomolecules.

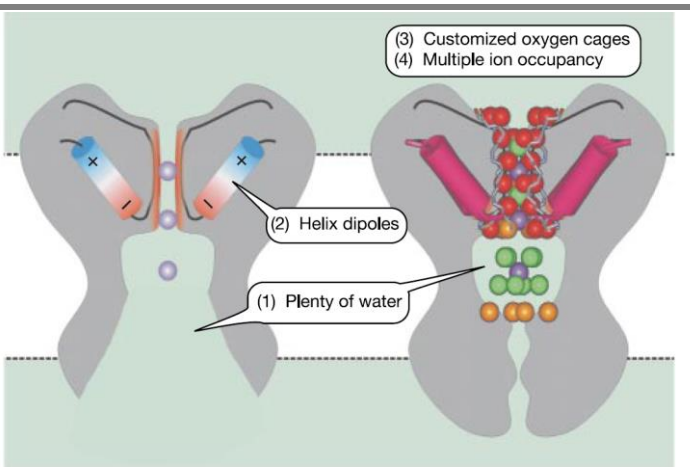

Figure 2-1. Schematic of a voltage-gated potassium channel in open (left) and close mode (right). The purple spheres indicate the potassium ions. There is a water-filled cavity in the middle of the membrane protein. The backbone oxygens of the selectivity filter (red spheres) provide a good match to the hydration environment for the potassium ions. A trapped potassium ion is surrounded by eight water molecules (green spheres) in the water filled cavity in closed mode. Reprinted from (Yellen, 2002) with permission.

Will these features lead to similar human-made membranes containing several types of controllable nanopores of different missions?

That is the question, which can be answered in a not-too-far future.

2.2 Gating

2.2.1 Definition

Controlling the ionic and molecular transport through nanoconduits was among the first objectives of nanofluidic research since it has begun. As it was explained in 1.4.1, the original properties of nanometer size conduits such as selectivity and rectification made it possible to control the ionic transport (Tian et al., 2012). However, continuous and active control of the ionic transport, so called ‘‘gating’’, that is performed in cells by ion channels has to be reproduced in solid-state counterparts.
Steric exclusion, field effect and liquid reconfiguration are the paradigms that have been introduced for performing gating in nanoconduits. In the following sections, we discuss about the working principles of these methods and compare their characteristics.

2.2.2 Gate effectiveness

The gate effectiveness is defined as the ratio of on- to off-state conductance (G_{on}/G_{off}) in order to compare the performance of the gating methods in different conditions.

2.3 Steric effect

The steric effect originates from the definite volume that every particle naturally occupies in space and cannot share with other particles. Two distinct particles can not be in the same spatial position at a given moment.
This effect has been exploited to gate the nanofluidic transport. The keyword ‘‘bioinspired’’ or ‘’biomimetic’’ in nanofluidics usually implies that this effect is used in nanofluidic conduits. The steric effect gating of nanochannels is normally performed by immobilizing macro-molecules on the walls of nanopores or nanochannels. The macro-molecules can be switched between two conformation states by changing the temperature, pH or any other factor that can be used as an external stimulus. The working principle of all the nanoconduits that use the steric effect for gating is similar. They use the steric exclusion to physically open and close the conduit.
For the first time, ssDNAs were immobilized in a conical nanopore and used to rectify the fluidic transport (Harrell et al., 2004). The conformation change of the DNA molecules in response to an electric field resulted into gating property of a nanopore. The electrophoretic movement of the electrostatically charged DNA molecules inward and outward the conical tip, called ‘‘mouth’’ of the nanopore, resulted in closing and opening it (Figure 2-2.a). Although one end of the DNA chain was immobilized, in an electrophoresis experiment, the anionic chain ex-

tended linearly in the direction of the anode. Accordingly, it could occlude or unclog the nanopore, depending on the direction of the applied electric field.
Later, gating the nanopores using smart polymer brushes was reported by some research groups. Using temperature sensitive polymers to gate the fluidic transport inside nanopores (Yameen et al., 2009b) showed good results. The electrical con-

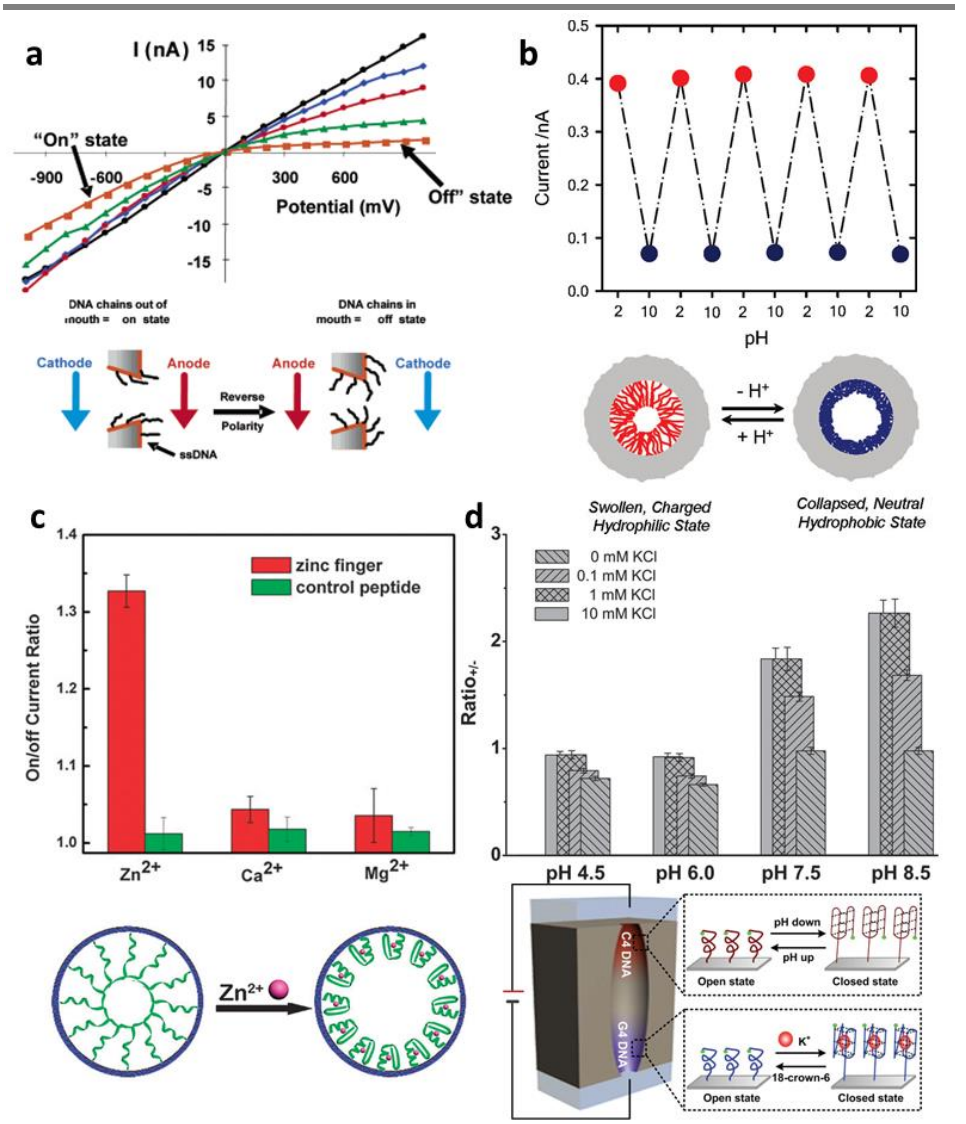

Figure 2-2. **a**) Rectification of ionic current by immobilizing ssDNAs on a conical nanopore. Black dots show the I-V curve before modification while the orange ones show the nanopore coated with 45 mer DNA. The chain length of DNA defines the rectification degree. Reprinted from (Harrell et al., 2004) with permission. **b**) A proton gated nanopore. The pH sensitive polymers open and close the channel. reprinted from (Yameen et al., 2009b) with permission. **c**) Gating effectiveness of a zinc activated nanochannel. The graph shows the high sensitivity of the channel to zinc ions relative to others which is due to coating the wall with zinc finger peptide protein. The conformation of this protein is dependent on the presence of zinc ion. Reprinted from (Tian et al., 2010) with permission .**d**) A double gated nanochannel that is sensitive to pH and potassium ion. The channel is opened at high pH and high concentration of potassium. Reprinted from (Liu et al., 2015) with permission.

ductance of a nanopore increased more than four times by a temperature rise of 17 °C. A similar approach was taken for pH sensitive polymer brushes (Yameen et al., 2009c). The ratio of on-state to off-state conductance was about 4 (Figure 2-2.b).

More recently, using the polymers which are sensitive to a molecule of interest have interesting applications in both sensing and gating. Some polymers have been used which are sensitive to special ions like zinc (Tian et al., 2010), potassium (Hou et al., 2009), mercury (Tian et al., 2013) or even proteins (Ali et al., 2013).

A combination of two factors in a single nanopore has also been investigated. The potassium and pH gated nanochannels (Liu et al., 2015) and the multiple pH- and voltage-gated nanopore (Buchsbaum et al., 2014) are two examples of double-gated nanopores. Using a combination of two or even more factors will enhance the selectivity and resolution of gating. Figure 2-2.d shows a double gated nanochannel that is sensitive to pH and potassium ions. The channel is opened at high pH and high concentration of potassium.

Using smart polymers for gating results in a versatile method for gating and sensing. Specially, the combination of two or even more factors in a single nanopore results in a finer control on the type, size and charge of ionic species subjected to the gating effect, which is very promising for the fabrication of synthetic nanopores with the same roles as the ones of ion channels.

Overall, exploiting the smart polymers for gating is still in its infancy period. The advances in polymer science will have a strong impact on this subject. Moving toward multiple gating factors is another fact that can result in more nature-like nanofluidic gates.

2.4 Field effect

2.4.1 Origin of the field effect gating in nanofluidics

Beside the inspiration from the biological ion channels, the field effect was first used to modulated the ionic concentration inside a microfabricated nanometer size channel (Gajar and Geis, 1992). The fabricated device was called ionic liquid-channel field effect transistor (ILCFET) that was designed to resemble the metal oxide field effect transistor (MOSFET) using conductive liquid channels. Later, as described by (Daiguji et al., 2004), the experimental results that showed the modulation of ion transport in protein ion channels due to translocation of biomolecules (Kasianowicz et al., 1996) attracted attentions toward the ion transport in nanoscale channels. Advances in microfabrication technologies allowed fabricating synthetic nanopores and studying of bimolecular transport through them (Li et al., 2001).

A few years later, a numerical simulation was carried out to solve the equations from theoretical modeling of ionic transport inside a nanochannel (Daiguji et al., 2004). The modeling supported the idea of fabricating a unipolar ionic field-effect transistor. Based on this, the same group introduced the nanofluidic field effect transistor (FET) (R. Karnik et al., 2005). Using a combination of fluorescence and electrical measurements, they demonstrated that the gate voltage modulated the concentration of ions and molecules in the channel and controlled the ionic con-

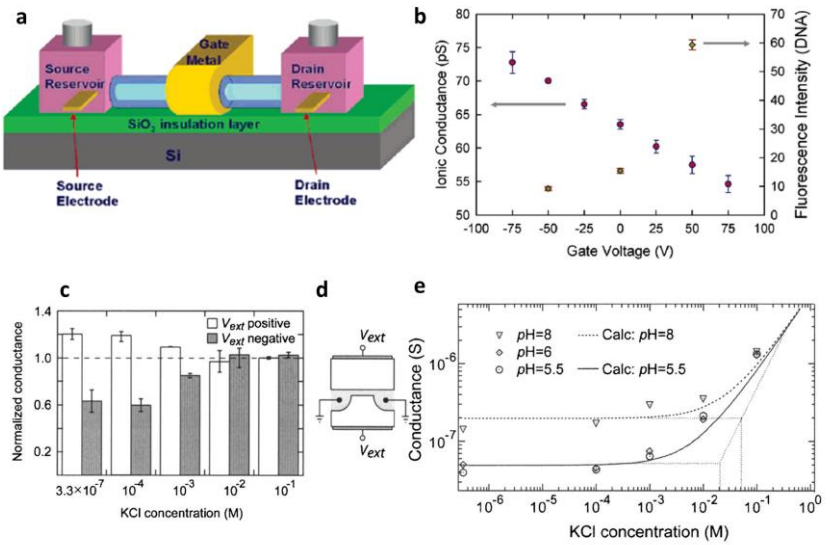

Figure 2-3. **a**) Schematic of the nanofluidic FET proposed by Karnik *et al.* and **b**) the evolution of ionic conductance and fluorescent intensity *versus* gate voltage (The gate electrode was 500 nm apart from the nanochannel wall. Reprinted from (R. Karnik et al., 2005) with permission. Copyright 2005 American Chemical Society. **c**) The effect of external gate (around 500 µm apart from the nanochannel) on the electric conductance of nanochannel at both nanochannel walls as sketched in (**d**). **e**) Dependence of the electric conductance of nanochannel on its wall surface charge. the wall surface charge varies by changing the pH of the solution. Reprinted from (Schoch and Renaud, 2005) with permission.

ductance (Figure 2-3.a-b). They used a negatively charged dye in KCl solutions of various concentrations to demonstrate the field effect. When the gate potential was positive, the gated part of the nanochannels became positively charged and induced an attractive force on the negatively charged dye and increased the concentration intensity of fluorescent dye in the nanochannel. When a negative gate potential was applied, the nanochannels became more negatively charged, which repelled negatively charged dyed molecules from the gated portion of the nanochannels, leading to a decrease in the concentration of the negatively charged dye and fluorescence intensity. The nanofluidic FET was introduced as a building block of integrated nanofluidic circuits for the manipulation of ions and molecules at the small-scale. This application can occur even in non-overlapping EDL regime. The numerical simulation proved that in overlapping EDL conditions, it is possible to control the flow of only counter-ions through the nanochannel. Accordingly, the nanofluidic diode was introduced (Daiguji et al., 2005).

At the same time, other groups working on nanofluidics discovered the effect of external electric field on the nanofluidic transport (R. B. Schoch and Renaud, 2005). As Figure 2-3.c represents, they also reported a considerable change of the electrical conductance of nanochannels while varying the wall surface charge by using solutions having different pH (Figure 2-3.d). Similar works were also reported for controlling the electroosmotic flow in microchannels (Schasfoort et al., 1999; van der Wouden et al., 2005).

Changing the wall surface charge by immobilizing molecules of different charge on the nanochannel wall was also studied (Rohit Karnik et al., 2005) and combined with the gate electrode effect (Fan et al., 2005).

2.4.2 Nanofluidic platforms for FET

All the works mentioned in previous sections used nanochannel or nanotube platforms. Nanopores, in spite of their geometrical similarity to ion channels, were less successful in employing the FET concept mostly due to fabrication limitations.

Some groups reported that they successfully tuned the ionic transport through their FET configured nanopores (Jiang and Stein, 2010; Joshi et al., 2010; Kalman et al., 2009; Nam et al., 2009). However, there are some limitations in fabricating an ideal nanofluidic FET in a nanopore platform. The main challenging problem is the limitations for the insulation of the gate electrode. An ideal nanofluidic FET necessitates an insulating layer in order to prevent the current leakage from the gate electrode into the conduit. For the case of nanopore, it is not simple to insulate the gate electrode. The reported insulating layers such as evaporated silicon dioxide (Kalman et al., 2009) or atomic layer deposition (ALD) of titanium dioxide (Nam et al., 2009) or aluminum oxide (Jiang and Stein, 2010) are not very resistive to the electric current when they are in contact with electrolyte. Firstly, they are limited by the possible thickness of the dielectric layer. Secondly, the quality of deposited insulator is not good enough to insulate the gate electrode. The presented data in the mentioned works illustrates clearly their problem of current leakage. Even for the case of deposited thermal oxide (Joshi et al., 2010) that should have the best quality, the author discussed about the electric current leakage from the gate. The leakage was not preventable for the case of thermally oxidation of tungsten (Wu et al., 2013), either. The current leakage problem limits the applied gate voltage and consequently, the gating cannot be carried out effectively.

For the case of nanopipet platform, fabrication of any gated feature has not been reported yet. It is difficult to integrate an insulated gate to an unconventionally fabricated device. Nevertheless, fabricating such a device can be impactful and will have many applications due to the user-friendly properties of nanopipets.

2.4.3 Modeling the nanofluidic transport in presence of field effect

2.4.3.1 Analytical modeling

Since the beginning of nanofluidic studies, analytical modelings and numerical simulations have been carried out. The first two publications from Daiguiji et al. (Daiguji et al., 2005, 2004), introduced the concept of the effect of the electrostatic field on nanofluidic transport. The paper by Burgreen and Nakache (Burgreen and Nakache, 1964) was likely the first work in the field, even if they didn't use the word ''nanofluidic''. Later, Levine *et al.* (Samuel Levine et al., 1975) developed an analytical model for the electrokinetic flow through a narrow parallel plate channel. They reported that the classical Smoluchowski expression is reduced while the height to EDL thickness ratio tends to zero. They also modeled

the electroosmotic flow at high zeta potential for small capillaries of the same radius as the EDL thickness (S Levine et al., 1975a).

Beside the gating phenomenon, some research groups focused on developing the governing equation in electrokinetic flow inside nanochannels (Pennathur and Santiago, 2005). Some others tried to justify their experimental results by means of simple modeling (Smeets et al., 2006).

More recently, some more developed analytical modelings have been reported. A full multi-ion model for analyzing the surface charge property and EOF in gated nanofluidic devices by FET have recently been reported (Yeh et al., 2012). Trying to model the surface reactions as well as their influence on the wall surface charge is the advantage of this model.

There are two challenging points in all analytical models. Firstly, the surface charge density of the nanochannel wall depends on the kinetics of the surface reactions. Secondly, some models in surface chemistry have been developed for parallel plates. Applying these models to a cylindrical or rectangular nanochannel may not be correct. In Chapter 4, the analytical modeling of the nanofluidic transport is discussed in detail.

2.4.3.2 Numerical simulations

Numerical simulations, as a complementary method, has been conducted by some research groups in order to clarify the nanofluidic transport in the presence of the field effect. The more comprehensive the modeling is, more accurate solution is obtained. As an example, the ionic transport in a nanofluidic FET was simulated numerically by Singh et al. (Singh et al., 2011). They investigated that the effectiveness of the ionic current control by the gate decreases with increasing the surface charge density. They attributed this effect to a change in zeta-potential and overall electro-neutrality condition. Nevertheless, this result was extracted from a constant surface charge model while the effect of the activity of H^+ ions on the wall surface charge was not considered. Although, these kinds of modeling can explain some aspects of the physical phenomena, they are far from practical use. The reason is that unlike the well-developed computational fluid dynamics (CFD), the physical modeling still needs to be improved and validated for the case of nanofluidic transport.

More recently, based on the latest findings in nanofluidics, Pardon and van der Wijngaart modeled and simulated the electrostatically gated nanochannels (Pardon and van der Wijngaart, 2013). In addition to basic governing equations used in previous works, they modeled the surface reactions and considered the activity of H^+ ions in their simulation. They observed a higher gating effectiveness at the pH values close to the point of zero charge (PZC) and at low ionic concentrations where the EDLs overlapped.

2.4.4 Limitations

2.4.4.1 Breakdown limit

As discussed briefly in 1.3.3, the performance of nanofluidic FETs are limited by the current leakage from the gate. Not only nanopores, but nanochannels and

nanotubes suffer from this limitation. The breakdown limit changes depending on the quality of the insulating layer that depends on the method of deposition, thickness and dielectric material.
Karnik *et al.* observed a dielectric breakdown in their nanofluidic transistor circuit (Karnik et al., 2006). They attributes this breakdown to inadequate step coverage of dielectric oxide layer or due to a breakdown caused by the sharp edge. Even having a thermal oxide over the gate couldn't prevent the current leakage from gate (Oh et al., 2009). As mentioned before, a similar result was also reported in nanopore platform (Joshi et al., 2010). As it is shown in Figure 2-4.a the leakage current is relatively higher at negative gate voltages.

The dielectric layers that have been used in the nanofluidic FETs are normally used in MEMS devices as insulating layers and works properly with an acceptable breakdown limit. In nanofluidic FETs, the non-perfect dielectric layer is in contact with the electrolyte. The electrolyte can penetrate through the defects in the dielectric layer and the insulating role of the dielectric layer breaks down. Jiang and Stein (Jiang and Stein, 2010) tried to investigate how surface chemistry influences the breakdown limit for field-effect control over micro- and nanofluidic systems. They measured the breakdown limit of silicon dioxide layers that was deposited with different techniques (Figure 2-4.b-c). The thermal oxide had the best result of about 0.6 *V/nm.* The result for ALD was one order of magnitude lower. Shin *et al.* (Shin *et al.*, 2012) claimed that their fabrication method was capable of fabricating large-scale nanofluidic FET that had a competitive gating effectiveness. In

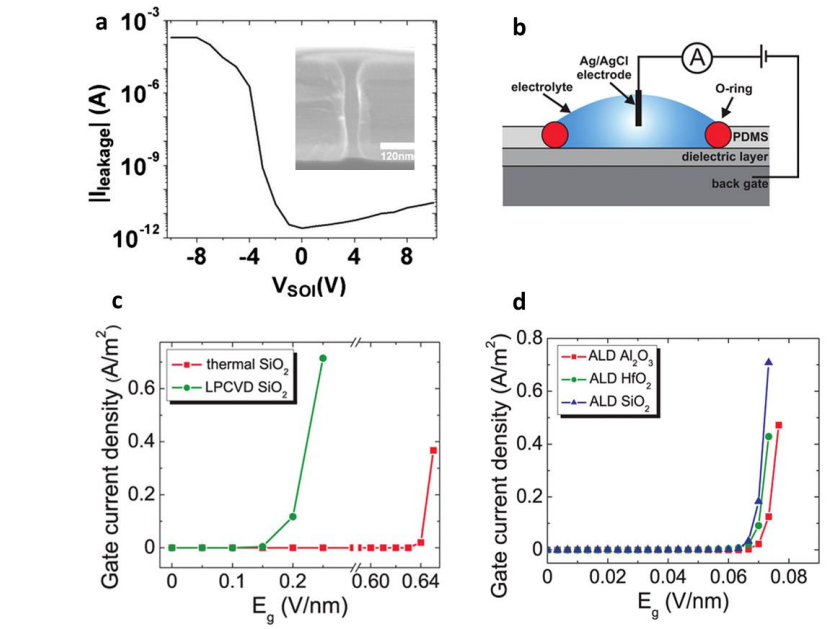

Figure 2-4. **a**) The current leakage from a 60 nm thermally grown silicon dioxide to the SOI substrate versus substrate bias at 10 μM hydrochloric acid. Adapted from (Joshi et al., 2010) with permission. **b**) Schematic of the current leakage measurement setup for different types of insulators. **c** and **d**)The results show that thermally grown silicon dioxide has the best resistance to current leakage while the breakdown limit for ALD layers is one order of magnitude lower. Adapted from (Jiang and Stein, 2010) with permission.

their work, they compared the current leakage from different types of dielectric layers in order to demonstrate the better quality of their anodized aluminum layer. The current leakage decreases the possible gating effectiveness by limiting the applied gate voltage.

2.4.4.2 Configuration limit

This limitation concerns only the nanofluidic FETs fabricated in nanochannel platform. The gated wall adjusts the wall electric potential only on one side while the charge of the other side, which is tens of nanometers away, cannot be modulated in the same way. Therefore, the gating will not be as effective as the gate-surrounded nanotubes (Figure 2-5). The reported gating effectiveness for the nanochannel configuration is lower than the one of the nanotubes (R. Karnik et al., 2005).

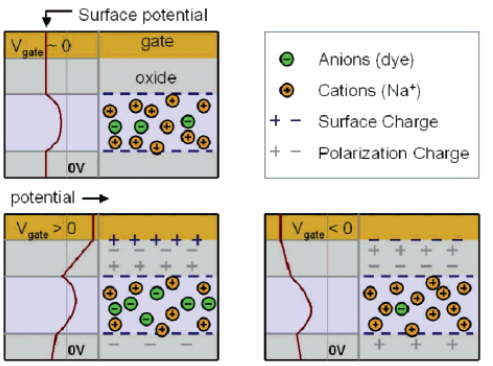

Figure 2-5. Schematic illustration of the charge and electric potential distribution inside a one-side-gated nanochannel. reprinted from (R. Karnik et al., 2005) with permission.

To overcome this limitation, one can design the nanofluidic FET with two gate electrodes on top and bottom of the channel, which adds some fabrication cost and time. Using the ‘‘etching and deposition’’ technique described in 1.3.2 suggests a better possibility of having gate electrodes around the channel. A similar approach was reported by Oh *et al.* (Oh et al., 2008).

2.5 Liquid reconfiguration

Utilizing wettability properties for gating purpose in nanochannels is one of the novel and interesting methods that has been presented recently. Applying a transmembrane voltage to silicon nitride nanopores was reported to gate the nanochannel via changing the wettability of the wall surface (Powell et al., 2011; Smirnov et al., 2011). According to the published results, the peculiar behavior of water in hydrophobic nanopores can lead to a gating system for aqueous solutions.

The idea of using liquid to reconfigure the pore has also been employed recently for gating the multiphase fluidic transport in micropores (Hou et al., 2015). The pore is firstly filled with a strongly wetting liquid. Then, based on the fact that an immiscible fluid requires a certain level of pressure to deform the interface, the pore will allow or prevent the fluid to pass through. This pressure threshold is dif-

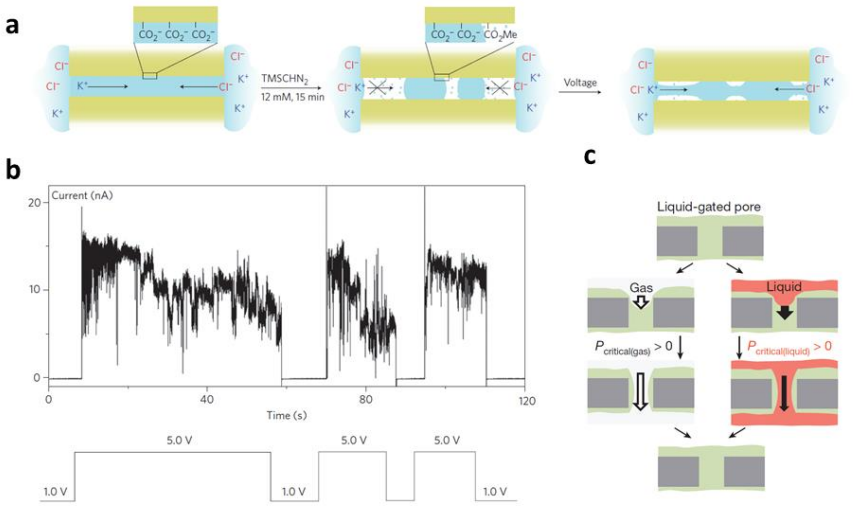

Figure 2-6. **a**) Modification of the surface leads to have hydrophobic clusters. Applying an electric field across the membrane results in an open-state for fluidic transport. **b**) The electric current shows the open state when 5 V are applied across the membrane. Reprinted from (Powell et al., 2011) with permission. **c**) Working principle of gating when the pore is filled with a strongly wetting liquid (green). Pressure induced deformation of the gating liquid surface allows both gases and liquids to flow through the pore. Reprinted from (Hou et al., 2015) with permission.

ferent for gas and liquid or even for two immiscible liquids. This method is capable of gating the fluidic transport in nanopores, too. The main difference is that smaller pores necessitate higher pressure for opening.

2.6 Compare and contrast

Hundreds of types of ion channels in cell membranes benefit from various physiochemical embedded architectures that enable gating. The biomimetic solid-state nano size conduits should be designed to offer similar properties. To date, some similar approaches have been taken in synthetic nanofluidic features as described in previous sections. However, gating the nanofluidic transport is not limited to these few methods. As discussed before, this field is now far from a well-developed situation since it is still close to the start point.

In order to better explain the current situation of nanofluidic gating, Table 2-1 demonstrates some information extracted from the published results in the subject of gating the nanofluidic transport.

Most of the works used the nanopore platform for gating purpose. The nanochannel and nanotube platforms were only used in the field effect gating. The size of the conduits varies from less than 10 nm up to 35 nm, which is much larger than the 2-3 nm size of ion channels. Although much larger channels experience transport regimes different from the ones in apertures of a few nanometers, their application can also be different. For example, instead of sub-nanometer size ions, they can be used for gating, sensing and manipulation of large molecules like DNA, *etc*.

One of the important but not always available information about the nanofluidic gating is the time response of the gate. At the nanoscale, the traveling time of the species goes down. Therefore, an efficient gate is necessary for performing the manipulating commands. Only a few authors studied the response time of the gates. The liquid reconfiguration method has shown a quick time response relative to other methods. For the field effect, only one work (Fan et al., 2005) has studied the transient time response and reported to be in order of hundreds of seconds. The response time is limited by the time needed for the ions to diffuse into the nanochannel. For the steric effect, the time response is dependent on the type of the smart polymer that is used for gating. Among the studied works, there is only one reported response time which is very long (Xia et al., 2008).

In terms of gating effectiveness, although the reported devices can modulate the ionic transport, the range of modulation is not broad enough to be able to open or close the channel completely. This level of sensitivity allows the nanofluidic device to be used for sensing applications. Nevertheless, comparing to the ion channel, that allows only a specific ion of interest to pass, the solid-state counterparts still need more enhancement. Apart from the liquid reconfiguration method, that physically closes the channel; the reported values for gating effectiveness are mostly less than one order of magnitude for the field effect and the steric effect. To enhance the gating resolution and performance, different gating methods should be combined. The advances in related technologies can lead to an increase in gating effectiveness.

Diversity of types of stimuli used in steric effect gating makes it the most versatile method used in both gating and sensing. Field effect, in spite of its ability to sieve the particles of similar charge, has been only used in general fundamental studies. Likewise, the few examples of using liquid reconfiguration have not had specific applications yet.

2.7 Perspective

The future gating mechanisms in nanofluidic transport are expected to make use of various gating methods in order to enhance the gating performance and selectivity in a similar way as in the biological counterparts.

New gating methods might also be introduced as far as the fluid transport at the nanoscale is better understood and the related technologies are developed.

Table 2-1. The results of gating for different published research

Article	Category	Pore size (nm) (best result)[2]	Platform	Gating stimulus	Time response (s)	Gate effectiveness[3] (maximum reported)
(Xia et al., 2008)	Steric	20	nanopore	pH	Long 36-60ks	10
(Hou et al., 2009)	Steric	18	nanopore	Potassium ion	-	1.3
(Yameen et al., 2009b)	Steric	tens of nm	nanopore	Temperature	-	3.4
(Yameen et al., 2009c)	Steric	15	Nanochannel membrane	pH	-	4
(Tian et al., 2010)	Steric	28	nanopore	Zinc ion	-	1.3
(Tian et al., 2013)	Steric	~30	nanopore	Mercury	-	3.2
(Liu et al., 2015)	Steric	21	Nanochannel membrane	pH and/or potassium ion	-	2.3
(Powell et al., 2011)	LR[4]	20	nanopore	Transmembrane voltage	Short <1s	Ideal gating
(Smirnov et al., 2011)	LR	120	nanopore	Transmembrane voltage	Short	Ideal gating 3 orders of magnitude
(Hou et al., 2015)	LR	200-20000	micropore	Pressure	short	Ideal
(Fan et al., 2005)	FE[5]	40-50	nanotube	Gate voltage	Not short 400 s	2.9
(R. Karnik et al., 2005)	FE	~35	Nanochannel nanotube	Gate voltage	-	1.3 2.9
(R. B. Schoch and Renaud, 2005)	FE	50 nm	nanochannel	Gate voltage	-	1.6
(Nam et al., 2009)	FE	<10	nanopore	Gate voltage	-	9
(Joshi et al., 2010)	FE	34	nanopore	Gate voltage	-	2.6
(Jiang and Stein, 2010)	FE	~20	nanopore	Gate voltage	-	1.2

[2] The size of nanoconduits that has the best result is reported here. for the case of conical nanopores, the tip size is reported.
[3] Gate effectiveness is defined as the ratio of on- to off-state conductance. For the case of field effect, the maximum and minimum achieved conductance is considered as open- and close-state, respectively.
[4] Liquid reconfiguration
[5] Field effect

Chapter 3
Methods and Materials

Studying the fluidic transport at the nanoscale necessitates to access or build nanoscale features. The features not only should allow the fluid to flow at the nanoscale, but they should provide the possibility of conducting small-scale investigations such as optical observation, electrical characterization, etc. In this chapter, the fabrication process of a versatile nanofluidic device is explained. Moreover, the procedure applied for measuring the electric conductance of the nanochannels is discussed.

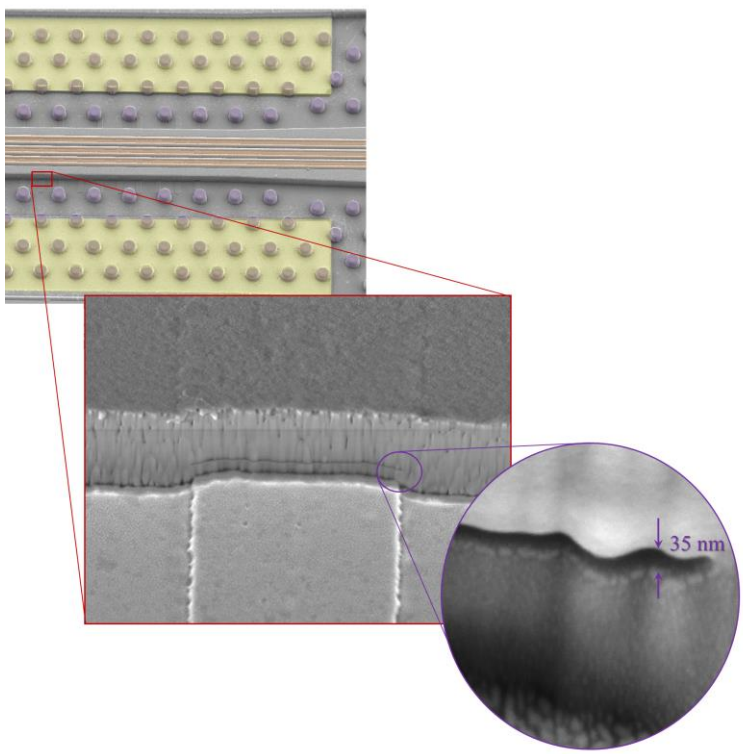

3.1 Microfabrication process

3.1.1.1 Platform

As discussed in 1.3.5, the nanofluidic platform should be selected based on the working objectives of the nanofluidic device. The nanochannel platform was selected in this thesis since the aim was to study fundamental aspects of the nanofluidic transport. The possibility of optical observation and the simpler integration of sensors and electrodes are the main advantages of using the nanochannel platform.

3.1.2 Fabrication method

The method ‘‘etching and bonding’’ had been used for the fabrication of one- and two-dimensional nanochannels and nanoslits at the microsystem laboratory (LMIS4) for about a decade. Based on this experience and according to the need for integration of electrodes close to the nanochannel, the ‘‘sacrificial layer’’ method was selected. This method has been widely used in the fabrication of both one- and two-dimensional nanochannels since the nanofluidic studies begun. In this method, a sacrificial layer is patterned to form the planar shape of the nanochannel using standard photolithography techniques. Then, the patterned layer is covered by a capping layer usually a transparent oxide. The capping layer is then etched to provide access to the sacrificial layer and finally, the sacrificial layer is removed and the nanochannel opens. The manufacturing process will be explained in detail in 3.1.6.

The accuracy of this method relies on the selectivity of the final etching step between the sacrificial layer and the capping layer. In other words, the process for releasing the sacrificial layer should not etch the capping layer since the thickness of the sacrificial layer determines the height of the nanochannel.

Different materials have been used as a sacrificial layer. The amorphous- or polysilicon is a common sacrificial layer that is widely used in the fabrication of microelectromechanical systems (MEMS). It can be released by xenon difluoride (XeF_2) gas etching when the capping layer is selected to be silicon dioxide or silicon nitride. A very high selectivity to the mentioned oxide layers has been reported. Apart from silicon, various types of materials and releasing process have been used in the fabrication of nanochannels. The combination of silicon dioxide and polymers was also utilized in the fabrication of nanochannels. Testing different types of metals such as aluminum, chromium, platinum, etc. in the fabrication of nanochannels has also been reported (Duan et al., 2012). Duan *et al.* reviewed in detail the different materials reported as sacrificial layer for the fabrication of nanochannels.

3.1.3 Sacrificial layer

Two materials were evaluated for their use as a sacrificial layer in this thesis; amorphous silicon (a-Si) and chromium. Similar patterns of 40 nm in thickness of both materials were created on a float glass substrate and covered with a sputtered silicon dioxide layer. After accessing to both sacrificial layer sides, they were re-

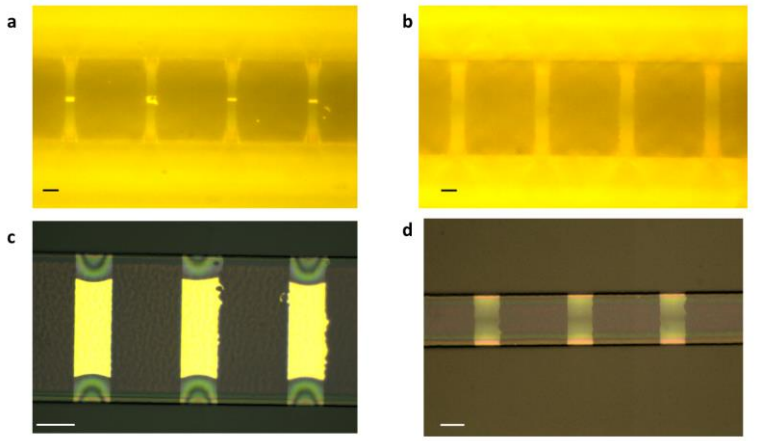

Figure 3-1. Optical microscope images of the nanochannel during the fabrication process. a) Chromium etching of a 25µm long nanochannel for 14 hours. A few micrometers of chromium are still present inside the nanochannels. b) The chromium was released completely leaving the wafer in the etchant for a longer time. c) After 10 minutes of DRIE, a-Si still is present in a 50µm long, while it is completely released (d) in a 15 µm long nanochannels. The scale bars in all figures indicate 5µm.

leased using specific etching recipes. The chromium was etched using a solution ($(NH_4)_2Ce(NO_3)_6 + HClO_4$). The etch rate of chromium in small openings of nanochannels was slow. After 14 hours in the etchant, the chromium layer was released in the nanochannels of 15 µm in length but not in longer channels. For example, 25 µm nanochannels needed more etching time as shown in Figure 3-1-a and b.

For the case of the a-Si layer, it was released using a dry fluorine-based (SF_6) chemistry. The mentioned recipe was reported to have fast etch rate and high selectivity to silicon dioxide sacrificial layer. Only ten minute of etching is enough to release the a-Si in a nanochannel of 15 µm in length. Figure 3-1-c and d show the optical microscope photographs of the nanochannels of different length after 10 minutes of etching. Later, the etching process for a-Si release was changed to XeF_2 chemistry, which was reported to have better selectivity to the oxide layer.

Finally, the a-Si was selected because:

- The etch rate is higher relative to the chromium.
- The selectivity to the oxide layer is higher, specially for the case of XeF_2 *etching.*
- The problems caused by wet etching, like the channel collapse due to the final drying or channel clogging because of contaminated etchant, are not present in the mentioned methods for a-Si release.
- The Si-release is widely used in different MEMS fabrication.

3.1.4 Insulating layer

In this thesis, the integrated electrodes are used for both sensing and gating purposes. It means that both circuits for nanofluidics and the integrated electrodes should be isolated so that the potential difference between the gate and the ionic

solution does not make a considerable electric current in the insulating layer. For example, as discussed in 2.4.4.1, the insulating layer in nanofluidic FETs should be resistive enough to prevent the current leakage from the gate. . The thinner the insulator, the lower the potential difference it can withstand. On the other hand, a thicker insulator is less effective in terms of sensing and fluidic transport stimulation. Consequently, the minimum possible thickness of insulator should be selected. Previous works have used dielectric thicknesses from tens of nanometers in nanopores to hundreds of nanometers in nanochannel platforms. The quality of the insulating layer is dependent on its thickness.

In this work, the quality of different thicknesses of sputtered and chemical vapor deposited layers of silicon dioxide were examined. Finally, a 500 nm oxide layer deposited using low temperature chemical vapor deposition (LPCVD) was considered as insulating layer. The LPCVD deposition was followed by an annealing step to improve the quality of the layer. The results prove that there is no considerable current leakage in our application.

3.1.5 Integration to microscale

Needless to say that the nanochannel should be integrated with the large-scale so that it can be filled with the solutions. Two microscale channels were integrated so that they can deliver the solution from large reservoirs to the entrance of the nanochannel. The mechanism of nanoscale to macroscale integration is explained in 3.2. In this section, the subject is the fabrication procedure that was carried out for the fabrication of microchannel part.

Other reported works fabricated the microchannel on an additional substrate and then bonded it to the nanochannel device (R. Karnik et al., 2005). This approach prolongs the fabrication process and adds some uncertainties due to the often limited bonding quality. The bonding should prevent any nanoscale opening that has similar effect as the nanochannels. Moreover, irreversible bonding is less convenient since it makes the rinsing of the microchannel more complicated, when it is necessary.

In this project, the goal was to fabricate both micro- and nanochannels on the same wafer in order to avoid the mentioned challenges of the previous methods. An epoxy based negative photoresist known as SU8 was utilized in order to fabricate the microchannels in the same device as the ones that contain nanochannel. This method did not work because of the difficulties in setting the exposure dose. The design included reflective metal parts in the critical area of the patterns where the largest aspect ratio of the SU8 structure should have been achieved. Furthermore, the auto-fluorescent properties of SU8 resulted in limitations in optical observations inside the nanochannel. The solution was to use a thin shadow layer between the SU8 and the nanochannel, which was not considered since it increased the fabrication time and cost relative to the conventional methods.

A simpler and cost effective method was finally chosen. Getting access to the openings of the nanochannels necessitated etching the oxide layer. In this case, the microchannels were etched in the 7 μm thick oxide layer deposited in the previous steps (Figure 3-2.c and d). Capping the etched layer with a polydime-

thylsiloxane (PDMS) rubber closed the microchannels. The PDMS part was not irreversibly bonded to the device. It only stuck to the device by a pressure applied from the screws in the mounting part (further explanation in 3.2.). The PDMS part could also be patterned in the same way as the microchannels so that larger microchannels were created and the filling and rinsing process became easier (Figure 3-2.f).

3.1.6 Process flow

Based on the key points mentioned in previous subsections, the fabrication process was designed.
Fused silica wafer (thickness 525±25, Ø 100±0.5 mm) was the only possible option due the desired objectives and design restrictions:

- The substrate should be transparent to provide the possibility of optical observation.
- The substrate should not be conductive to allow the high resistance electrical measurements.
- The wafer should withstand high temperature. It is a requirement for deposition of high quality insulating layers.

The fabrication steps are as follows:
The wafer was rinsed in a 10:1 mixture of sulfuric acid (H_2SO_4) and hydrogen peroxide (H_2O_2) known as Piranha solution to clean the residues.
Then, a thin layer of a-Si was sputtered on the substrate. The thickness of this layer defined the height of the nanochannels. The thickness was selected between 30-45 nm in different fabrication rounds and designs. This layer was patterned using normal photolithography techniques followed by a deep reactive ion etching (DRIE) step (Figure 3-2.a). The reasons supporting the choice of a-Si as for sacrificial layer were described in 3.1.3. in brief:

- It can withstand high temperature.
- There is a well-known procedure for releasing a-Si layer with a perfect selectivity to silicon dioxide.
- Its releasing rate is acceptable.

Another Piranha rinsing was performed to remove any organic residues on the wafer. A 500 nm low temperature dioxide (LTO) layer was deposited using LPCVD as for the insulating layer (Figure 3-2.b). This was followed by an annealing step to improve the insulating property of the layer. Further details were discussed in 3.1.4. In brief:

- The deposited layer by LPCVD has a better quality relative to other deposition methods.
- Its breakdown limit increases by annealing at high temperature.

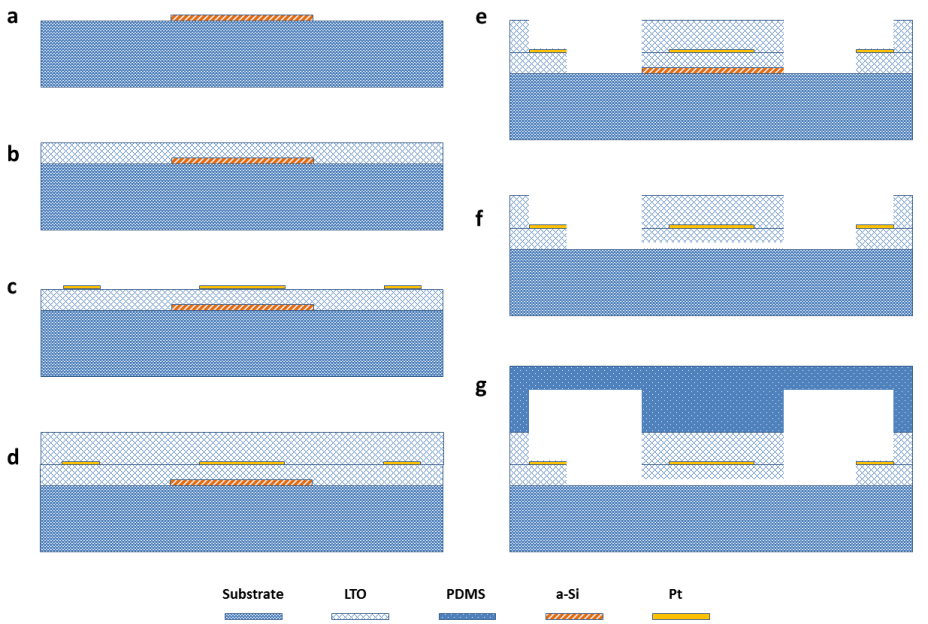

Figure 3-2. Process Steps to fabricate the nanochannels. a) A thin a-Si layer is deposited on the fused silica substrate. b) The layer is covered by an LTO layer followed by c) patterning electrodes. d) The electrodes are insulated by another LTO layer. e) The LTO layers are etched and the entrance of the nanochannels are accessible. f) The a-Si layer is released and the nanochannel is opened. g) A patterned PDMS part caps the microchannels.

- It is transparent.

Lift off technique was utilized to pattern a 20/200 nm titanium/platinum layer on the LTO (Figure 3-2.c). This layer is used as the measurement and gate electrodes. This material was selected because:

- Titanium works as an adhesion layer between platinum and silicon dioxide.
- Platinum is inert and is less likely to react relative to other metals.
- It has an acceptable selectivity in the following etching steps so that the layer can survive while etching both silicon dioxide and sacrificial silicon.

The layer was then covered by a 6 μm LTO layer (Figure 3-2.d). The thickness of this layer defines the height of the microchannel. For the case of patterned PDMS the height of this layer can be lower.

DRIE of LTO layers was then carried out in order to access the a-Si layer at the bottom (Figure 3-2.e). The right recipe should be selected at this step in order to provide an appropriate selectivity to platinum. A wrong recipe will lead to etching of the metal parts. In order to have the best result, the presence of oxygen and hydrogen should be avoided. At this condition, there is no need to use a hard mask for etching.

At this step, the opening of the nanochannel is available and the sacrificial layer can be released (Figure 3-2.f). High selectivity of XeF_2 etching to silicon dioxide makes it an appropriate option for releasing a-Si. The etch rate is strongly dependent on the chamber pressure, the pulse time and the exposed area. In our case, the net etching time for 110 μm in length and 40 nm in height nanochannels for a full wafer was about 30 minutes while the etching pressure was set to 500 Pa. It is worth noting that a short isotropic DRIE of SF_6 chemistry at the beginning can help to have a uniform opening of the nanochannel and uniform etching in all regions of the wafer.

Finally, the microchannels were capped by a patterned (or non-patterned) PDMS part. The PDMS part can whether be bonded to the device or just seal it by applying pressure. The fabrication process was performed at the Center of MicroNano Technology (CMI, EPFL).

Figure 3-3 shows SEM images of a fabricated device. The round pillars in the mi-

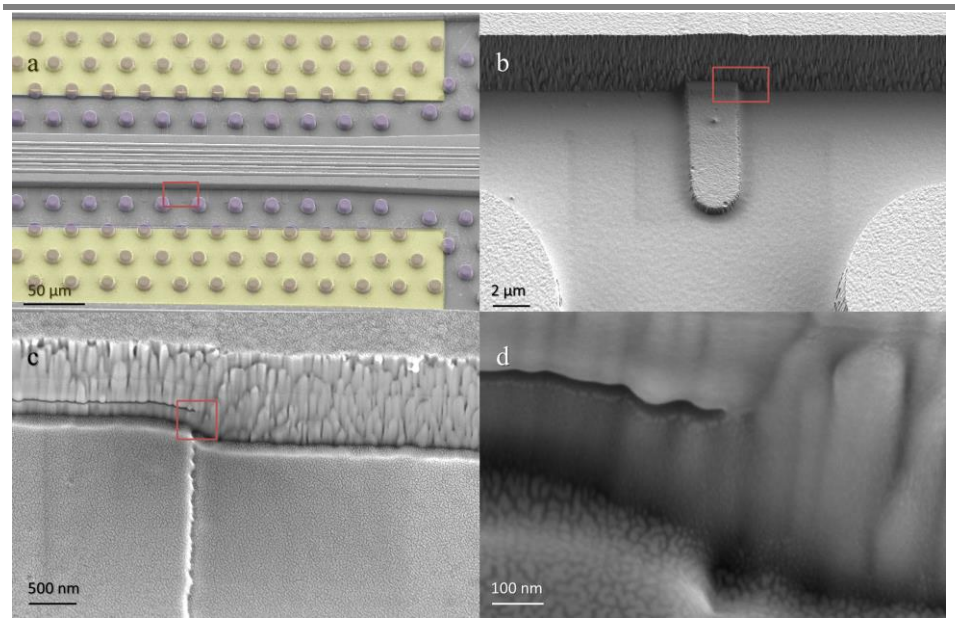

Figure 3-3. SEM image of a fabricated device. a) Two microchannels including round pillars (purple) and platinum electrodes (yellow). The entrance of a single nanochannel is marked by a red rectangle. b) Zoomed in to the marked area in (a) that shows the entrance of a single nanochannel . c) 23 kX magnification of the entrance of the nanochannel. The tilt angle is 30 degrees. d) The marked area of (c) . 124 kX magnification of the entrance of the nanochannel.

crochannels (colored in orange in Figure 3-3.a) were designed to avoid the upper PDMS collapse into the microchannel. As mentioned before, it is possible to use a non-patterned PDMS only for closing the microchannels and as an intermediate tool for large-scale integration. The platinum electrodes (colored in yellow) were embedded close to the entrance of the nanochannels in order to discard the additional effects of microchannels in the measurements. The entrance of a single nanochannel is marked with a red rectangle and its zoomed views are shown in Figure 3-3.b-d. The entrance of a 35 nm in height channel is shown in Figure 3-3.d.

3.1.7 Design of the device

Figure 3-4 demonstrates a schematic of the fabricated device. A set of forty nanochannels is present at the center of a 15 mm in 20 mm chip. The geometry of nanochannel varies from chip to chip for different designs. The height of the nanochannel, which is defined by the thickness of the sacrificial layer, from 30 to 45 nm for different fabrications. The width of the nanochannels varies between 2 to 5 μm. The nanochannel lengths are in the range of 20 to 110 μm.

Two microchannels bring the solution to the entrance of the nanochannels. The width of the microchannels is 110 μm. Theirs height varies from 7 to 120 μm according to the thickness of the second LTO layer (process flow, Figure 3-2.e) and the size of the additional channel in PDMS (process flow, Figure 3-2.g).

Close to the nanochannel entrances, two platinum electrodes are embedded in the microchannels. These electrodes, indicated by a symbol Ω in the Figure 3-4.a, are utilized for the electrical measurements of the ionic transport through the nanochannels.

Some other electrodes are present in the microchannel. They are used for different purposes such as sensing the ionic strength of the solution in every microchannel or checking the discontinuities due to bubbles presence. These electrodes are marked by symbol *I*.

There is another electrode integrated over the nanochannel with the purpose of sensing or gating (Figure 3-4.c). This platinum electrode is placed 500 nm above the nanochannel and insulated by the LTO layer as described in Process . The number of gate electrodes varies from 1 to 5 while their widths are in the range of 5 to 72 μm. These electrodes are used in the experimental studies of the effect of temperature on the nanofluidic transport that will be discussed in Chapter 5 and Chapter 6.

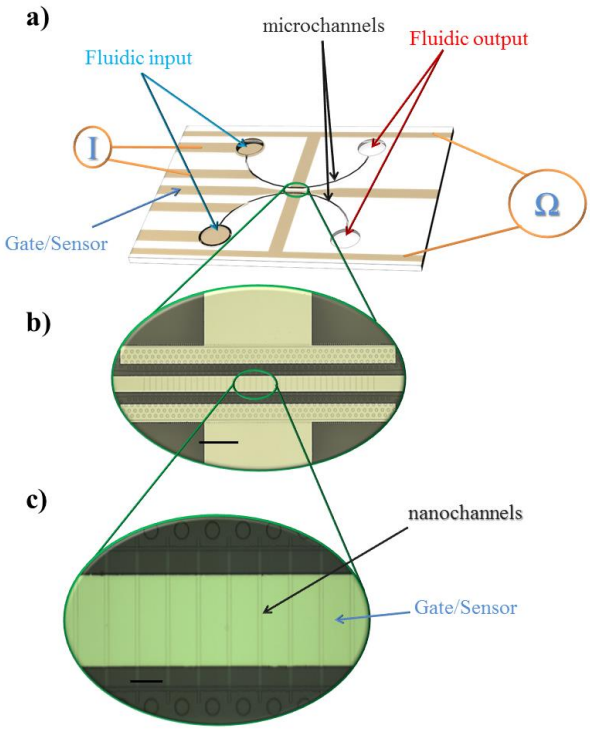

Figure 3-4. a) Schematic of a fabricated device. The two microchannels bring the solution to the entrances of the nanochannels. The electrodes indicated by Ω are designed to measure the impedance of the nanochannel. The ones with the symbol *I* can measure the ionic strength of the solution by relating it to the conductivity. One or more electrodes are embedded over the nanochannel with the purpose of sensing or/and gating. b) Microscope view of a fabricated device showing both the measuring electrode and the gate/sensor one over the nanochannels. The scale bar indicates 200μm. c) Optical microscope view of a horizontal electrode over the vertical set of nanochannels. The scale bar represents 25 μm.

3.2 Integration to macroscale

3.2.1 Fluidics

Figure 3-5 displays the setup that was used to provide a fast and easy connection, manipulation and investigation of the fluid flow toward and within the device. Liquid delivery to the entrance of the nanochannel is carried out by integrating micro- and mini-channels in a soft PDMS part and a polymethylmethacrylate (PMMA) adaptor. The PDMS part plays the role of sealing and interconnecting the microchannel to the outside mini-channels. The soft PDMS prevents the liquid leakage while it is under pressure of the mounting screws. The PMMA adaptor allows the liquid to pass through external tubes toward the reservoirs in the PDMS part. The external tubes are in Polytetrafluoroethylene (PTFE) with the outer diameter of 1.07 mm and inner diameter of 0.56 mm (Fisher Scienntifitc, W39241), which are connected to syringes that contain the solutions. The liquid is pushed to the device using a syringe pump (Harvard apparatus, PHD 2000).

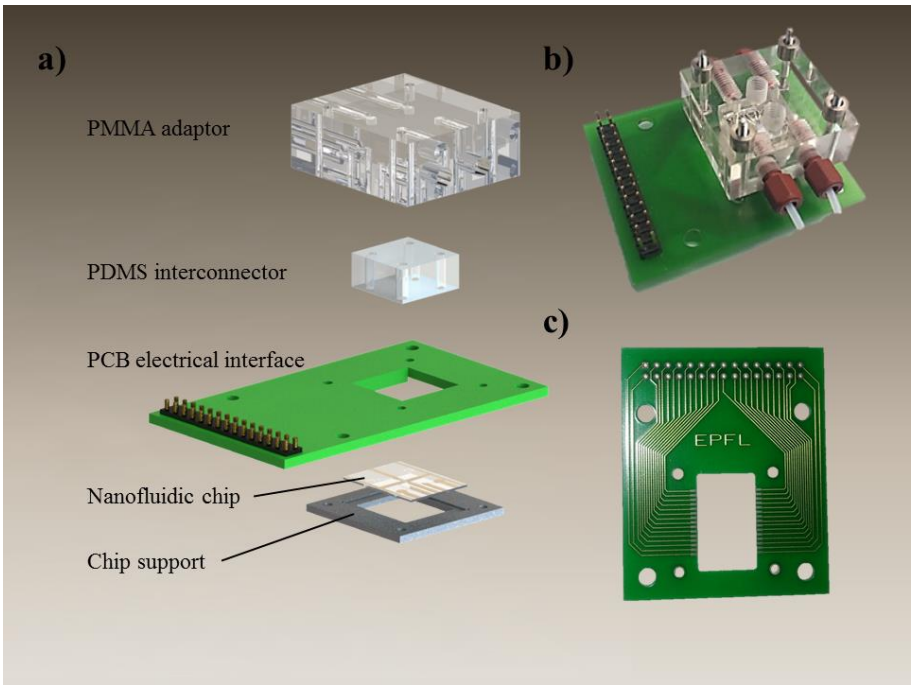

Figure 3-5. a) Exploded view of the mounting parts of the setup. The device is put on an aluminum support and is fastened to the PCB interface using screws. A PDMS interconnecting block stays between the device and the PMMA adaptor that prevents liquid leakage while it is kept under pressure. b) A photograph of a mounted setup. c) Simple design of the PCB.

3.2.2 Electric

The integrated electrodes are connected to the outside large-scale instrument by means of a printed circuit board (PCB) interface. The small spring connectors on the PCB interface provide good contacts with the electrodes while being kept under pressure.

3.3 Solutions

In most of nanofluidic studies, potassium chloride (KCl) solutions in water have been used as the main fluid in the system. The potassium chloride is highly solvable in water and KCl solutions are widely used water-based solutions in different fields of research. It is very stable which allows reproducible measurements. It is used as the calibration solution for conductivity meters or as electrolyte filling solution for silver/silver chloride reference electrodes. The presence of the potassium ion in physiological medium is vital and many biological solutions contain this ion. The potassium chloride solution is a symmetric electrolyte with monovalent ions, which implies that simpler analytical model can be used. Moreover, both potassium and chloride ions have a similar ionic radius. The similarity of their ionic radius leads to similar migration properties like the ionic mobility and diffusion constant, which facilitates the analysis of experimental results.
Depending on the desired concentration, different amounts of potassium chloride salt (Sigma, P9541) were solved in certain volumes (normally 100 mL) of deion-

ized water (DI water 18 MΩ.cm, supplied by the center of micro-nanotechnology CMI, EPFL). The conductivity and pH value of the solution was measured (METTLER TOLEDO, China) and recorded.
The solutions at acidic pH values were prepared by adding hydrochloric acid to the solution. For preparing basic pH solutions, potassium hydroxide was added to the solution. A high concentration potassium hydroxide solution was prepared following the same method as for the potassium chloride solution.

3.4 AC impedance measurements

The impedance spectroscopy has been widely used in different fields of study for many years. The electrochemical impedance spectroscopy and the use of impedance spectroscopy in the studies of biological cells and tissue are some of the applications. Particularly, the application of impedance spectroscopy in screening the ion channel activities in the cell membrane illustrates how powerful this method can be.
In nanofluidics, most of the reported measurements were performed using large electrodes that applied direct current (DC). However, the AC electrical measurement of nanochannel was done at LMIS4 since the nanofluidic studies begun. Schoch (Schoch, 2006) reported the use of impedance spectroscopy in his thesis. Wu *et al.* (Wu et al., 2015) used impedance spectroscopy to sense the immobilization of single- and double-strand DNA molecules in alumina nanopores.
In the present study, the integrated microelectrodes at the entrance of nanochannels were used for electrical measurements of the nanochannel. This way the measurement benefits from the electrodes being placed very close to the nanochannel. Difficulties in integration of a reference electrodes close to the channel entrance and the electric potential limitations, in addition to overpotential of non-reference electrodes (Girault, 2004) and their diffusion limited DC current causes the AC measurements to be more beneficial for monitoring the electric conductance of nanochannels. Moreover, the AC measurement of nanochannel conductance does not suffer from the side effects of DC measurement such as the transient effects (Fan et al., 2005; Schoch, 2006), time-dependent preconcentration of ions at the entrance of nanochannel (Schoch et al., 2006) and non-preventable resistance of the microchannels, etc.

3.4.1 The resistor capacitor model for nanochannel

As an equivalent electric circuit, the nanochannel is modeled as a resistor. The electrochemical properties of an electrode causes an EDL to be produced on the polarizable electrodes, which leads to an equivalent capacitor in the circuit (Girault, 2004). Moreover, a small capacitance effect created by the device and the experimental setup, exists in the circuit. It is called parasitic or stray capacitance (Schoch, 2006). Figure 3-6.a shows the equivalent electric circuit of the nanochannel suggested by Schoch. Another equivalent circuit was also suggested by Wu *et al.* for an alumina nanoporous membrane in order to enhance the precision of modeling (Wu et al., 2015), which is depicted in Figure 3-6.b.

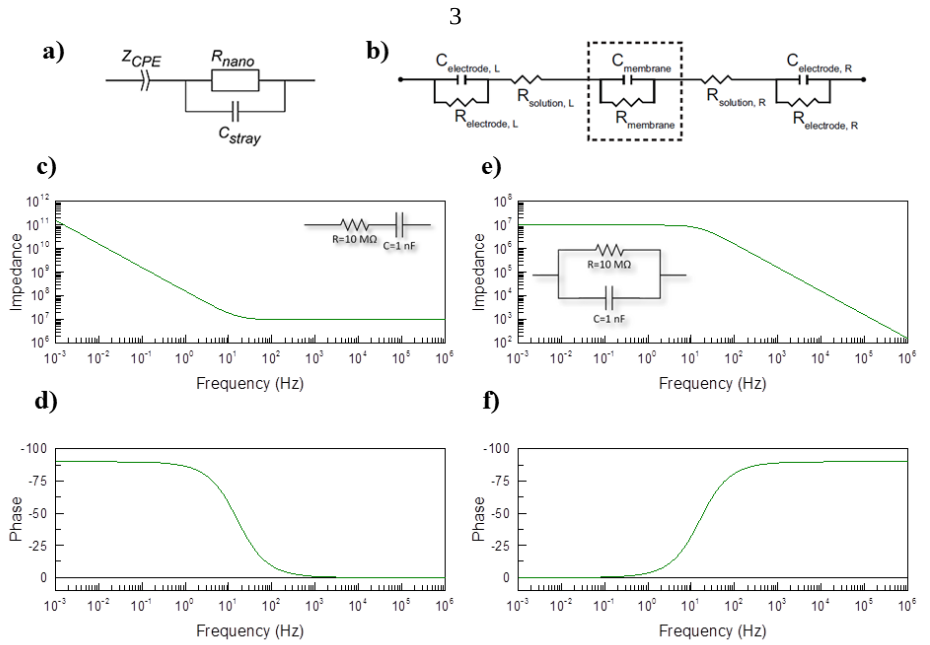

Figure 3-6. **a**) The equivalent RC circuit suggested by Schoch (Schoch, 2006). Z_{CPE} the impedance of the constant phase element modeling the EDL on the platinum electrodes **b**) The equivalent RC circuit for a nanoporous membrane suggested by Wu *et al.* (Wu et al., 2015). **c** and **d**) Bode diagram and phase angle variation for the impedance of a resistor and a capacitor in series. **e** and **f**) Bode diagram and phase angle variation for the impedance of a resistor and a capacitor in parallel.

Having an equivalent resistor-capacitor (RC) circuit implies that only at specific frequency range, the measured impedance corresponds to the DC resistance of the channel. Figure 3-6.c-f show the Bode diagrams and phase angle variations of two resistors and capacitors in series and parallel. The impedance of the circuit does not emphasize the value of the resistance in a large frequency range. This implies that the AC measurement should be performed in a specific frequency range so that it can be related to the resistance of the resistor in the circuit.

Therefore, the AC measurement of nanochannel should be performed in the right frequency that corresponds to the resistance of nanochannel. To this aim, an impedance spectroscopy for a wide range of frequencies should be conducted.

3.4.2 Experimental procedure

3.4.2.1 Impedance spectroscopy

The impedance of the nanochannel was measured at a frequency range of 40 Hz to 4 MHz using an impedance analyzer (Hewlett Packard Agilent 4294A precision impedance analyzer). The impedance spectrum was then analyzed to find the right frequency where the impedance corresponds to the nanochannel resistance. The nanochannel resistance corresponds to the impedance where the phase is closest to zero, according to the equivalent electric circuit of the nanochannel discussed in the previous section.

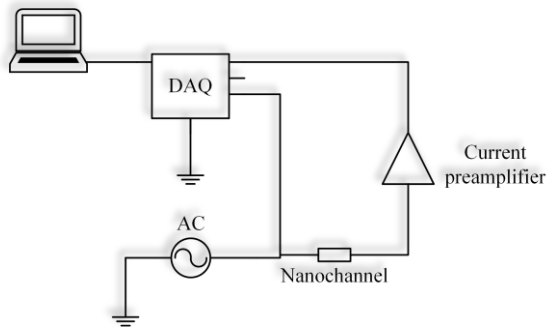

Figure 3-7. Schematic of the low frequency impedance measurement setup. A signal from function generator enters the nanochannel, then a low noise current preamplifier reads , amplifies and converts it to a voltage to be read by DAQ.

3.4.2.2 AC electrical conductance measurement at fixed frequency

While the frequency of measurement was defined according to the results of impedance spectroscopy, the measurements can be done at a fixed frequency. To this aim, a simple measurement setup was designed and used.

A 50 mV sinusoidal signal was applied using a function generator (Agilent 33220A, Malaysia). A low noise current preamplifier (Stanford Research System SR750, USA) was used to read the current, filter the noise and convert the current to a voltage signal. The signal was then read by a data acquisition card (DAQ) (National Instrument PCI-6251, USA).

This circuit was used not only for measuring the resistance of the nanochannels, but for the microchannels as will be described in 4.7.2 and the integrated platinum electrodes (temperature sensors) as will be described in 5.3.1.2. Figure 3-7 shows the schematic of the measurement setup. A computer interface (LabVIEW, 2013) was used to acquire and analyze the data and produce a control command for the setup.

3.4.3 Low frequency impedance spectroscopy

In order to validate the suggested models for the fabricated nanochannels, the impedance measurement was performed in a wide range of frequencies at different ionic concentrations. For the frequencies below 100 Hz the setup presented in 3.4.2.2 was utilized while for higher frequencies, the normal impedance analyzer mentioned in 3.4.2.1 was used. Figure 3-8 shows the Bode diagram and phase angle variations for the impedance of a nanochannel set in a frequency range of 50 mHz to 400 kHz. The measurements from the impedance analyzer are not sufficient to validate the RC models for the nanochannel. Particularly, at low ionic concentrations, the results from the impedance analyzer only indicate a parallel set of resistor and capacitor since it shows a behavior like the one shown in Figure 3-6.e. The information about the electrochemical capacitance of the electrode can only be observed if low frequency measurements are performed.

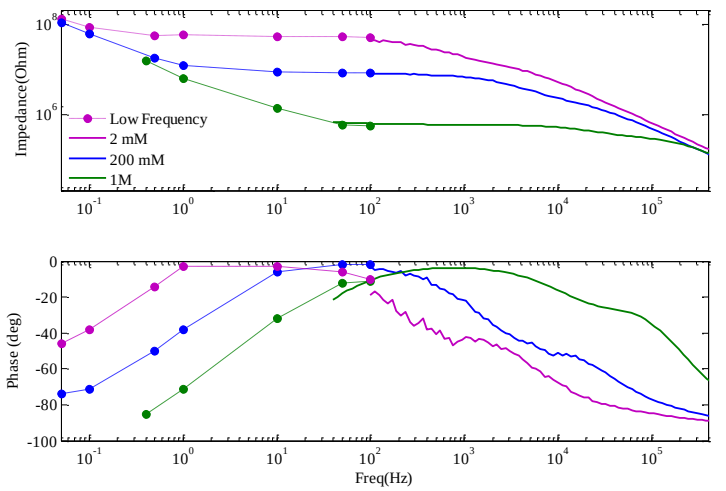

Figure 3-8. Bode diagram and phase angle variation for the impedance of a set of nanochannels (40× 35 nm in height 49 μm in length and 5 μm in width channels). The solid lines depict the impedance analyzer data while the circles correspond to the low frequency measurement setup. The dashed lines are only drawn to illustrate the trend. Without considering the results from low frequency measurements, it is impossible to find the equivalent RC circuit.

3.5 Highlights

The microfabrication process was explained in detail:

- The method used is more cost- and time-effective relative to other reported fabrication methods since it integrates the microchannels in the same wafer as the nanochannel's.
- a-Si was used as sacrificial layer since it can be released easily with a very good selectivity to the insulating oxide layer.
- The best deposition method for the insulating layer is the one that offers higher resistance to current leakage.
- AC impedance measurement was performed to characterize the nanochannel:
- The right frequency that corresponds to the resistance of nanochannel should be selected in AC measurements.

Chapter 4

Electric Conductance of Nanochannel

Scaling down the fluidic channels to nanometer regimes creates different conditions for the fluidic transport. The theoretical analysis and experimental investigations imply that the nanochannel conductance does not follow the macro-scale models. It is generally accepted that the electric conductance of nanochannels deviates from the bulk and tends to a constant value at low ionic concentrations. In this chapter[6], the analytical modeling of the nanochannel conductance is discussed; a new analytical modeling approach is introduced and finally, the model predictions are compared with the experimental measurements.

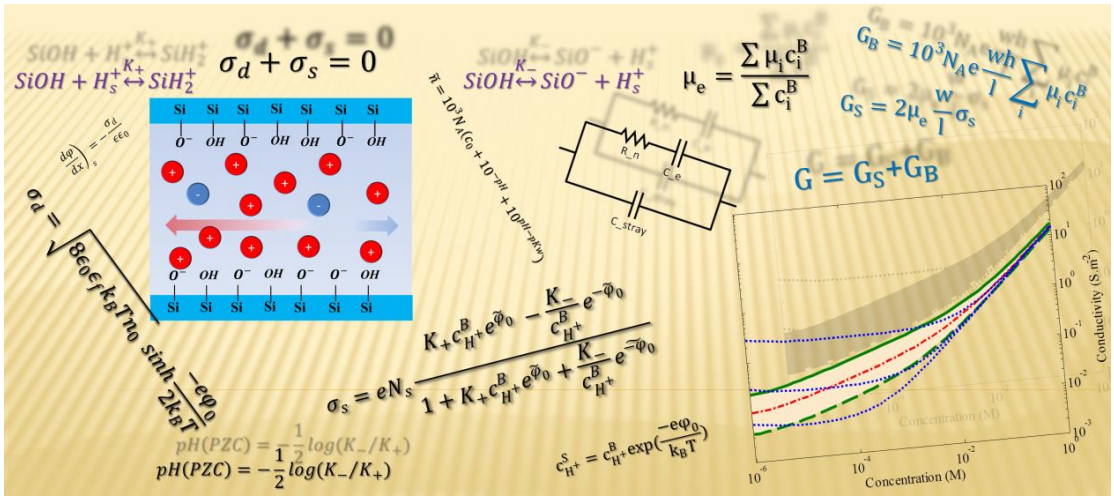

[6] Based on : Taghipoor, M., Bertsch, A., Renaud, P., 2015. An improved model for predicting electrical conductance in nanochannels. Phys. Chem. Chem. Phys. 17, 4160–4167. doi:10.1039/C4CP05338A

4.1 Electrical measurements in nanofluidics

Optical observation of molecular transport, using fluorescent dye molecules, is often used in nanofluidic studies. However, the electrical characterization of nanofluidic channels is indeed a very complementary method, which also offers the possibility to perform label free measurements on such systems. Using the electrical measurements in nanofluidic studies is so common that almost all the experimental works benefit from it. Characterization of nanofluidic channels (R. B. Schoch and Renaud, 2005; Stein et al., 2004; Taghipoor et al., 2015), single molecule translocation (Lorenz J. Steinbock et al., 2013) and detection (Raillon *et al*., 2012), characterization of nanofluidic field effect transistors (R. Karnik *et al*., 2005; Wu *et al*., 2013) and diodes (Karnik *et al*., 2007; Wu *et al*., 2013) and estimation of fluid temperature by electrical conductance measurement (Jonsson and Dekker, 2013) are some of the reported works that used the electrical measurements in nanofluidic studies.

Most of the research groups measured the electrical resistance of nanochannels. Both AC and DC measurements were reported. The resistance of nanochannels depends on the electric current carriers *ie:* ions, whose concentration is influenced by the nanochannel wall. In the following sections, this phenomenon will be discussed.

4.2 Electrical conductivity of aqueous solutions

In electrolytes, the electric current is carried by charged species (ions) traveling in response to a bias electric potential. The response of ions to a unique electric potential is different since their radii and charges are different. For example, the H^+ ion has been reported to have the highest response to electric field due to its very small ionic radius, while larger ions like Na^+ migrate about 7 times slower.(Barry and Lynch, 1991) The electric migration of ions in an electrolyte depends also on the viscosity of the electrolyte, since friction is the only dominant resistive force against the ionic migration, especially at low ionic concentrations. At high ionic concentrations, ion-ion interactions take part and should be considered as a resistive force. Furthermore, the degree of ionic dissociation also influences the total resistivity of the solution. Lower dissociation constants result in a lower number of ions and less electric conductivity.

In order to quantify the electric migration of different ions in electrolytes, the ionic mobility μ_i ($m^2V^{-1}s^{-1}$) of an ion is defined as its traveling velocity in response to a unit electric potential, which is expressed as

$$\mu_i = \frac{|z_i|e}{6\pi r_i \eta} \tag{4-1}$$

where z_i , e, r_i *and* η are the charge number of ith ion, the electron charge, the ionic radius (including water mantle) of ith ion, and the dynamic viscosity of the electrolyte, respectively. The electrical conductivity of a solution can then be related to the mobility of the solvated ions.

Moreover, a higher number of ions results in a higher number of current carriers and consequently a higher electric conductivity. Therefore, the electrical conductivity is dependent on the concentration of ionic species c_i $(\mathrm{mol.\,L^{-1}})$, too. The electrical conductivity or specific conductance γ $(\mathrm{S.\,m^{-1}})$ of an electrolyte containing different ions depends on the concentration of ionic species and their ionic mobility via

$$\gamma = 10^3 N_A e \sum_i \mu_i c_i \tag{4-2}$$

where N_A (mol^{-1}) is the Avogadro constant, and e (C) is the electron charge.

4.2.1 Kohlrausch's Law

Since the conductivity of an electrolyte depends on its ionic concentration, the term molar conductivity Λ_m $(\mathrm{S.\,M^{-1}m^{-1}})$ is defined as the electrical conductivity of the electrolyte divided by its ionic concentration.

$$\Lambda_m = \frac{\gamma}{c} \tag{4-3}$$

As mentioned before, although the conductivity of an electrolyte increases by increasing the number of charge carriers, the increased electrostatic interactions among the charged species causes a slight decrease in the net mobility of ions. Kohlrausch's Law models this decrease for a strong electrolyte, which is dissociated completely in the solution.

$$\Lambda_m = \Lambda_m^\infty - K\sqrt{c} \tag{4-4}$$

where Λ_m^∞ is the limiting molar conductivity of the solution *i.e.* the limit of the infinite dilution and K is an empirical constant. Λ_m^∞ is the summation of molar conductivities of different ions inside the solution.

$$\Lambda_m^\infty = \sum |z_i| \Lambda_{m,i}^\infty \tag{4-5}$$

$\Lambda_{m,i}^\infty$ is the limiting molar conductivity of an ion *i* that is related to its mobility *via*

$$\Lambda_{m,i}^\infty = N_A e \mu_i \tag{4-6}$$

4.3 What makes the nanochannel different?

At the nanometer scale, the fluidic transport behavior changes, mostly due to the surface effects, which cannot be neglected anymore. Particularly, the electrostatic charge of the nanochannel walls has a significant impact on the molecular transport in nanometer size apertures. The charged walls attract counter-ions and repel co-ions. This causes a charged layer to appear close to the charged wall. The

layer is known as the electric double layer (EDL) as has been studied in colloid and surface chemistry since decades (Helmholtz, 1853). At low ionic concentrations, the thickness of the electrical double layer can be of the same order as the nanochannel height or even more. Consequently, not only the concentration of ions inside the nanochannel can be higher than the bulk, but also as it is sketched in Figure 4-1, the selectivity of the nanochannel to certain types of ions makes the condition completely different from bulk. Therefore, the conductivity of the solution inside the nanochannel does not follow the bulk one as the ionic concentration decreases. Many experimental investigations have confirmed a deviation from bulk conductance for the case of nanometer size confinements.(R. B. Schoch and Renaud, 2005; R. Karnik et al., 2005; Rohit Karnik et al., 2005; Wu et al., 2012; Stein et al., 2004; Smeets et al., 2006; Siria et al., 2013; Nam et al., 2009)
In addition to the salt ions, there will always be a certain level of dissociated water molecules inside the solution, which cannot be neglected since they take part in electric current through the nanochannel. Specially, when their concentration is of the same order as the salt ions one, they make the solution composition inside the nanochannel different from one of the neutral bulk.
Moreover, the nanochannel surface charge is defined by the reactions occurring at the surface, which are dependent on the concentration of ions inside the nanochannel. Particularly, the concentration of H^+ ion inside the nanochannel has a significant influence on the nanochannel wall surface that influences the ionic transport through the nanochannel.
Overall, considering the solution inside the nanochannel similar to the bulk is a wrong assumption since the composition and concentration of ions inside the nanochannel is different.
In the following sections, we study the wall-ion interactions inside a nanofluidic channel.

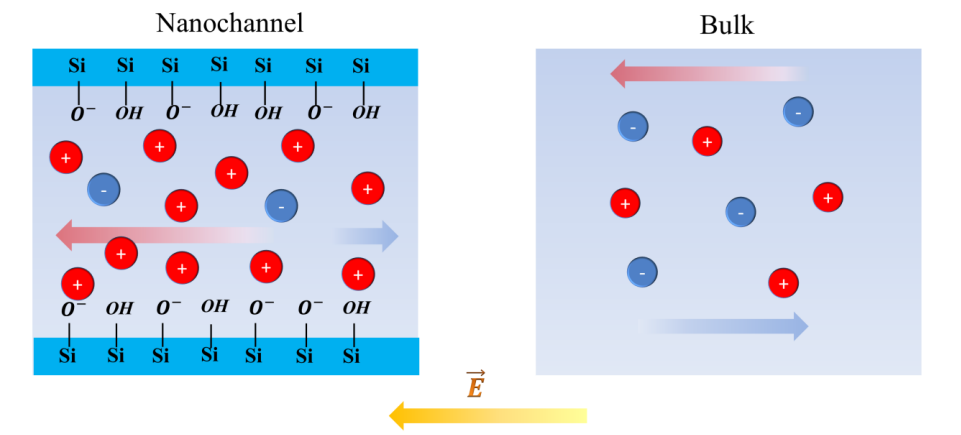

Figure 4-1. Comparison of the transport in the bulk and the nanochannel. The left drawing shows the selectivity of nanochannel to counter-ions as well as their enrichment. There is a net electroosmotic flow inside the nanochannel that pushes the small amount of co-ions present inside the channel along the electric field. The red arrows show the migration direction of positive ions while the blue arrows correspond to the negative ions.

4.4 Wall-electrolyte interface

Theoretical modeling of the surface charge density of different kinds of metal oxides has attracted attention in the field of colloid chemistry (Iler, 1979; Yates *et al*., 1974), geophysicist (Reppert and Morgan, 2003a; Scales et al., 1992) and different chemical sensor studies (van Hal et al., 1996). Yate *et al*. (Yates *et al*., 1974) developed a site-dissociation model describing the surface charge density at the oxide-electrolyte interface (equation (4-17)) that has been used in different fields of study. This model was utilized beside Grahame's model (Grahame, 1947, section4.4.4.1) to estimate the surface charge density and Stern layer potential in a silicon dioxide porous media (Revil and Glover, 1997). The surface charge density decreases while lowering the concentration (Davis *et al*., 1978; Revil and Glover, 1997) which implies that the nanochannel conductance models that assume the surface charge constant, need to be revised. Here, I present the the modeling details for a silicon dioxide surface. However, the model is applicable for all kinds of oxide surfaces.

4.4.1 Surface reactions at oxide-electrolyte interface

For a silicon dioxide surface, considering the surface of the wall covered by SiOH groups, H^+ and OH^- ions can be adsorbed to the surface by protonation and deprotonation of surface silanol groups,

$$SiOH \overset{K_-}{\leftrightarrow} SiO^- + H_s^+ \tag{4-7}$$

$$SiOH + H_s^+ \overset{K_+}{\leftrightarrow} SiOH_2^+ \tag{4-8}$$

Where K_- and K_+ are the equilibrium constants for these amphoteric reactions. The first reaction tends to charge the oxide surface negatively, while the second reaction charges the surface positively. Salt ions can also bind to the surface (Stumm, 1987),

$$SiOH + K^+ \overset{K_K}{\leftrightarrow} SiOK + H_s^+ \tag{4-9}$$

$$SiOH + Cl^- \overset{K_{Cl}}{\leftrightarrow} SiCl + OH^- \tag{4-10}$$

Where K_K *and* K_{Cl} *are the intrinsic equilibrium constants of the adsorbtion reactions* (4-9) *and* (4-10). The salt adsorption reactions imply that the adsorption of K^+ occurs mainly at high pH values while Cl^- ions are adsorbed more likely in acidic conditions *i.e.* low pH values.

4.4.2 Wall surface charge

According to the mentioned chemical reactions, there will be five different groups on the surface, SiOH, SiO^-, SiH_2^+, SiOK and SiCl. The total surface site density N_s $(\text{site}.\,\text{nm}^{-2})$ can be defined as the summation of site densities of every single group,

$$N_s = N_{SiOH} + N_{SiO^-} + N_{SiH_2^+} + N_{SiOK} + N_{SiCl} \tag{4-11}$$

In our study, we do not consider the adsorption of potassium and chloride ions as in other similar works in this field (Glover et al., 1994; Pardon and van der Wijngaart, 2013; Reppert and Morgan, 2003a; Revil and Glover, 1997; Wildhaber, 2014; Windbacher, 2010; Yates et al., 1974). The salt ions in aqueous solution are shielded by water molecules and can not be close enough to the surface and be adsorbed (Windbacher, 2010). Therefore, the binding site density of the surface can be expressed as

$$N_s = N_{SiOH} + N_{SiO^-} + N_{SiH_2^+} \tag{4-12}$$

Moreover, using the same approach as the site binding model (Yates *et al*., 1974) and writing the equilibrium conditions in terms of the equality of electrochemical potentials for the mentioned reactions, the equilibrium constants of the reactions can be written as

$$K_- = \frac{C_{H_s^+} N_{SiO^-}}{N_{SiOH}} \tag{4-13}$$

$$K_+ = \frac{N_{SiH_2^+}}{C_{H_s^+} N_{SiOH}} \tag{4-14}$$

Where $C_{H_s^+}$ expresses the concentration of H^+ right at the surface. Using the equations (4-12) to (4-14) the total binding site density is given as,

$$N_s = N_{SiOH}\left(1 + \frac{K_-}{C_{H_s^+}} + K_+ C_{H_s^+}\right) \tag{4-15}$$

The net charge on the surface can be calculated by subtracting the number of positive and negative sites. Therefore, the surface charge density can be written as,

$$\sigma_s = e(N_{SiH_2^+} - N_{SiO^-}) \tag{4-16}$$

Using all the equations (4-12) to (4-16) leads to the site binding equation for the charge density of the wall surface,

$$\sigma_s = eN_s \frac{K_+ c_{H^+}^S - \frac{K_-}{c_{H^+}^S}}{1 + K_+ c_{H^+}^S + \frac{K_-}{c_{H^+}^S}} \tag{4-17}$$

4.4.3 Ionic activity

The activity of any species in a solution is defined since the concentration of a reactant might differ in one area of the solution due to different factors. For our subject of study, the only dominant factor is the electrostatic charge of the wall surface. The electrostatic potential of the wall due to its surface chage leads to a different concentration of the H^+ ion close to the wall where the chemical reactions

occur. At this condition, it would be incorrect to use the bulk concentration of H^+ ion in calculations. Instead, the definition of the activity of the H^+ ion is used to explain the distribution of H^+ ion concentration in a solution by relating its concentration at the wall surface $c_{H^+}^S$ and in the bulk $c_{H^+}^B$. Assuming isothermal, isobaric, ideal and reversible system in equilibrium, the wall surface charge concentration of H^+ ions can be expressed as:

$$c_{H^+}^S = c_{H^+}^B exp(\frac{-e\varphi_0}{k_B T}) \tag{4-18}$$

where k_B, T and φ_0 are the Boltzmann constant, absolute temperature and electric potential of the Stern layer, respectively.

4.4.4 Wall electric potential

The surface charge density is obtained using equations (4-17) and (4-18).

$$\sigma_s = eN_s \frac{K_+ c_{H^+}^B e^{\tilde{\varphi}_0} - \frac{K_-}{c_{H^+}^B} e^{-\tilde{\varphi}_0}}{1 + K_+ c_{H^+}^B e^{\tilde{\varphi}_0} + \frac{K_-}{c_{H^+}^B} e^{-\tilde{\varphi}_0}} \tag{4-19}$$

With $\tilde{\varphi}_0 = -e\varphi_0/k_B T$, describes a dimensionless electric potential of the Stern layer. The wall surface charge influences the ionic distribution and the electric potential in the EDL. Conversely, the wall surface charge depends on the H^+ concentration distribution, which is a function of the electric potential according to equation (4-18). This implies that more information is needed to calculate the electric potential.

4.4.4.1 Grahame's model

Grahame (Grahame, 1947) solved the Poisson-Boltzmann equation for a symmetric electrolyte to estimate the charge density inside the diffuse layer. To this aim, he assumed a constant permittivity of the electrolyte and applied the Gauss law to the EDL. This model was used later by Yate *et al.* (Yates *et al*., 1974) in their site binding model. Many other works in different fields also used Grahame's model in their analytical modelings (Reppert and Morgan, 2003a; Revil and Glover, 1997).

The Poisson-Boltzmann equation for a symmetric electrolyte is given as,

$$\frac{d^2\varphi}{dx^2} = \frac{2ec_0}{\epsilon\epsilon_0} sinh(\frac{e\varphi}{k_B T}) \tag{4-20}$$

Where ϵ_0, ϵ_f, c_0 (M) and φ are the dielectric constant of vacuum, the relative dielectric constant of the fluid, the concentration of salt ions in the bulk and the electric potential, respectively. Grahame could integrate equation (4-20) by introducing the identity (4-21),

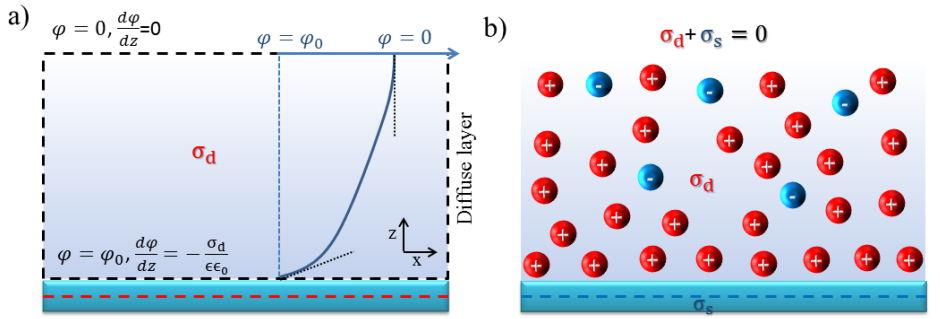

Figure 4-2. a) The boundary conditions used in Grahame's model. b) Schematic of the overall electroneutrality requirement.

$$\frac{d^2\varphi}{dx^2} = \frac{1}{2}\frac{d}{d\varphi}\left(\frac{d\varphi}{dx}\right)^2 \tag{4-21}$$

Which after substituting into equation (4-20) and integration gives:

$$\left(\frac{d\varphi}{dx}\right)^2 = \frac{4c_0 k_B T}{\epsilon\epsilon_0}\left(cosh\left(\frac{e\varphi}{k_B T}\right) - 1\right) \tag{4-22}$$

The electric potential has been assumed zero in the bulk *i.e.* $\varphi = 0$ and $d\varphi/dx = 0$ Figure 4-2.a describes the boundary condition used for the integration of the Poisson-Boltzmann equation.

Now, according to Gauss' law, the slope of change of the electric potential at the surface is proportional to the charge density in the diffuse layer σ_d,

$$\left.\frac{d\varphi}{dx}\right)_s = -\frac{\sigma_d}{\epsilon\epsilon_0} \tag{4-23}$$

The charge density σ_d was described by Grahame as ''*The total charge in a column of liquid of unit cross section extending from the plane in question (the one to which* $d\varphi/dx$ *refers) on into the body of the solution where* $\varphi = 0$.''(Grahame, 1947)

Combining equations (4-22) and (4-23) leads to a relation that is known as Grahame's model.

$$\sigma_d = \sqrt{8\epsilon_0\epsilon_f k_B T n_0}\ sinh\frac{-e\varphi_0}{2k_B T} \tag{4-24}$$

Here, we replaced the term concentration c_0 with the number density n_0 $(m^{-3})$of every ion in order have the equation in a more compact form.

4.4.4.2 Modification for pH

Taking into account the electroneutrality requirement of free electrolyte ($c^B_{K^+} + c^B_{H^+} = c^B_{Cl^-} + c^B_{OH^-}$) and using the definition of the Debye length, Revil and Glover (Revil and Glover, 1997) improved equation (4-24) to be applicable in all pH

values. Having a similar approach, the term n_0 in equation (4-24) was replaced with the term $\tilde{n}$, which is described as

$$\tilde{n} = 10^3 N_A (c_0 + 10^{-pH} + 10^{pH-pKw}) \tag{4-25}$$

Where pKw represent the dissociation constant of water and pH corresponds to the pH value of the bulk.

4.4.5 Conservation of charge

Assuming that the surface charge of the wall should be neutralized by the oppositely charged ions, the summation of equations (4-19) and (4-24) should be zero (Figure 4-2.b).

$$\sigma_d + \sigma_s = 0 \tag{4-26}$$

Altogether, the Stern layer electric potential φ_0 can be calculated by solving the system of equations (4-19), (4-24), (4-25) and (4-26).

4.5 The surface charge of a nanochannel wall

As discussed in section 4.4, the surface charge of different oxides was the subject of several studies in different fields. Some analytical methods were utilized for estimating the surface charge of the oxide surfaces. Similar methods were later employed in some nanofluidic transport model (Baldessari and Santiago, 2009; Jensen *et al*., 2011; Smeets *et al*., 2006; Yeh *et al*., 2012). They considered the surface chemistry of the nanochannel wall and modeled the nanochannel conductance based on a non-constant wall surface charge. However, they used a variety of models for the description of the surface charge and the wall electric potential.
The model discussed in the previous section was developed for a flat plat in contact with a symmetric electrolyte. For the case of the nanochannel walls, the validity of the model needs to be examined. For the case of Grahame's model (equation (4-24)), although the governing equations are similar, the boundary conditions should be revised. For the case of site binding model, the only change is due to the activity of the H^+ ion that can be different depending on the transport regime.

4.5.1.1 Different nanofluidic transport regimes

Based on the number of unbalanced charges inside the enriched nanochannel at different ionic concentrations two transport regimes are defined in nanofluidic studies. At high ionic concentrations where the EDL thickness is very small (Figure 4-3. a), the main part of the channel does not screen the electrostatic effects from the suface. Therefore, a neutral electro osmotic flow (EOF) will occur in the main region of the nanochannel. The conductivity of the solution inside the channel can be considered as the bulk's since the EDL is very small. Decreasing the ionic concentration will lead to thickening the EDL. As long as there is no EDL overlap, the ions contained in the EDL screen the wall surface charge while

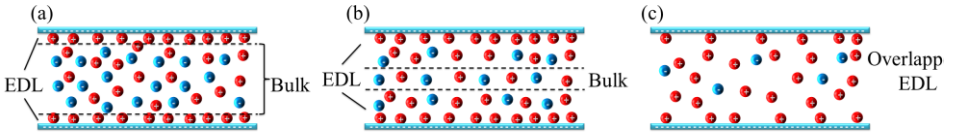

Figure 4-3. Schematic view of the EDL in a nanochannel. (a) At high concentration, the EDL thickness is very small and the conductance is mainly the bulk conductance. (b)When the EDL thickness gets larger, both bulk and surface-effect conductance are important. (c) At low concentrations, the EDL of walls overlap and the nanochannel conductance is only influenced by the wall surface charge

a neutral solution is present at the center of the nanochannel (Figure 4-3. b). Decreasing further the ionic concentration results in overlapping EDL, where ions whose charge is opposite to that of the walls (counter-ions) will fill the channel (Figure 4-3. c). In this condition, the ionic and fluidic transport regime is completely different. The nanochannel is more conductive than the bulk in normal nanofluidic devices where the wall electric potential is high enough to attract ions.

4.5.1.2 Wall surface charge of nanochannel at different transport regimes

Thin EDL guarantees the validity of the flat plate models since the nanochannel walls do not have any influence on each other. They can be considered as two isolated plates following the flat plate condition. Therefore, the developed model can be used in non-overlapping EDL conditions.

When the EDL overlap, the distributions of the ions inside the nanochannel as well as the boundary conditions are not similar to the case of flat plat. Analytical model of the ionic transport for the case of overlapping EDL resulted in complicated mathematical relationships. Levine *et al*. (S Levine et al., 1975b) solved the governing equations for a narrow parallel plate channel and suggested a relationship for the electric potential inside the channel. At that time, no one knew that these analytical studies might be much more impactful in the next few decades.

Recently, a full multi-ion model was reported that solved the equations with the boundary condition for the EDL overlapping regimes (Ma et al., 2015). They studied the effect of taking into account the EDL overlapping condition. Their result showed that using the similar model for both the overlapped and non-overlapped EDL could be acceptable. Specially, at neutral pH the results are very close. Therefore, in this thesis, the non-overlapping EDL relations are utilized for simplicity. However, some more modifications are applied that will be discussed later.

4.5.1.3 Dependency on the pH and ionic concentration

The system of equations[7] was solved for a potassium chloride solution in contact with the silicon dioxide wall. For the silicon dioxide nanochannel surface, the surface charge density increases with increasing concentrations whereas the magnitude of the electric potential of the Stern layer decreases (Figure 4-4). This de-

[7] Equations (4-19), (4-24), (4-25) and (4-26).

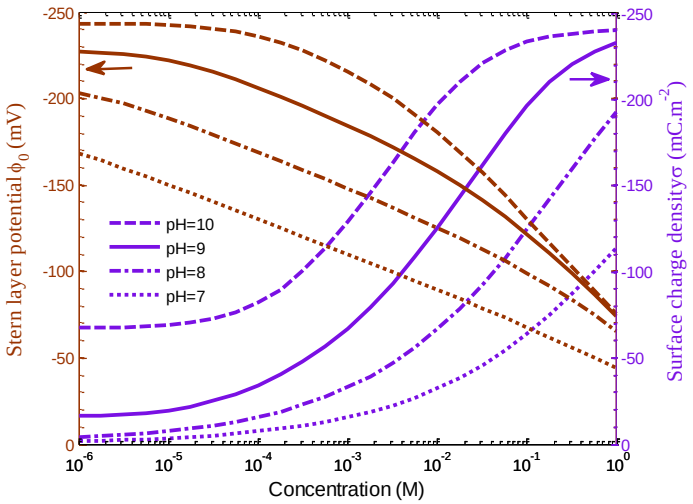

Figure 4-4. Surface charge density and Stern layer potential versus electrolyte concentration for different pH values for a silicon dioxide surface ($pK_- = -6.3, N_s = 1.5\ site.nm^{-2}$).The surface charge density increases with increasing salt concentrations whereas the magnitude of the electric potential of the Stern layer decreases.

crease of the magnitude of Stern layer potential is related to the fact that more ions are present beside the wall. In other words, the concentration of ions close to the wall increases and according to the Gauss law, the potential decreases. This also happens in the case of a constant surface charge simulation (Alishahi et al., 2015; Pardon and van der Wijngaart, 2013). The increase of magnitude of the zeta potential at low ionic concentrations for silicon dioxide surfaces has been validated experimentally by various research teams (Scales *et al.*, 1992; Siria *et al.*, 2013; Yates and Healy, 1975). The zeta potential is directly related to the stern layer potential and they have similar trends at different ionic concentrations. This implies that at lower ionic concentrations, silicon dioxide surfaces better attract counter-ions due to their larger potential. However, the diffusion of counter-ions due to the concentration gradient, limits the attraction toward the wall. Here, the results are obtained for a silicon dioxide surface, at room temperature, with a density of binding sites of $1.5\ sites.nm^{-2}$ and equilibrium constants $pK_+ = -0.3$ and $pK_- = -6.3$ (Revil and Glover, 1997).

Concerning the reason of the decrease in the surface charge by lowering the ionic concentration, the logarithm of the ratio between the Stern layer and bulk H^+ concentration is depicted in Figure 4-5. At low salt concentrations, the H^+ concentration in the nanochannel is about three orders of magnitude higher than the one in the bulk for pH=7, while at high salt concentrations, this difference is even less than one order of magnitude. It means that for a negatively charged surface, the increase of the H^+ concentration in the Stern layer is much higher at low ionic concentrations than at high concentrations and consequently, the wall tends to be less negatively charged according to equation (4-7). The more the wall attracts H^+ ions, the more the number of negative SiO^- groups decreases due to surface reactions and consequently the H^+ attraction becomes weaker. Finally, there is a bal-

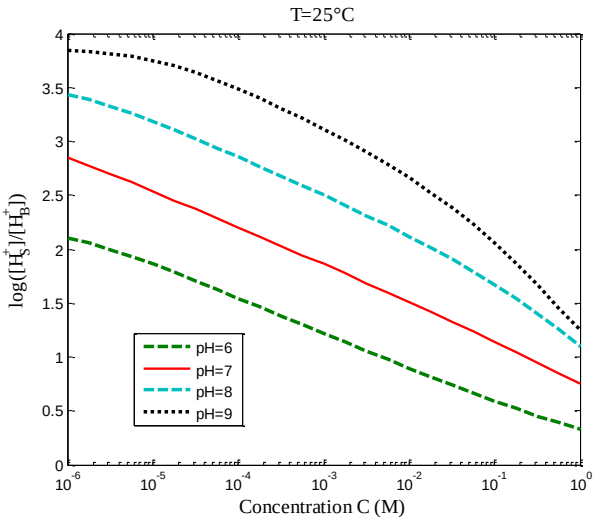

Figure 4-5. Evolution of the logarithm of the Stern layer to bulk H^+ concentration ratio with the ionic concentration and pH. It illustrates that for a negatively charged surface, the increase of the H^+ concentration in the Stern layer is much higher at low concentrations than at high concentrations

ance between H^+ ions attraction by the wall charge, and its surface charge density, which means that the wall surface charge is not constant for all ionic concentrations.

Figure 4-6 shows the evolution of the surface charge density with the pH for different values of the ionic concentration. The model predicts a maximum possible surface charge density when all the binding sites have a similar charge. Higher ionic concentrations move the maximum surface charge density to lower values of the pH. The point of zero charge (PZC) is defined as the pH where the surface charge density and subsequently the electric potential is zero. Given $\sigma_s = 0$ *and* $\tilde{\varphi}_0 = 0$ in (4-19), the pH at the PZC is calculated as

$$pH(PZC) = -\frac{1}{2} log(K_-/K_+) \tag{4-27}$$

For a silicon dioxide surface, the this value is estimated to be *pH(PZC)=3*, which is inline with the reported values in the literature (Pardon and van der Wijngaart, 2013).

The magnitude of the electric potential at the Stern layer $|\varphi_0|$ increases at higher pH values. As it is shown in Figure 4-7, lower ionic concentrations experience a higher increase in the magnitude of the Stern layer potential. The electric potential at the Stern layer does not increase after the maximum surface charge is achieved.

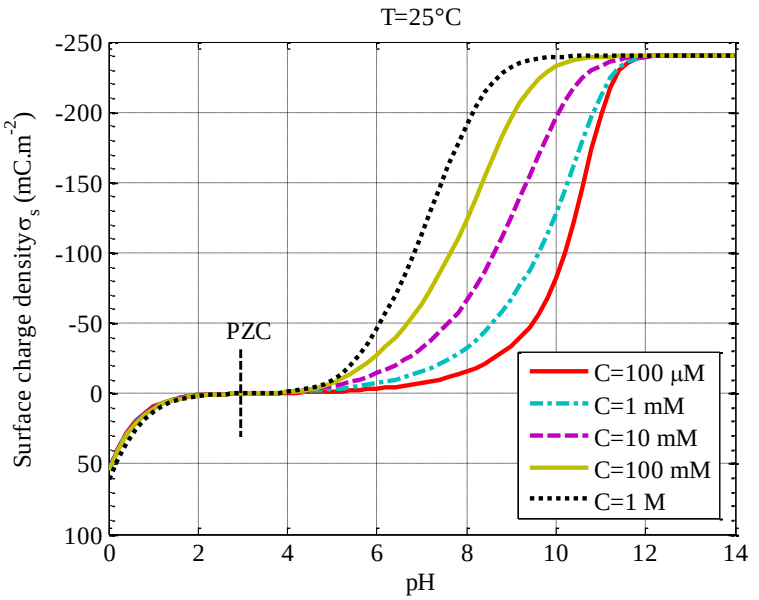

Figure 4-6. Evolution of the Surface charge density versus pH at different ionic concentrations for a silicon dioxide surface ($pK\_ = -6.3, N_s = 1.5\ site.nm^{-2}$). The point of zero charge is at pH=3 and the maximum possible charge density is -240 mC/m^2.

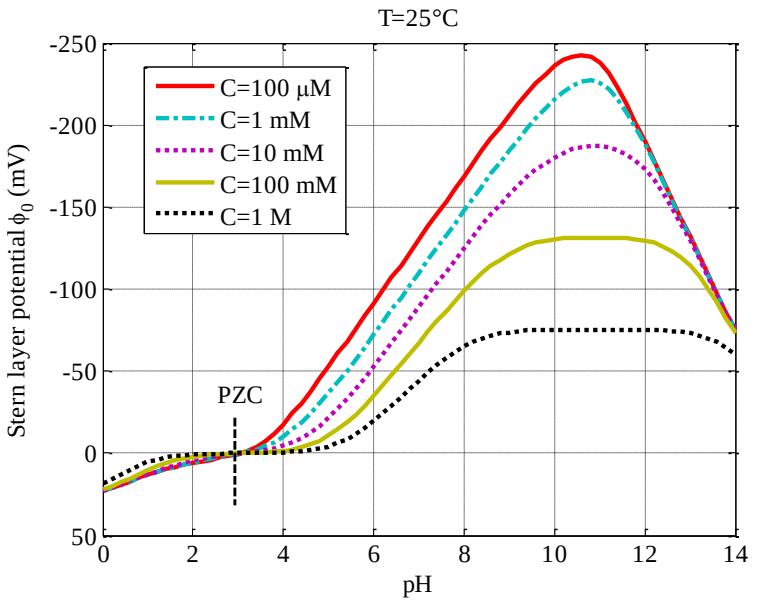

Figure 4-7. Evolution of the Stern layer potential φ_0 versus the *pH* at different ionic concentrations for a silicon dioxide surface ($pK\_ = -6.3, N_s = 1.5\ site.nm^{-2}$). The electric potential does not increase anymore after the maximum possible charge achieved.

4.6 Electrical conductance of nanochannel - Analytical modeling

A reliable model for the nanochannel conductance is needed for predicting the experimental results. It can also help to detect the probable defects in the fabricated nanochannels and experimental setup.
Since the beginning of nanofluidic studies, theoretical modeling of nanochannel conductance has been done. There have been two main approaches in nanochannel conductance calculations. The first approach uses the dependency of the electrolyte conductivity on the ionic concentration to calculate the nanochannel conductance (Rohit Karnik et al., 2005; Martins et al., 2013; R. B. Schoch and Renaud, 2005; Smeets et al., 2006). The second assumes a bias electric field and calculates the ionic current due to the ionic migrations inside the nanochannel (Baldessari and Santiago, 2009; R. Karnik *et al*., 2005; Stein *et al*., 2004). In most of the cases, the charge density inside the nanochannel was considered constant (R. Karnik et al., 2005; Rohit Karnik et al., 2005; R. B. Schoch and Renaud, 2005; Siria et al., 2013; Stein et al., 2004) whereas assuming a constant wall surface charge density at all ionic concentrations is a simplification that does not correspond to reality. Some studies in surface chemistry have shown that this assumption was not correct (Davis *et al*., 1978; Revil and Glover, 1997; Scales *et al*., 1992; Yates and Healy, 1975). Also, it leads to a constant nanochannel conductance at low ionic concentrations which is not consistent with the experimental results (Rohit Karnik *et al*., 2005; Smeets *et al*., 2006; Wu *et al*., 2012). Here, an improved model is introduced by considering the dependence of the wall surface charge on the ionic concentration based on the first approach.

4.6.1 Schoch and Renaud model

As mentioned before, the first approach in modeling the electric conductance of nanochannels is based on the dependency of conductivity of the solution on the concentration of ions *ie*: equation (4-2). Schoch and Renaud developed their model based on the fact that the variation of the EDL thickness with concentration results in different transport regimes (section4.5.1.1). For the bulk regime, the electric conductance can be estimated using equation (4-2) since the nanofluidic effects are negligible. For the EDL overlapping regime, they calculated the excess concentration of counter-ions inside the nanochannel and developed an analytical model for this regime.

4.6.1.1 The excess nanochannel charge

Assuming that the overall electroneutrality requirement is satisfied, Daiguji *et al*. (Daiguji *et al*., 2004) estimated the difference in ionic density as a function of wall surface charge. This estimation was later used by Schoch and Renaud to calculate the excess mobile ion concentration c_e inside the nanochannel. They assumed that the charge of the nanochannel is completely equilibrated by the counter-ions inside the nanochannel.

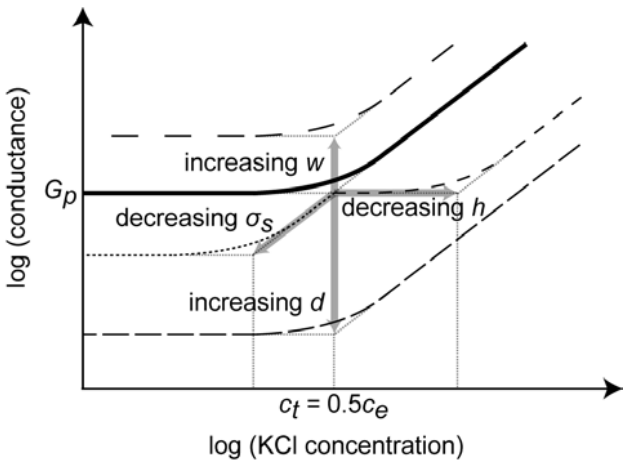

Figure 4-8. Schematic of a log-log diagram of the electric conductance of nanochannels versus the ionic concentration. The effect of the surface charge density σ_s, the width w, the length d, and the height h of the nanochannels on its electric conductance is shown. Reprinted from (Schoch, 2006). For detailed explanation, please see the reference.

$$c_e = \frac{2\sigma_s}{hN_a e} \tag{4-28}$$

Where h is the height of the nanochannel and N_a is the Avogadro number.

4.6.1.2 One relation for all regimes

Combining equations (4-2) and (4-26), they introduced two terms whose summation gives the nanochannel electric conductance. One term explained the bulk conductance and the other estimated the influence of the wall surface charge on the electric conductance. Their model of nanochannel conductance G for a KCl solution is given as

$$G = 10^3 N_A e(\mu_{K^+} + \mu_{Cl^-})c\frac{wh}{l} + 2\mu_{K^+}\sigma_s\frac{w}{l} \tag{4-29}$$

Where w, h and l (m) are the nanochannel width, height, length and the effective wall surface charge density. The model predicts a linear bulk conductance dependence to the concentration at high ionic concentrations while the conductance reaches an offset (a plateau in log-log scale) at low ionic concentrations (Figure 4-8). The figure shows the effect of different parameters on the electric conductance of the nanochannel (Schoch, 2006)

4.6.2 Modifications

4.6.2.1 Variation of wall surface charge

Although Schoch and Renaud's model has the advantage of simplicity, there is doubt as to the existence of a low concentration plateau, inspecting the experimental and numerical results reported by different research groups (R. B. Schoch and Renaud, 2005; R. Karnik et al., 2005; Rohit Karnik et al., 2005; Wu et al., 2012; Smeets et al., 2006; Baldessari and Santiago, 2009; Pardon and van der Wijngaart, 2013).

The assumption of a constant surface charge at all ionic concentrations results in a constant electric conductance in the EDL overlapping regime. Different research groups made similar assumptions in order to predict the electrical conductance of nanofluidic devices, which led to a saturated conductance at low ionic concentrations (Bocquet and Charlaix, 2010; R. Karnik *et al*., 2005; Siria *et al*., 2013; Stein *et al*., 2004; Wu *et al*., 2012). As discussed in sections 4.44.5, the wall surface charge depends on the ionic concentration and a pH of the solution, which should be taken into account.

4.6.2.2 Dissociated H^+ and OH^-

As it can be figured out from Figure 4-5, the concentration of H^+ ions in the EDL is different from the bulk. The considerable activity of the H^+ ion inside the nanochannel can affect the nanochannel conductance since its ionic mobility is higher than the mobility of other salt ions. Except in a few works that studied the problem for acidic conditions (Jensen *et al*., 2011; Martins *et al*., 2013), this effect was neglected in previous models that assumed an effect of the bulk pH only on the wall surface charge. Specially, when the salt concentration is of the same order as the ones of H^+ ions, the effect of H^+ ions is dominant. Similarly, the role of OH^- should be considered for a positively charged wall.

For the case of a monovalent salt solution, it is possible to define an effective ionic mobility as the concentration weighted average of participating ions' mobility values. Assuming a Boltzmann distribution of all ions, the proportion of each ion concentration in the diffuse layer and in the bulk is the same. The effective ionic mobility μ_i is then defined as:

$$\mu_e = \frac{\sum \mu_i c_i^B}{\sum c_i^B} \tag{4-30}$$

where μ_i and c_i^B are the ionic mobility and concentration of counter-ions in the bulk. For instance, for a negatively charged surface and a potassium chloride solution, the effective ionic mobility is

$$\mu_e = \frac{\mu_{K^+} c_{K^+}^B + \mu_{H^+} c_{H^+}^B}{c_{K^+}^B + c_{H^+}^B} \tag{4-31}$$

Where $c_{K^+}^B$ and $c_{H^+}^B$ are the bulk concentrations of K^+ and H^+ ions respectively.

4.6.3 The improved Model

Based on the dependency of the electric conductivity of the solution on the ionic mobility and concentration, and applying the mentioned modifications, the improved model is developed. It is composed of two terms. The bulk term that is defined as:

$$G_B = 10^3 N_A e \frac{wh}{l} \sum_i \mu_i c_i^B \tag{4-32}$$

And the surface term which is defined as:

$$G_S = 2\mu_e \frac{w}{l} \sigma_s \tag{4-33}$$

The total conductance is the summation of both G_B and G_S.

$$G = G_S + G_B \tag{4-34}$$

At high ionic concentrations, the surface term has a small influence on the total conductance, the conductance is governed by channel geometry and a linear dependency of conductance to the ionic concentration is observed. At low ionic concentrations, on the other hand, the bulk term is negligible relative to the surface term and the total conductance is mainly the surface term. In fact, when decreasing the ionic concentration, the nanochannel conductance does not follow the bulk conductance nor does it reach a plateau of constant value, even if the latest case may happen in some conditions. Figure 4-9 shows the calculated evolution of the conductivity for different values of the pH as a function of ionic concentration. The term ‘‘conductivity ρ ’’ is defined here as the average conductivity of the solution inside the nanochannel using the relation,

$$\rho = G \frac{l}{wh} \tag{4-35}$$

Using the average conductivity allows to discuss about the nanochannel conductance without being concerned about the geometry. When the H^+ or OH^- concentrations are higher than the electrolyte concentration, the ionic strength does not change by diluting the solution any more. In this situation, the nanochannel conductance remains constant and is not influenced by dilution. The conductance may even increase in the case of lower pH, when H^+ ions of higher ionic mobility replace the K^+ ions inside the nanochannel. Moreover, it might be possible for the case of high pH values that the electric potential rise is high enough to concentrate more salt ions since in lack of H^+ ions the surface charge does not change as much as at lower values of the *pH*. In this case, the nanochannel conductance changes less at low concentrations.

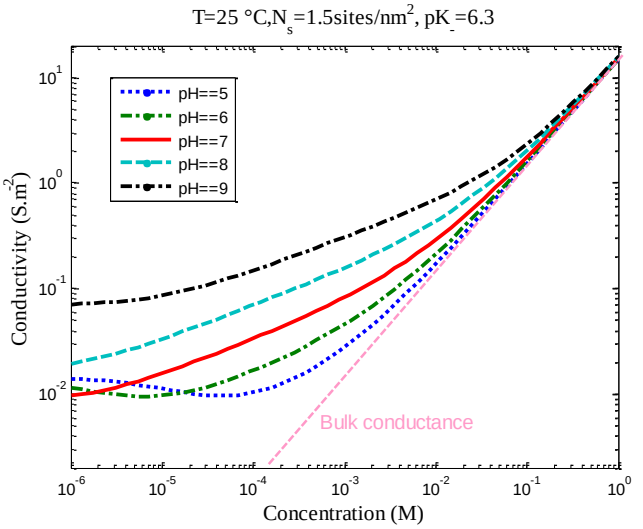

Figure 4-9. Conductivity versus concentration for a silica surface nanochannel. The nanochannel length to width ratio is $d/w = 10$ and its height is $h = 35\ nm$. A higher surface charge density tends to a higher deviation from bulk.

In this improved model, the binding site density and the equilibrium constant are the parameters that define the behavior of the nanochannel walls, and its surface charge density. For the case of a silicon dioxide surface, the equilibrium constant for the creation of negatively charged sites K_- (reaction (4-7)) is the only equilibrium constant to take into consideration since the reported K_+ values are extremely small. In the literature, the value of pK_- is reported to be between $pK_- = 6$ and $pK_- = 7.5$ (Pardon and van der Wijngaart, 2013; Revil and Glover, 1997). The number of binding sites has been reported to be between $N_s = 4\ sites/nm^2$ and $N_s = 8\ sites/nm^2$ (Iler, 1979; Pardon and van der Wijngaart, 2013; Reppert and Morgan, 2003a) for silicon dioxide. The lower limit is reported to be $N_s = 1.5\ sites/nm^2$ for a silicon dioxide surface (Revil and Glover, 1997). Figure 4-10 shows the evolution of conductance with concentration for various values of the equilibrium constant and binding site densities. A higher number of binding sites as well as higher values of equilibrium constant lead to a larger deviation from bulk line. The red dashed line in Figure 4-10 corresponds to the values used in this study while the blue lines indicate the extreme deviations in the reported range of parameters. The yellow area indicates all possible results. For the range of reported values, the variation of electrical conductivity is less than one order of magnitude.

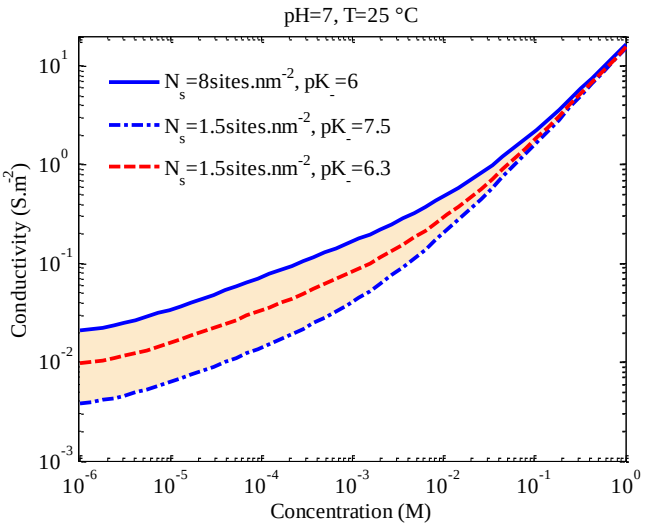

Figure 4-10. Conductance at pH=7 for different surface parameters. The larger number of binding sites and larger equilibrium constant leads to higher deviation from the bulk. The selected values are taken from the maximum and minimum reported values in the literature. The yellow area indicates the conductivity for all the possible values of surface parameters in the reported range.

4.7 Electrical conductance of nanochannel- Experimental validation

4.7.1 Comparison with the reported experimental results

In Figure 4-11, the model is compared with the data, previously published by other research groups (R. Karnik et al., 2005; R. B. Schoch and Renaud, 2005; Smeets et al., 2006) at different pH values.

The model estimates a higher bulk conductance for the measurements at high ionic concentrations. This looks reasonable since ion-ion interactions that happen at high concentrations have been neglected. As discussed in 4.2.1, The ionic mobility reduces with the increase of concentration (William M. Haynes, 2014, pp. 5–76). Neglecting this effect results in an overestimation of the nanochannel conductance at high ionic concentrations. The experimental measurement of the bulk conductivity (the blue circles) depicts the reduction of ionic mobility at high concentrations in Figure 4-11. The bulk values correspond to the measurements of the conductivity of the bulk solution as measured by a standard conductivity meter (METTLER TOLEDO, China).

The electroosmotic flow (EOF) can also induce a certain level of electrical conductivity at high ionic concentration, which has been neglected in our model. However, the model overestimates the electric conductance at high ionic concentration.

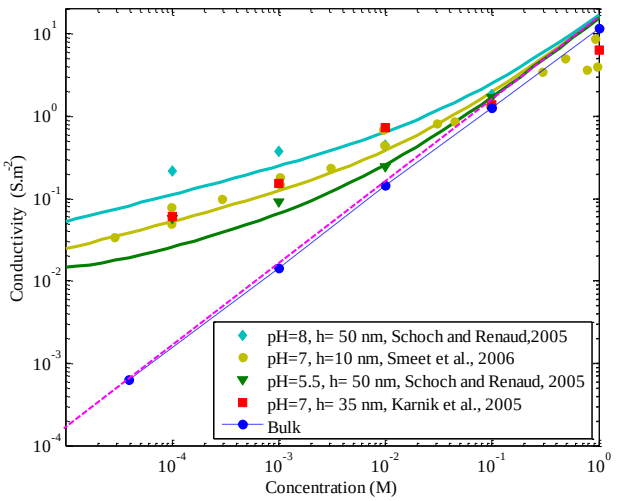

Figure 4-11. Comparison of our model with the data, published by other research groups (R. Karnik et al., 2005; R. B. Schoch and Renaud, 2005; Smeets et al., 2006). Lines show the model result for corresponding values of the pH. The modelling parameters are $N_s = 15\ sites/nm^2$ and $pK\_ = 6$. The blue circles are the experimental measurements of the bulk conductivity while the pink line is a guideline for its slope regardless of the ionic mobility decrease at high concentrations.

4.7.2 On-site measurements

The improved model was compared with the results from controlled experiments measuring the electrical conductance using AC impedance measurements[8]. As explained in 3.1.7, two platinum electrodes were placed in the microchannels for the bulk conductivity measurements. The bulk conductivity has a linear dependency on the concentration. Hence, the two electrodes can be calibrated for measuring the concentration of the solution according to a prior reference solution measurement. Measurements were performed in a shielded cage and connections to the measuring instruments used coaxial cable to avoid electromagnetic noise.

Figure 4-12 shows the measurements of the electrical conductance versus the ionic concentration obtained for different designs of nanochannels (different number of nanochannels, width, length but the same height) at $pH=7$. Here, the number of binding sites is 1.5 $sites/nm^{-2}$ and $pK\_ = 6.3$ (Revil and Glover, 1997). There is a very good agreement between the model and the experiments. Different symbols in the figure represent different devices.

[8] The procedure for AC measurement of the nanochannel conductance was described in 3.4.2.

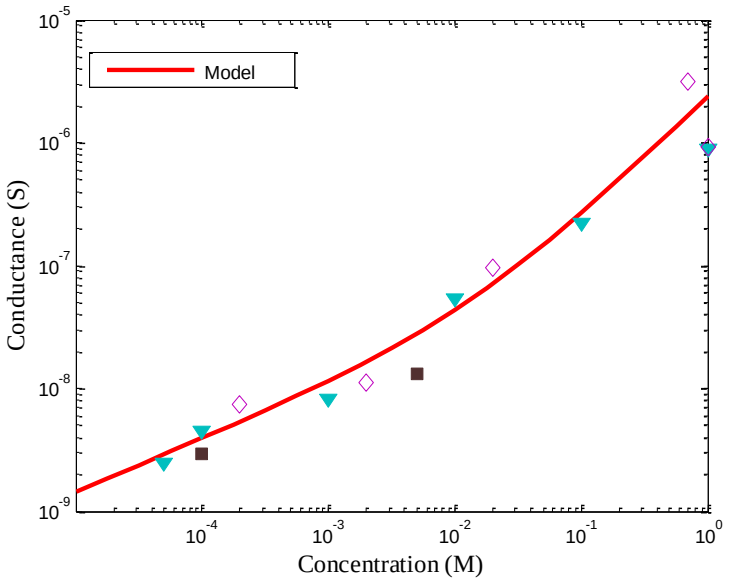

Figure 4-12. Nanochannel conductance versus concentration at $\mathrm{pH} = 7$ for a silica surface ($\mathrm{pK}_{-} = -6.3, \mathrm{N}_s = 1.5\ \mathrm{site.nm^{-2}}$). The nanochannel length to width ratio is $d/w = 10$ and its height is $\mathrm{h} = 35$ nm. Different symbols represent different devices.

4.8 Highlights

The main messages from this chapter are:

- The surface charge of nanochannel depends on the ionic concentration of the solution.
- Due to the wall surface charge, the concentration of ions inside the nanochannel is not similar to the bulk. The H^+ ions are not exceptions.
- The presence of a considerable amount of H^+ ions in the nanochannel changes the electric conductance by contributing to the surface reactions and enhancing the net ionic migration.
- The electric conductance of the nanochannel is not constant for the EDL overlapping regime. It decreases smoothly with diluting the solution.

Chapter 5

Temperature and Nanofluidic Transport

Electrical conductivity of electrolytes is known to be dependent on temperature. However, the similarity of the temperature sensitivity of the electrical conductivity for bulk and nanochannels has not been validated. In this chapter[9]*, we present the results from experimental measurements as well as analytical model that show the significant difference between bulk conditions and the nanoscale. The temperature sensitivity of the electrical conductance of nanochannels is higher at low ionic concentrations where the nanofluidic transport is governed by the electrostatic effects from the wall. Neglecting this effect can result in significant errors for high temperature measurements. Additionally, the temperature sensitivity of the nanochannel conductance allows to measure the enthalpy change of surface reactions at low ionic concentrations.*

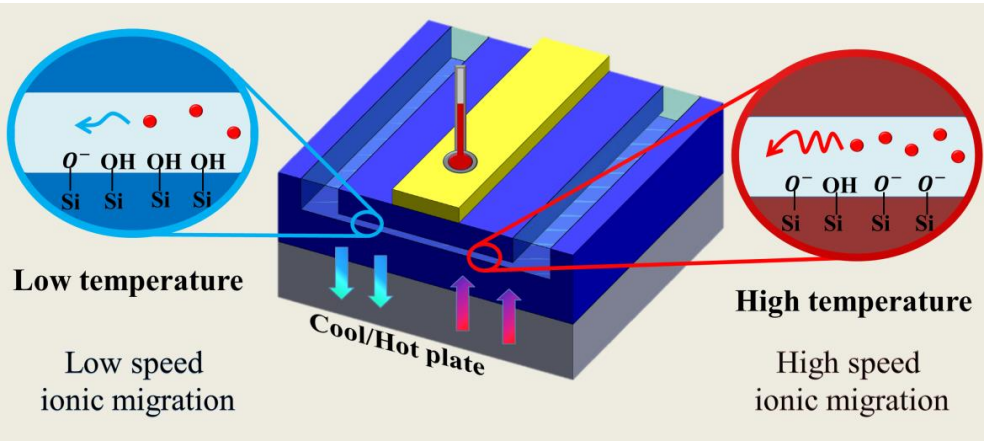

[9] Based on: Taghipoor, M., Bertsch, A., Renaud, P., 2015. Temperature Sensitivity of Nanochannel Electrical Conductance. ACS Nano. doi:10.1021/acsnano.5b01196

5.1 Motivation

The electrical conductivity of an electrolyte depends on its temperature since the mobility of ions changes with temperature. Aqueous solutions show an increase in electrical conductivity with temperature since the decrease of water viscosity makes it easier for the ions to migrate. Different ions have different mobilities and the sensitivity of their mobility to temperature change is different (Sluyters and Sluyters-Rehbach, 2013), too. The evolution of the electrical conductivity of different solutions with temperature has been studied by many research groups and reported to raise with temperature (William M. Haynes, 2014, pp. 5–74).

Moreover, the electrical conductance of nanochannels is known to differ from the bulk due the distinctive effect of the nanochannel wall that is electrostatically charged (R. Karnik et al., 2005; R. B. Schoch and Renaud, 2005; Stein et al., 2004; Taghipoor et al., 2015; Wu et al., 2012). As discussed in the previous chapter, the wall electrostatic field leads to overlapping EDL, where the concentration of counter-ions is more than the bulk and this extra concentration makes the nanochannel more conductive. Despite many studies focused on modeling and testing the influence of the wall effect on the electrical conductance (Baldessari and Santiago, 2006; Pardon and van der Wijngaart, 2013; Yeh et al., 2012), less attention has been devoted to the study of the influence of temperature change on the nanochannel conductance.

Failing to understand how the electrical conductance depends on temperature will result in errors in all related applications. For example, sensing applications that calibrate the measured conductance of nanochannels to estimate the temperature (Jonsson and Dekker, 2013), need to validate if the temperature dependence of an electrolyte in a nanochannel is similar to the one in bulk conditions. As another example, the electrical measurements were exploited to illustrate the gating function of temperature sensitive polymers in nanopores (Yameen et al., 2009b). The right estimation of the temperature dependency of the electrical current at the nanoscale is necessary, in order to define the proportion of the gating effectiveness due to the channel clogging by the polymers.

Is the temperature sensitivity of nanochannel conductance similar to the bulk?

That is the main question I try to answer in this chapter.

5.2 Analytical investigation

5.2.1 Temperature sensitivity of related physical parameters

Some of the physical parameters that participate in the analytical model of the electrical conductance of nanochannels, presented in previous chapters, vary with temperature. The temperature dependency of these variables defines the overall temperature dependency of the electric conductance. In the following subsections, these variables are introduced and their temperature sensitivity is discussed.

5.2.1.1 Temperature sensitivity

First, an expression needs to be introduced. In this chapter, the term ‘‘*temperature sensitivity*’’ of a variable v is defined as its relative rate of change with respect to temperature difference. In terms of mathematical expression:

$$\alpha_v \equiv \frac{1}{v}\frac{\partial v}{\partial T} = \frac{\partial ln(v)}{\partial T} \tag{5-1}$$

5.2.1.2 Equilibrium constant

The rate of chemical reactions is significantly influenced by temperature variation. The nanochannel wall reactions are not exceptions. The equilibrium constant K_{eq} of a reaction is related to the standard Gibbs free energy of the reaction ΔG° and absolute temperature T *via*

$$\Delta G^{\circ} = -RT\, lnK_{eq} \tag{5-2}$$

Where *R* is the gas constant. For the surface reaction at constant pressure, differentiation of K_{eq} with respect to temperature gives

$$\frac{dlnK_{eq}}{dT} = -\frac{1}{R}\frac{d(\Delta G^{\circ}/T)}{dT} \tag{5-3}$$

The right term of the equation (5-3) is related to the standard reaction enthalpy using the Gibbs-Helholtz equation.

$$\frac{d(\Delta G^{\circ}/T)}{dT} = -\frac{\Delta H^{\circ}}{T^2} \tag{5-4}$$

Now, combining both equations (5-3) and (5-4) leads to a relationship between the enthalpy of reaction and its equilibrium constant called Van’t Hoff equation.

$$\alpha_{K_{eq}} = \frac{dlnK_{eq}}{dT} = \frac{\Delta H^{\circ}}{RT^2} \tag{5-5}$$

In this equation, the enthalpy of the reaction is assumed constant, which is a correct approximation while the temperature dependence of the reaction enthalpy is very weak in many cases (Atkins and de Paula, 2013), specially for small temperature ranges.

As for many nanofluidic devices, the enthalpy change of reaction of a silica surface has been reported to be in the range of $\Delta H^{\circ} = -15\ \mathrm{kJ.mol^{-1}}$ to $\Delta H^{\circ} = -90\ \mathrm{kJ.mol^{-1}}$ (Reppert and Morgan, 2003a). Hence, the temperature sensitivity of the equilibrium constant at room temperature will be in the range of $\alpha_{K_{eq}} = 2\%$ to $\alpha_{K_{eq}} = 12\%$. This relatively high temperature sensitivity implies that the temperature sensitivity of the electrical conductance of the nanochannel will be different from the bulk when it is determined by the wall surface charge.

In order to calculate the value of the equilibrium constant at different temperatures, equation (5-5) should be integrated. Given the value of ΔH° *and* K_1 at T_1, K_1 at temperature T_2 is

$$lnK_2 = lnK_1 - \frac{\Delta H^{\circ}}{R}\left(\frac{1}{T_2} - \frac{1}{T_1}\right) \quad (5\text{-}6)$$

Since the number of binding sites that contribute to the surface reactions depends on the *pH* value, the enthalpies of surface reactions might be *pH* dependent, too. Some groups (Kallay et al., 1999; Machevsky and Anderson, 1986) reported the dependency of enthalpies of the surface reactions on the *pH* for different metal oxides. Some others measured the enthalpy of surface reactions only at the PZC (De Keizer et al., 1990) since the measurements outside the PZC region cannot simply be justified by normal stoichiometric calculations. In fact, the enthalpy change of surface reactions can be expressed as a summation of the standard and the electrostatic contributions (Kallay et al., 1999). As far as the temperature variation can change the electrostatic properties of the surface, the enthalpy change of the surface reactions might be dependent on temperature, too.

In this work, the enthalpy change of surface reactions of silicon dioxide was assumed constant since the temperature range is small. However, different enthalpies can be utilized at different pH values.

5.2.1.3 Ionic mobility

The only temperature dependent variable that can influence the conductivity of an electrolyte is the ionic mobility. The ionic mobility, itself, is a function of water viscosity according to equation (4-1). Since the viscosity of water decreases by increasing the temperature, (William M. Haynes, 2014, pp. 6–1) the ionic mobility of solvated ions and consequently the conductivity of water increases. The temperature sensitivity of water dynamic viscosity is $\alpha_{\eta} = -2.1\%$ (William M. Haynes, 2014) and subsequently, the temperature sensitivity of the ionic mobility is $\alpha_{\mu_i} = 2.1\%$.

The ionic mobility is used directly in the analytical modeling of the electrical conductance of nanochannels as in equations (4-30), (4-32) and (4-33).

5.2.1.4 Electric permittivity

The electric permittivity of liquid water is known to decrease by increasing the temperature (Kaatze, 1997; Malmberg and Maryott, 1956; William M. Haynes, 2014). The relationship suggested by Malmberg and Maryott (Malmberg and Maryott, 1956) was used here to calculate the temperature sensitivity of the electric permittivity, which is given as

$$\epsilon = 87.740 - 0.40008\theta + 9.398(10^{-4})\theta^2 - 1.410(10^{-6})\theta^3 \quad (5\text{-}7)$$

where θ is the temperature in degrees Celsius. The temperature sensitivity is then $\alpha_{\epsilon} = -0.45\%$ at $25°C$.

The electric permittivity of the solution is utilized for calculating the surface charge and the wall electric potential as in equation (4-24).

5.2.1.5 Dissociation constant of water

Autoprotolysis of water and its dependence to the electric field was studied numerically for a nanofluidic field effect transistor (Pardon and van der Wijngaart, 2013). Like any chemical reaction, the dissociation of water molecules is temperature dependent and should be considered in our study. At low ionic concentrations where the salt concentration is of the same order as the ionized water molecule concentration (*i.e.* H^+ and OH^- concentration) considering self-ionization of water is necessary. Specially, in surface chemistry studies, as the surface charge is strongly influenced by the *pH*, neglecting the self-ionization of water can result in errors. Additionally, the ionization of water, like any other chemical reaction, is temperature dependent and its dissociation constant pK_w decreases by increasing the temperature (William M. Haynes, 2014). Although the temperature sensitivity of pK_w is very small, its variation with temperature is taken into account in our modeling since the wall surface charge is strongly dependent on the *pH* value of the solution.

5.2.1.6 Thermal voltage

The thermal voltage is an expression of the thermal energy of ions in the solution in terms of the electric potential. It is related to the absolute temperature T and the electron charge e *via*

$$V_T = \frac{k_B T}{e} \tag{5-8}$$

where k_B is the Boltzmann constant. It influences the ionic distribution toward the wall and since it is explicitly related to the temperature, its variation with temperature can influence the nanochannel electrical conductance. At room temperature, the thermal voltage is about $V_T \approx 26$ mV which is in the same order of magnitude as the wall electric potential for a silica surface in normal conditions. Its temperature sensitivity is $\alpha_{V_T} = 1/T$, which is about 0.3% at room temperature.

5.2.1.7 Debye length

The Debye length is a characteristic length that depends on the thermal energy and ionic strength of the solution and is independent of the wall electric field.

$$\lambda_D = \left(\frac{\epsilon_f \epsilon_0 k_B T}{2e^2 I}\right)^{\frac{1}{2}} \tag{5-9}$$

where ϵ_f, ϵ_0 and I are the relative dielectric constant of electrolyte, dielectric constant of vacuum and the ionic strength of the solution, respectively. Its temperature sensitivity can be expressed as a function of α_ϵ and α_{V_T}. The relative rate of change of the Debye length can then be expressed as

$$\alpha_{\lambda_D} = \frac{1}{2}\frac{1}{\epsilon_f T}\frac{\partial(\epsilon_f T)}{\partial T} = \frac{1}{2}\left(\frac{1}{\epsilon_f}\frac{\partial \epsilon_f}{\partial T} + \frac{1}{T}\right) = \frac{1}{2}(\alpha_\epsilon + \alpha_{V_T}) \tag{5-10}$$

Table 5-1. Temperature sensitivity of important physical parameters

Parameter (p)	Relationship	α_p (%)
Equilibrium constant K	$\Delta G^{\circ} = -RT\ lnK_{eq}$	2-12
Ionic mobility μ_i	$\mu_i = \frac{\lvert z_i \rvert e}{6\pi r_i \eta(T)}$	2.1
Dielectric constant ϵ_f	Eq. (5-7)	-0.45
Thermal voltage V_T	$V_T = \frac{k_B T}{e}$	0.3
Debye length λ_D	$\lambda_D = (\frac{\epsilon_f \epsilon_0 k_B T}{2e^2 I})^{\frac{1}{2}}$	-0.06

According to the estimated values, its temperature sensitivity is $\alpha_{\lambda_D} = -0.06\%$, which is relatively low. This means that temperature has a minor effect on the screening length of the wall electric field.

5.2.1.8 Comparison

The mathematical relationships and temperature sensitivity of the studied parameters are summarized in Table 5-1.

Figure 5-1 compares the normalized values of the mentioned parameters in a temperature range of 10 to 70 degrees Celsius. All the values are normalized by dividing by their value at *T=10°C*. As it is depicted, the increase of the equilibrium constant *K* and the ionic mobility μ_i are dominant. It means that increasing the temperature will increase the electrical conductance *via* the ionic mobility increase. Likewise, increasing the temperature changes the electrical conductance by changing the wall surface charge as discussed before.

Of course, having a high temperature sensitivity of a parameter does not necessarily show a significant impact of that parameter on the temperature sensitivity of the electrical conductance. On the other hand, a parameter with low temperature sensitivity can have influential impact on the electric conductance. For example, the dissociation constant of water has the lowest temperature sensitivity relative to other mentioned parameters, but neglecting to consider its temperature dependency gives rise to a considerable error. Figure 5-2 compares the surface charge of nanochannel wall at 80°C and *pH=9* while the pKw is considered as a function of temperature (solid line) or constant (dashed line). It shows up to 60% error at low ionic concentration if *pKw* is considered constant.

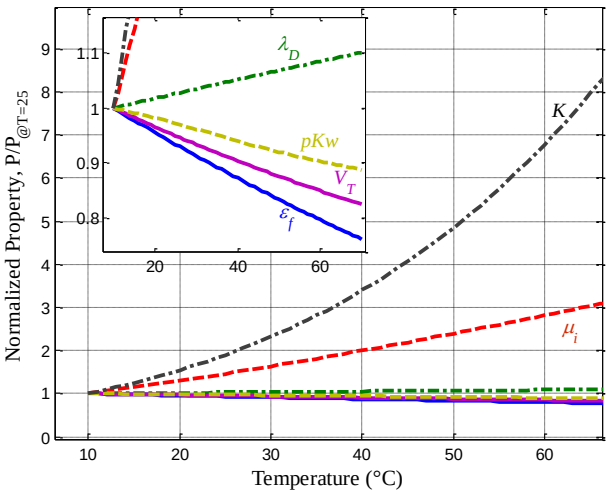

Figure 5-1. Normalized physical properties value *versus* temperature. The increase of the equilibrium constant K (Black dash-dot line) and the ionic mobility μ_i (red dashed line) are more dominant than other properties. In equilibrium constant calculations, the enthalpy change of the reaction was assumed constant and equal to $\Delta H^{\circ} = -30\ kJ.mol^{-1}$. The inset shows a zoomed view of the changes of Debye length λ_D (green dash-dot), dissociation constant of self-ionization of water pKw (yellow dashed), thermal voltage V_T (pink solid line) and the relative permittivity of water ε_f (blue solid line).

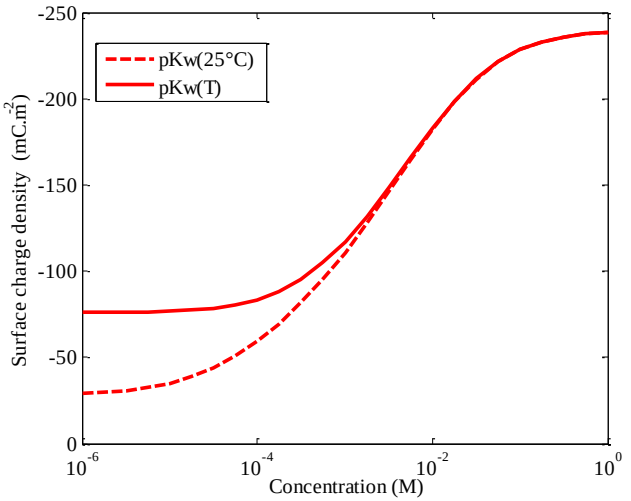

Figure 5-2. The impact of neglecting the temperature dependency of the dissociation constant of water on the estimation of the surface charge density. Both lines correspond to the analytical modeling of the wall surface charge at *T=80°C* and *pH=9*. The modeling parameters are $pK_{-} = -6.3$, $N_s = 1.5\ site.nm^{-2}$ and $\Delta H^{\circ} = -40\ kJ.mol^{-1}$. The dashed line shows a modeling that uses the value of *pKw* at *T=25°C* while the solid line uses the *pKw*, which is a function of temperature.

5.2.2 Temperature dependence of wall surface charge

Taking into account the temperature dependence of the mentioned variables, the surface charge density of a silica nanochannel wall was calculated in a temperature range of 0 to 70 °C using the analytical modeling presented in the previous chapter. Figure 5-3 shows the evolution of the calculated surface charge density *versus pH* at different temperatures. A higher temperature of the electrolyte leads to a higher magnitude of surface charge density. There is an exceptional case when all the binding sites of the surface are charged. In this condition, the temperature will not have any effect like the situation of the maximum surface charge density at high pH values.

Additionally, the PZC may be shifted to higher or lower values of the *pH*, if the values of enthalpy change of the surface reactions are different. Base on the equation equation (4-27), and considering the temperature dependence of the equilibrium constant, Eq.(5-5), the rate and direction of PZC shift can be estimated.

$$\frac{\partial pH_{PZC}}{\partial T} = -\frac{1}{2RT}(\Delta H_{-}^{o} - \Delta H_{+}^{o}) \tag{5-11}$$

The PZC shift with temperature change was observed previously and reported to approach the neutral point with increasing the temperature for a TiO_2 surface (Bérubé and de Bruyn, 1968).

As it is shown in the inset of Figure 5-4, the variation of the surface charge density has a direct impact on the wall electric potential. Some studies in surface chemistry (Revil et al., 1999) and geophysics (Reppert and Morgan, 2003a, 2003b) and recently in microfluidics (Hsu et al., 2012; Venditti et al., 2006) evaluated the effect of temperature change on the zeta potential for different surface types. Generally, the magnitude of the zeta potential has been reported to increase by increasing the temperature for the case of a silica surface. In the present analytical modeling, as Figure 5-4 illustrates, the magnitude of the wall electric potential increases with temperature, too. It shows that the normalized surface charge density σ_0 and the Stern layer potential φ_0 have positive slopes with respect to temperature increase.

The variation of surface charge density is not similar at all ionic concentrations. At low ionic concentration, the surface charge density is more sensitive to temperature change. Contrarily, the slopes of high ionic concentration curves are lower for the electric potential of the nanochannel wall. The dependency of temperature sensitivity of both surface charge and electric potential to concentration implies that the temperature sensitvity of the nanochannel electrical conductance can also be related to the concentration

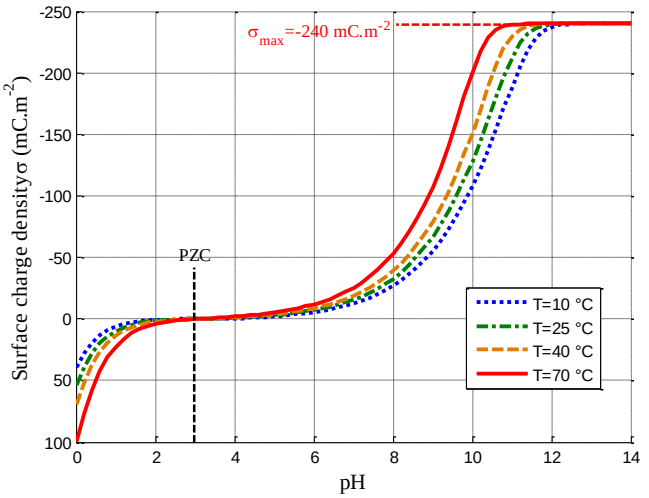

Figure 5-3. Evolution of modeled surface charge density *versus* pH for a silicon dioxide surface ($pK_{-} = -6.3, N_s = 1.5\ site.nm^{-2},\ \Delta H^{\circ} = -30\ kJ.mol^{-1}$) at 1 mM concentration of potassium chloride. The red solid line ($T = 70°C$), the orange dashed line ($T = 40°C$), the green dash-dot line ($T = 25°C$) and the blue dotted line ($T = 10°C$) show how the wall surface charge changes at different temperatures. The higher temperature of electrolyte leads to a higher magnitude of surface charge density.

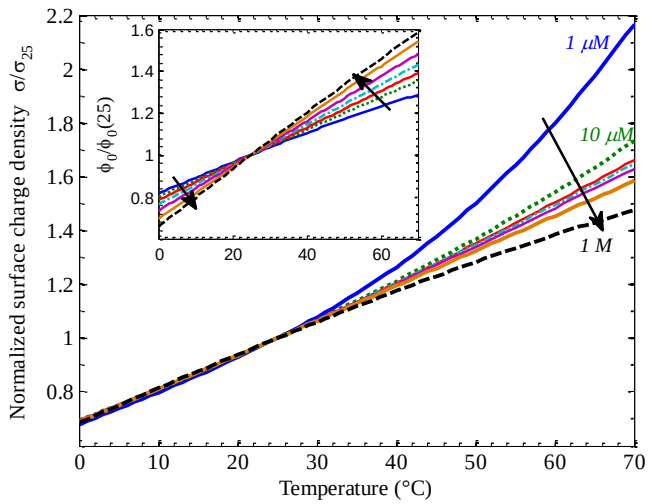

Figure 5-4. Change in normalized surface charge density σ/σ_{25} and normalized wall electric potential $\varphi_0/\varphi_{0_{25}}$ (inset) *versus* temperature at $1\ \mu M$ (blue line), $10\ \mu M$ (Green dotted), $100\ \mu M$ (red solid line), $1\ mM$ (cyan dash-dot), $10\ mM$ (pink solid), $100\ mM$ (orange solid) and $1\ M$ (black dashed) potassium chloride concentrations at pH=7. The graph shows that the magnitude of surface charge and electric potential increase with increasing the temperature, despite different slopes at different concentrations. The arrows show the increase of ionic concentration direction.

5.2.3 Temperature Sensitivity of the electrical conductance of nanochannels

As described in 4.5.1.1, two different regimes govern the nanofluidic transport according to the ionic concentration of the solution. The analytical model presented in 4.6, was composed of two terms that modeled the electric conductance of a nanochannel for these two regimes. Similarly, the temperature sensitivity of the nanochannel conductance should be inspected distinctively for both transport regimes.

5.2.3.1 Bulk regime

For the case of the bulk regime, according to equation (4-32), at high ionic concentrations, G_B which was defined as the electric conductance of the nanochannel for the bulk regime, is dominant and the only parameter that depends on temperature is the ionic mobility. Therefore, for a symmetric electrolyte, the temperature sensitivity of the electrical conductance α_{G_B} at neutral *pH* can be written as:

$$\alpha_{G_B} = \frac{1}{\sum \mu_i} \frac{\partial \sum \mu_i}{\partial T} \tag{5-12}$$

As mentioned before, α_{G_B} is known thanks to several works on conductivity meter calibrations. For instance, the temperature sensitivity of potassium chloride solutions has been studied by many research groups and reported to raise between 1.8-2 percent per degree Celsius at room temperature (William M. Haynes, 2014, pp. 5–74).

5.2.3.2 EDL overlapping regime

At low ionic concentrations where the surface effect is dominant and the EDLs are overlapping equation (4-33) is used to estimate the electric conductance of the nanochannel. Differentiating this equation with respect to temperature will lead to the temperature sensitivtiy of the electric conudctance for this regime.

$$\alpha_{G_S} = \frac{1}{\mu_e} \frac{\partial \mu_e}{\partial T} + \frac{1}{\sigma_n} \frac{\partial \sigma_s}{\partial T} = \alpha_{\mu_e} + \alpha_{\sigma_s} \tag{5-13}$$

The temperature sensitivity has an extra term α_{σ_s}. This means that the temperature sensitivity of the electrical conductance is different from the bulk. The extra term α_{σ_n} is directly related to the wall surface charge σ_s , which is an explicit function of temperature according to the site binding model (equation (4-19)).

In the mentioned equation, the surface charge is a function of an unknown electric potential and the system needs more equations to be determined. Subsequently, some more temperature dependent parameters contribute to the determination of the surface charge density. Moreover, the equilibrium constants as well as the wall electric potential are functions of temperature, which makes the problem more complicated.

The temperature dependent parameters that can play a role in the electrical conductance of a nanochannel were introduced in section 5.2.1. The temperature de-

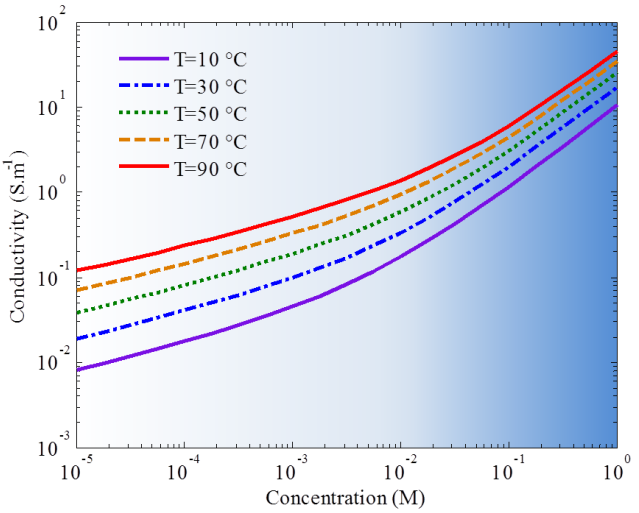

Figure 5-5. Calculated conductivity change *versus* salt concentration for different temperatures. The background color indicates different transport regimes. The blue color shows the bulk regime while the white represents the EDL overlapping regime. The gradient of blue color demonstrates the transient between these two regimes. It is obvious that the change of conductivity with temperature is higher at low ionic concentrations where it is governed by the wall surface charge. At high concentrations (blue region), a smaller effect is still observable since the conductivity of water increases with temperature, too. The solution is considered to be at $pH=7$ and the nanochannel surface is silicon dioxide ($pK\_ = -6.3$, $N_s = 1.5\ site.nm^{-2}$, $\Delta H^{\circ} = -40\ kJ.mol^{-1}$).

pendency of these parameters as well as the surface charge density (5.2.2) should be considered in the calculation of the electrical conductance of the nanochannel in the EDL overlapping regime.

Taking into account all the temperature dependent variables, the analytical model was used to calculate the average electrical conductivity[10] of the solution inside a 35 nm high nanochannel at different concentrations. As it is shown in Figure 5-5, a temperature rise makes the nanochannel more conductive. That is due to the known fact that solution conductivity increases by increasing the temperature (blue color background), which is related to the change in the ionic mobility of the salt ions. As expected, the nanochannel is more sensitive to the temperature change at lower concentrations since the effect of wall surface charge variation adds up to the bulk conductance variation. This is the key point that has not been considered in previous nanofluidic studies. The conductance increases more than one order of magnitude for a temperature rise of 80°C at ionic concentrations lower than 1 mM. The conclusion is that the nanofluidic transport in EDL overlapping conditions is influenced by temperature in a different way, as it is depicted in Figure 5-6. At low temperature, the silica surface of the nanochannel is less charged and a smaller number of ions can pass. At high temperature, the surface charge is higher, the concentration of counter-ions increases inside the channel, the water is less viscous and consequently, the ionic transport occurs faster. This results imply that for the case of thermally nanoactuated macromolecular gates

[10] What we call ‘‘nanochannel conductivity’’. See 4.6.3 for more information.

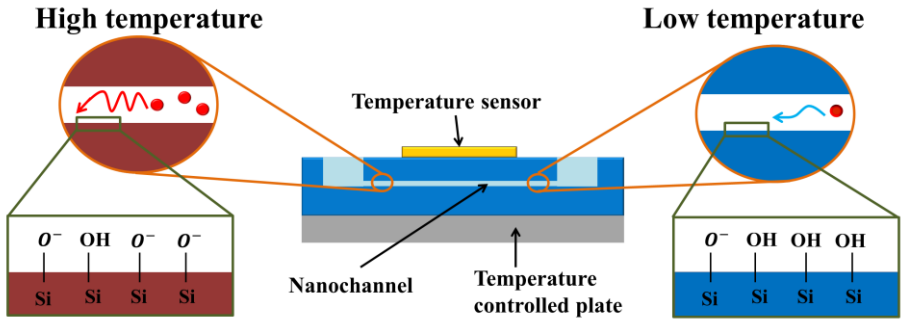

Figure 5-6. Schematic explanation of the temperature effect on the electrical conductance of a nanochannel. At low temperatures, the silica surface of the nanochannel is less charged and a small number of ions can pass. At high temperature, the surface charge is higher, the concentration of counter-ions increases inside the channel, the water is less viscous and consequently, the ionic transport occurs faster.

(Guo et al., 2010; Nasir et al., 2012; Yameen et al., 2009b), the temperature sensitivity of the wall surface charge should be taken into account. Specially, for the case of small pore diameter nano-conduits whose electrical conductance is governed by the wall surface charge, the role of wall surface charge is not negligible. Additionally, this significant change of nanochannel conductivity, especially at low concentrations, provides the possibility of modulating the nanofluidic transport by means of temperature change.

5.3 Experimental validation

5.3.1 Apparatus

5.3.1.1 Design of the device

As explained in 3.1.7, two microelectrodes close to the entrances of the nanochannel were used to measure the electrical conductance of the nanochannel. A thin platinum electrode that was calibrated and used as a nanochannel temperature sensor was integrated just 500 nm from the nanochannel. Figure 5-7.a and ure 5-7.b show the situation of the measurement electrodes and the temperature sensor using a SEM image and a schematic of the device.

5.3.1.2 Measurement setup

The device was mounted on a temperature controlled mini cool/hot plate and the electrical conductance of nanochannel was measured at different temperatures. The measurement procedure was similar to what explained in 3.4.2. Figure 5-7.c shows the measurement setup for the electrical conductance measurements as well as the situation of other sensors.

The temperature of nanochannel was measured using a setup as sketched in Figure 5-7.d. A function generator applied a relatively low electric potential AC sig-

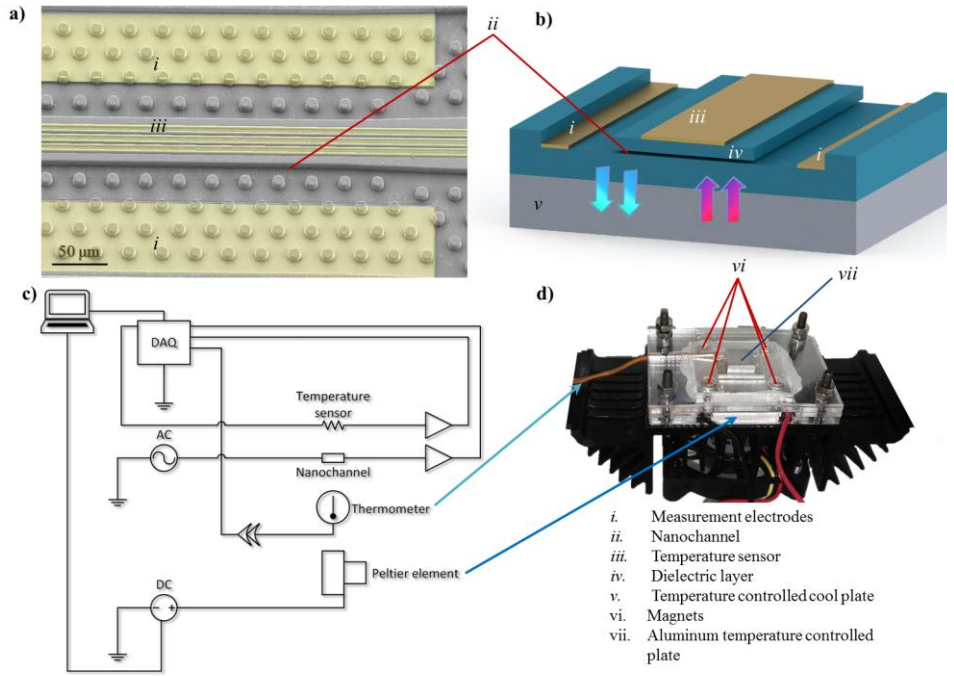

Figure 5-7. a) SEM image of a fabricated device showing the position of measurement electrodes as well as temperature sensors. b) Schematic of the device mounted on the temperature controlled plate. The arrows show the possibility of heating and cooling the device. c) The experimental setup. The temperature of the device is set by controlling the temperature of a mini cool/hot plate. The nanochannel temperature is measured by a platinum electrode that is integrated 500 nm away from the nanochannel wall. Two platinum electrodes are used for the nanochannel impedance measurements. The nanochannel conductance and temperatures are calculated in a LabVIEW interface using the data acquired by a data acquisition card (DAQ). d) Image of the temperature controlled plate apparatus. The Peltier element transfers the heat flux out of the aluminum plate using an aluminum finned sink. A fan produces a convective flow in order to increase the heat transfer rate. Four magnets are used to enhance the physical contact between the device and the plate.

nal to the temperature sensor in order to eliminate the Joule heating and electrostatic effects. A transimpedance amplifier was used to converted the current to voltage so that it can be read by DAQ (National Instrument PCI-6251, USA). The resistance of the platinum electrode was then calculated at different temperatures and calibrated for measuring the nanochannel temperature.

5.3.1.3 Temperature control

Figure 5-7.d shows how the setup was used to control the device temperature. A Peltier element (3.9A, 37.9 W, Laird, Russia) was utilized and controlled by a computer controlled DC power supply (Hewlett-Packard E3631A, USA) in order to set the device temperature. The device was mounted on top of an aluminum adaptor that was in contact with the Peltier and its temperature was controlled easily by controlling the current passing through the Peltier element. A thermally conductive paste was used between the device and the plate in order to enhance the heat transfer. The Peltier element transferred the heat flux out of the aluminum

plate using an aluminum heat sink supported by a fan (1.08 W, Master Cooler, China). The fan produced a convective flow in order to increase the heat transfer rate. Four magnets were used to enhance the physical contact between the device and the plate. A thermocouple was used to provide a temperature feedback, whose data was collected by DAQ. A computer interface (LabVIEW2013) was used to acquire the data and produce a control command for the power supply.

5.3.2 Results

The electrical conductance of the nanochannel was measured at a temperature range of 5 to 38 degrees Celsius. The variation of nanochannel conductance with temperature was then observed at different ionic concentrations. Figure 5-8 depicts the variation of the normalized nanochannel electrical conductance *versus* temperature at different ionic concentrations. The conductance was normalized to its value at 10 degrees Celsius. The electrical conductance of nanochannel increases about 3.4 times at 100 μM while its increase at 1M is only 1.5 times for the same temperature change of 25 degrees Celsius.

The figure clearly describes the difference in temperature sensitivity of the nanochannel electric conductance at different ionic concentrations. The temperature sensitivity of the electrical conductivity of aqueous solutions varies slightly with the ionic concentration (Katayama, 1976). However, the difference that was observed here cannot be justified only by the concentration difference. The conductivity meters use unique build-in functions to compensate the temperature at any ionic concentration while the results in Figure 5-8 emphasize that for the case of a nanochannel, every concentration follows its own modification formula.

In Figure 5-9, the experimental results are compared to analytical estimations. The slope of the normalized conductance is higher at low concentrations and both experimental and analytical results are consistent. The enthalpy change of surface reactions for a silicon dioxide surface was taken $\Delta H^{\circ} = -40\ \mathrm{kJ.mol^{-1}}$ in the analytical calculations.

This figure shows that because of the non-equal temperature sensitivity of the nanochannel conductance at different concentrations, different sensitivities should be specified for the applications that use the electrical conductance measurement to estimate the temperature inside the nanochannel. For instance, Jonsson and Dekker (Jonsson and Dekker, 2013) estimated the temperature inside their nanopore by measuring its electric conductance while they used the normal bulk relationships to correlate the temperature and the electric conductance.

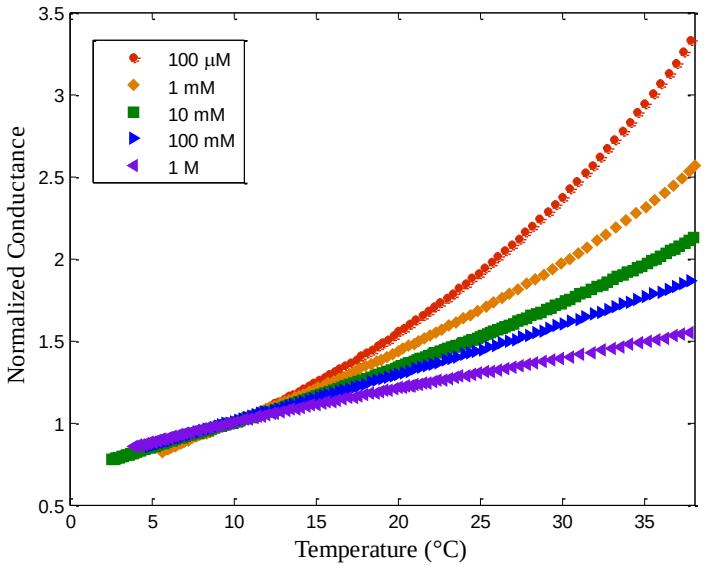

Figure 5-8. Evolution of normalized electrical conductance of a set of 45 nm high nanochannels *versus* temperature at different concentrations. At low ionic concentration, the electric conductance of the nanochannel is more sensitive to temperature changes. The conductance is normalized relative to its value at 10°C for all ionic concentrations.

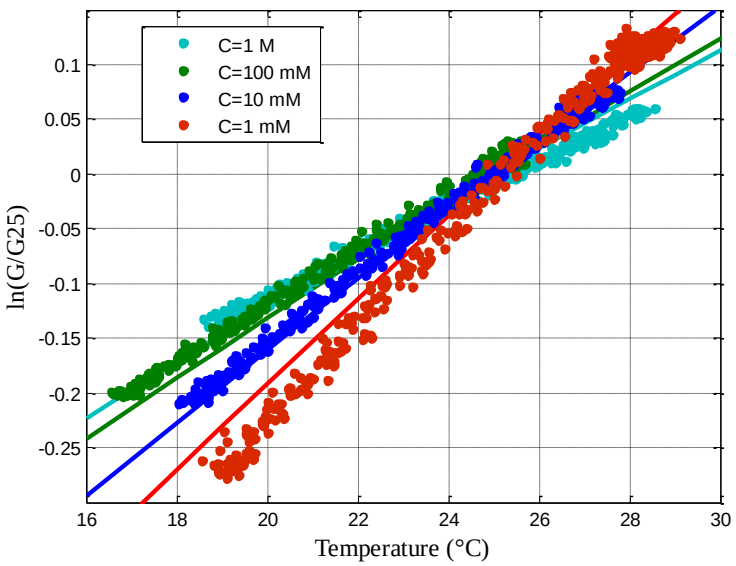

Figure 5-9. Evolution of the natural logarithm of the normalized conductance ($\ln(G/G_{25})$) from the measurements *versus* temperature at c= 1 M (Cyan circles), c= 100 mM (green circles), c= 10 mM (blue circles) and c= 1 mM (red circles). The colored lines are the modeled conductance for a silicon dioxide surface ($\Delta H^{\circ} = -40\ kJ.mol^{-1}$). The slopes show the temperature sensitivity of the electrical conductivity.

5.4 Discussion

5.4.1 Temperature sensitivity

Figure 5-10 illustrates the temperature sensitivity of the nanochannel conductance at different ionic concentrations. It compares the experimental results for two devices of different geometries with the model. It clearly proves that when the surface charge is the main factor in conductance calculation, the temperature sensitivity of the conductance is higher. According to the measured temperature sensitivity, an experimental measurement with only two degrees Celsius of temperature difference will have more than 8 percent error at low concentrations, which should be noticed in all of the nanofluidic applications that use the electrical measurements for characterization, sensing or any other purposes.
The bulk temperature sensitivity was also evaluated using the same experimental setup. The result is 1.9 percent, which is consistent with the known value from the literature (William M. Haynes, 2014). In analytical modeling, the enthalpy change value was selected to be $\Delta H^{\circ} = -40\ kJ.mol^{-1}$ for silicon dioxide surface.

5.4.2 The effect of enthalpy

As mentioned before, the enthalpy change of silicon dioxide surface reaction has been reported to be between -15 to -90 $kJ.mol^{-1}$ (Reppert and Morgan, 2003a). The higher enthalpy change results in higher temperature sensitivity of the electrical conductance at low ionic concentrations as it is shown in Figure 5-11. In this figure, the modeled temperature sensitivity of the nanochannel electrical conductance for different enthalpy changes is compared with the measured data for two different devices. According to the model, the temperature sensitivity is higher at low ionic concentrations for all enthalpies.

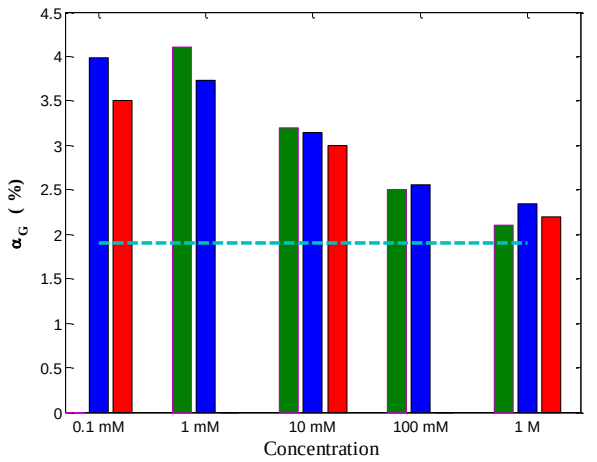

Figure 5-10. Comparison of temperature sensitivity of the measured electrical conductivity (red and green bars show different devices) with analytical model (blue bars) and bulk value (cyan dashed line) at room temperature. The measured temperature sensitivity is higher at low ionic concentrations where the conductivity is governed by the wall surface charge.

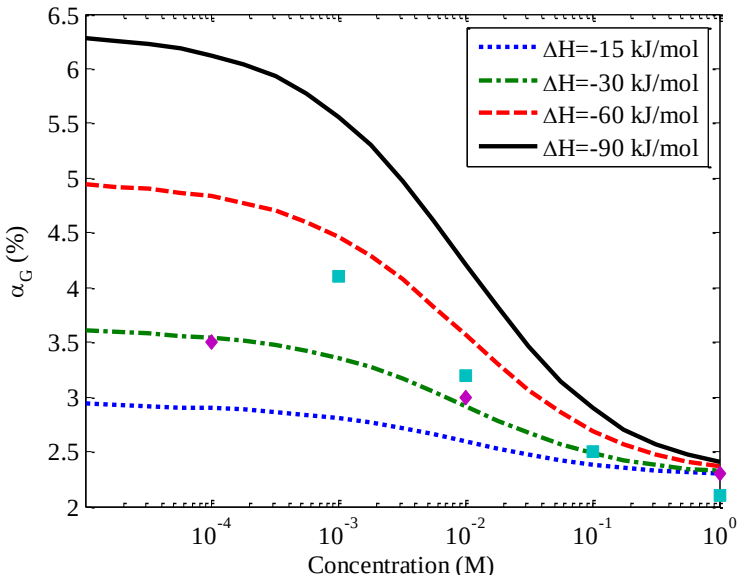

Figure 5-11. Comparison of the measured temperature sensitivity of the electrical conductivity with the results from the model for values of reaction enthalpy. The higher enthalpy change of the surface reaction leads to a higher temperature sensitivity at low ionic concentrations. Cyan squares and magnetite diamonds represent the experimental data for two different devices. The devices are of the same height but different width and length. The two devices are also different in terms of surface properties that can be the result of processing uncertainties and different number and type of adsorbed ions on the nanochannel wall.

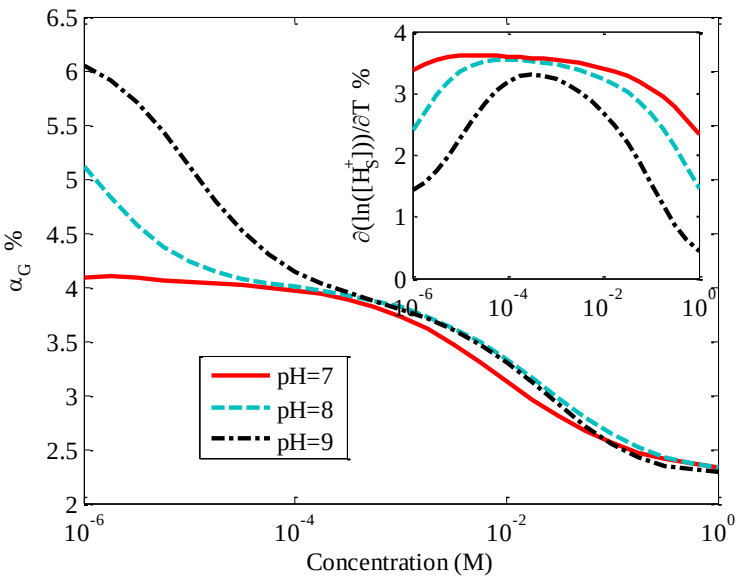

Figure 5-12. Evolution of temperature sensitivity of the electrical conductance of a nanochannel (35 nm in height) versus the ionic concentrations at different pH values. The inset shows the temperature sensitivity of the activity of H^+ ions. The decrease of temperature sensitivity of H^+ ions for high pH values (inset) justifies the increase of the temperature sensitivity of the nanochannel conductance at low ionic concentrations. The calculations were performed for a silicon dioxide surface ($pK_- = -6.3, N_s = 1.5\ site.nm^{-2},\ \Delta H^\circ = -40\ kJ.mol^{-1}$) at room temperature.

At high ionic concentrations, on the other hand, the values are lower, close to the bulk values and independent from the enthalpy change, which confirms that the temperature sensitivity is not dependent to the surface charge.

The electrical conductance of nanochannels have a temperature sensitivity at higher pH values. As depicted in Figure 5-12, the temperature sensitivity of the electrical conductance of nanochannels is higher for $pH=8$ and $pH=9$ for the EDL overlapping transport regime. The reason is that the temperature sensitivity of the wall surface charge is also higher at these pH values (see Figure 5-3). At $pH=7$, the activity of H^+ ions is more sensitive to the temperature, which means that the temperature sensitivity of the equilibrium constant moves the equilibrium in a direction that more number of charge sites are produced on the surface. Nevertheless, the higher temperature sensitivity of H^+ ions cancels a considerable part of the overall temperature sensitivity.

5.4.3 Measuring the enthalpy of surface reactions

Comparing the experimental data and the model provides the possibility of measuring the enthalpy change of surface reactions. Although calorimetry as the conventional method is normally used to measure the enthalpy of surface reactions (Kallay et al., 1999) this can also be introduced as a new method for measuring the enthalpy change of metal oxide surface reactions at the solid-electrolyte interface. According to Figure 5-13, the enthalpy change is a linear function of α_G and can be easily used for this purpose in nanofluidic studies as well as in other related fields like geophysics. In Figure 5-13, the enthalpy change of surface reactions is depicted versus the temperature sensitivity of the electrical conductance of nanochannels for a 1 mM potassium chloride solution at room temperature.

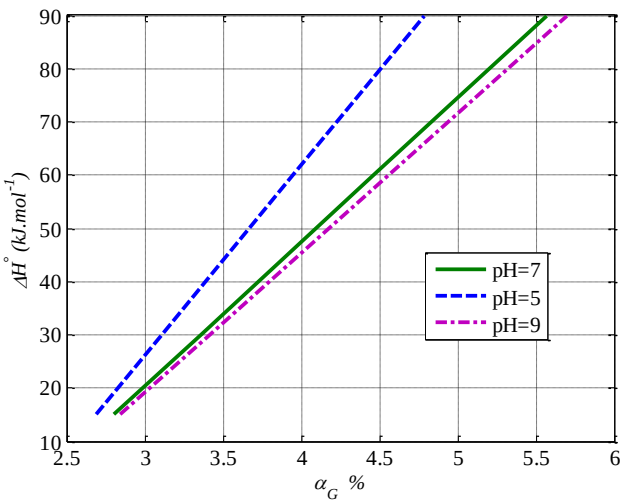

Figure 5-13. The enthalpy change of surface reaction is a linear function of the temperature sensitivity of the electric conductance of nanochannels. This linear dependency offers a new method to measure the enthalpy change of surface reactions. The calculations were performed for a silicon dioxide surface ($pK_- = -6.3, N_s = 1.5\ site.nm^{-2},\ \Delta H^\circ = -40\ kJ.mol^{-1}$) at room temperature and for a 1 mM potassium chloride solution.

5.5 Highlights

In this chapter, the effect of temperature on the nanochannel electrical conductance was studied. According to the analytical model and experimental measurements:

- The surface charge of nanochannel walls depends on temperature.
- The temperature sensitivity of the nanochannel conductance is different from the bulk at low ionic concentration.
- Neglecting the nanoscale effects may result in a measurement error of more than one order of magnitude at low ionic concentrations.
- The higher temperature sensitivity of ionic transport at the nanoscale suggests a new method for gating the nanofluidic transport.
- Based on the mentioned experimental setup, a new method for measuring the enthalpy change of surface reactions was introduced.

Chapter 6

Thermal Gating of Nanofluidic Transport

In this chapter[1], a nanofluidic gating mechanism that uses the thermal effect for modulating the ionic transport inside nanofluidic channels is introduced. The thermal gate controls the ionic transport more effectively than most of other gating mechanisms previously described in scientific literature. Gating in both bulk and overlapping electric double layer regimes can be obtained. The relatively short time response of opening and closing processes makes it a good candidate for manipulating small molecules in micro- and nanoscale devices.

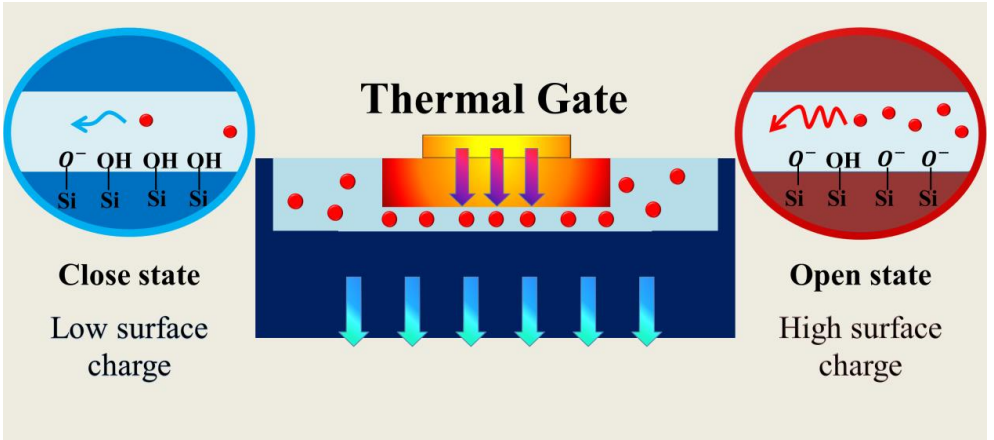

[1] Based on: M. Taghipoor, A. Bertsch, and P. Renaud, "Thermal control of ionic transport and fluid flow in nanofluidic channels", Nanoscale, 2015, DOI: 10.1039/C5NR05409E

6.1 Introduction

As discussed Chapter 2, controlling the fluidic and ionic transport inside nanochannels is one of the important applications of nanofluidics. Different phenomena were proposed and utilized in nanofluidic channels and pores to control the ionic and molecular transport in nanometer scale conduits. Using the electrostatic field effect (Fan et al., 2005; R. Karnik et al., 2005; R. B. Schoch and Renaud, 2005), steric effect (Xia et al., 2008; Yameen et al., 2009b) and liquid reconfiguration (Powell et al., 2011; Smirnov et al., 2011) are the three most reported phenomena.

According to theoretical and experimental results discussed in the previous chapter, at the micro and nanoscale, the variation of temperature influences the ionic transport. This temperature dependence of the ionic transport is due to some nanoscale phenomena as well as well-known macroscale ones. Increasing the ionic mobility enhances the ionic transport at both macro- and nanoscale whereas the temperature dependency of the surface properties of the nanochannel walls leads to a nanoscale effect on the ionic transport. The nanoscale effect appears only in EDL overlapping regimes[1] where the ionic transport is influenced by the wall effects. As it was illustrated in Figure 5-5, the electric conductance of a nanofluidic channel can be increased more than one order of magnitude by a temperature rise of 60°C at low ionic concentration for a silica nanochannel. This modulation factor can provide the possibility of gating in nanoscale fluidic channels.

In this chapter, a new phenomenon for gating the ionic transport in nanoscale channels is introduced.

To this aim, the nanofluidic device should be integrated with heaters that can increase the nanochannel temperature. Moreover, the response time of the gate to the external stimuli needs to be small enough, so that the channel opening and closing occurs in an acceptable time scale, which implies that the heating and cooling processes should be fast. Local heating of the nanochannel can decrease the response time as well as the required heat flux to assess a certain temperature. Joule heating of a thin layer of metal that is embedded close to the nanochannel or using plasomnic hot spot (Braun and Cichos, 2013; Nicoli et al., 2014) can appropriately heat up the nanochannel locally.

The local heating will generate a large thermal gradient, which may cause thermophoretic migrations (Belkin et al., 2014; Nicoli et al., 2014). The thermophoretic migration of species inside an electrolyte depends on various factors such as salinity and temperature of the solution, size, charge and hydration shell of the solute as well as the interactions between different solutes (Belkin et al., 2014; Braun and Cichos, 2013). The thermophoresis migration of species may cause a reduction or an increase of the electric current inside the nanochannel depending on the direction of migration.

[1] See 4.5.1.1.

6.2 Experimental setup

The nanofluidic devices used integrated micro-heaters over the nanochannels in order to control the fluidic transport. The micro-heaters are 72, 20 and 10 µm in width platinum electrodes placed over a 500 nm silicon dioxide layer on top of the arrays of nanochannels with 110 µm in length, 3 µm in width and 40 nm in height as described in 3.1.7.

The temperature controlled plate that was explained in 5.3.1.3 was used to keep the external chip temperature at 3±1 °C. A thermally conductive paste was used between the device and the plate in order to enhance the heat transfer. Working at low temperature helps to better illustrate the thermal gating phenomenon by increasing the working temperature range. The measurement circuit is also similar to the one described in 5.3.1.2.

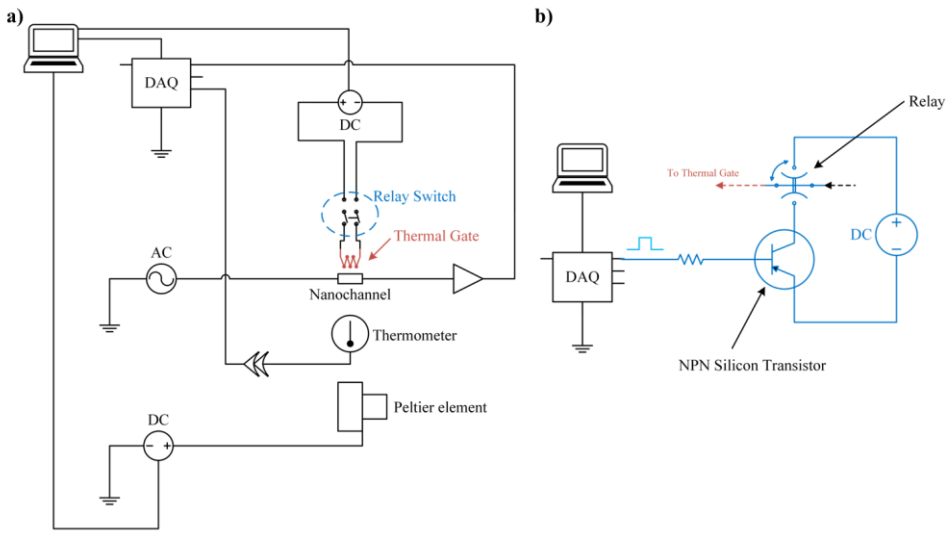

Figure 6-1. Sketch of the measurement and gate circuits. a) The Peltier element is used to keep the device temperature at 3±1°C. the measurement circuit is similar to the one used in the previous chapter. There is a relay switch that allows applying short heat pulses to the thermal gate. b) The schematic of the switch circuit. An NPN type transistor is used to drive the relay. The transistor, itself, is controlled by digital commands from DAQ.

The gate is in the off-state when the temperature is low and it turns to the on-state by heating up the micro-heater and the nanochannel. A relay switch was used to control the on-state pulse time in order to have a unique on-state time in all measurements. Figure 6-1.a shows the schematic of the experimental setup. The switch circuit, as depicted in Figure 6-1.b, uses an NPN silicon transistor (ST microelectronics, BD241) to derive the 2-pole relay (Tianbo, HJR1-2C). the operating and release time of the relay is 6 and 4 ms, which is in the right range while the minimum measurable pulse time is 50ms. Antisymmetric voltages were applied to the gate, so that the gate electric potential of the electrode over the nanochannel region was zero and no electrostatic gating effect appeared inside the nanochannel. Moreover, the 2-pole relay switches to both positive and negative voltages to prevent the transient electrostatic effects inside the nanochannel.

The nanochannel was heated up by applying electric DC current to the thermal gate. The resistance of the nanochannel was then measured by applying an AC signal to the measuring electrodes.

6.3 Liquid temperature inside the nanochannel

The average temperature of the liquid inside the nanochannel was estimated by relating the resistance of the nanochannel at 1 M to temperature. At high ionic concentration, the change of conductivity is dominated by the ionic mobility. As discussed in the previous chapter, the temperature dependence of the conductivity at high salt concentrations is converging to the bulk value, which is $\alpha = 1.8 - 2\ \%°C^{-1}$ for a potassium chloride solution. Therefore, measuring the conductance of the nanochannel at 1 M can be used to estimate the average temperature inside the nanochannel.

The term ‘‘average temperature’’ is used here since there is a variation of temperature from the hot region of the gate to the cold region of the reservoirs along the nanochannel. The average temperature represents the average conductivity of the nanochannel[1]. Figure 6-4.a-d depicts the temperature distribution inside the nanochannel while the gate temperature reaches 100 °C. The arithmetical average temperature inside the nanochannel is 88 °C for a gate of 72 μm in width while it is 62 °C and 69 °C for 10 μm and 20 μm in width gates. The temperature distribution was calculated using a numerical simulation that was conducted with the COMSOL finite elecment method software (COMSOL Multiphysics 4.4). The normal time-dependent heat transfer equations in solids were solved for the device geometry while its temperature at the bottom and top was kept at 5 °C and 25 °C, respectively. The heat pulse was modeled as a heat source in the platinum part over the nanochannel, just after the whole device reached the steady state in absence of the heat source. The water was assumed stationary in the whole device and was modeled as the solid.

In order to estimate the average temperature of the liquid present in the nanochannel experimentally, the temperature of the whole device was changed from 2 to 95°C with the temperature controlled Peltier element, *ie* the setup described in the previous chapter. The electrical conductance of the nanochannel was calibrated such that it can be used to estimate the average temperature inside the nanochannel at different applied gate powers for a 1 M potassium chloride solution. ure 6-4.e shows the evolution of average temperature versus the applied power to the gate of 72 μm in width. The values of power correspond to the proportion of power consumed in the nanochannel region of the gate electrode. Based on the data from numerical and experimental investigations of the nanochannel temperature (Figure 6-4), the maximum temperature of the 72 μm in width thermal gate is about 100 °C when a power of 575 mW is applied to the gate. ($V_{DC} = 8.0\ V$)

[1]The average conductivity was defined in 4.6, page 61.

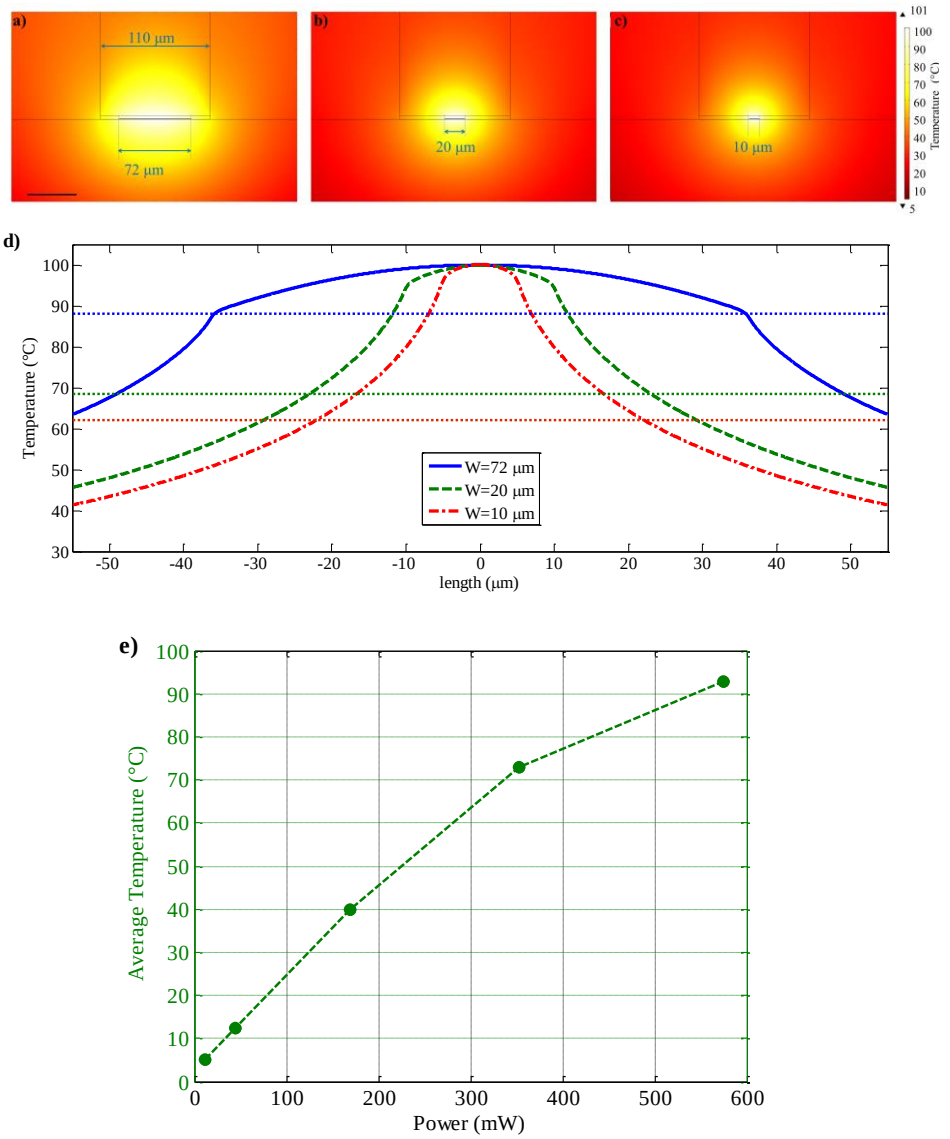

Figure 6-2. Simulation: The temperature distribution in the device 5 s after the thermal gate is turned on. The gate width is 72 µm (a) 20 µm (b) and 10 µm (c) while the nanochannel length is 110 µm. The gate temperature is around 100°C. the scale bar indicates 50 µm. d) Longitudinal temperature distribution at the middle of nanochannel 5 s after the gate is turned on. The dotted lines show the arithmetical average temperature. The wider the gate, the higher the average temperature. Experiment: e) The evolution of average temperature of the nanochannel measured by calibrating its electrical conductance versus the applied power.

6.4 Effectiveness of the thermal gate

Figure 6-3 depicts the effectiveness[1] of the thermal gate at different ionic concentrations and for deionized water for the gate width of 72 μm. Activating the the thermal gate increases the ionic flux more than one order of magnitude at low ionic concentrations. the electrostatic field caused by the wall surface charge influences the ionic transport since the electric double layer (EDL) overlaps at low ionic concentration. As mentioned in the previous chapter, heating the nanochannel will increase the surface charge density of the silica wall. More ions are attracted toward the nanochannel and its electric conductance increases. Moreover, heating up an aqueous solution increases the ionic mobility by decreasing its viscosity. This occurs for both the bulk and the overlapping EDL regimes. Therefore, a smaller relative change of the electric conductance happens at high ionic concentrations. Although the effectiveness is lower at high ionic concentration, modulating the ionic transport at high ionic concentrations is a clear advantage of the thermal gating method over its electrostatic field effect counterpart. The electrostatic field cannot be used to modulate the ionic transport at high ionic concentrations.

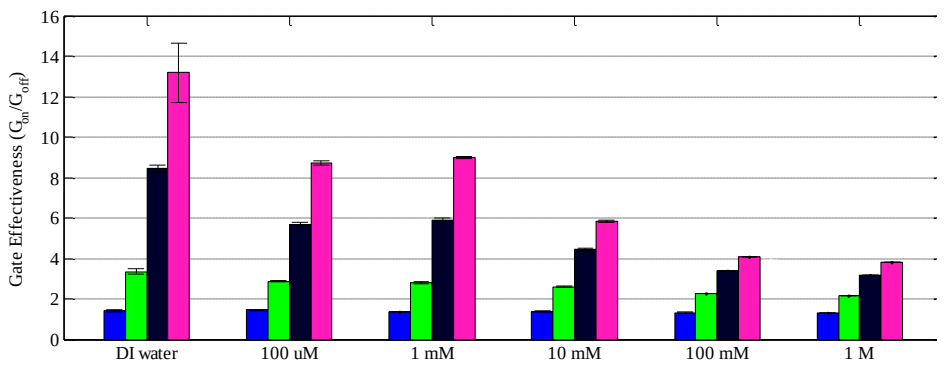

Figure 6-3. a) The gate effectiveness for $V_{DC} = 8.0\ V$ (pink), $V_{DC} = 6.0\ V$ (black), $V_{DC} = 4.0\ V$ (green), $V_{DC} = 2.0\ V$ (blue) at different ionic concentrations. The power applied to a 2.5 mm in length gate electrode is 570 mW at ΔT=90°C. The gate effectiveness is higher at low ionic concentrations. The nanochannel length is 110 μm while the width of the gate is only 72 μm. b) The gate effectiveness for a device with a gate of 20 μm in width. The error bars show the 95% confidence interval for 5 measurements.

The evolution of the gate effectiveness versus the average temperature is depicted in Figure 6-4 at different ionic concentrations. First, it emphasizes that controlling the temperature is a very powerful tool for modulating the ionic transport inside the nanochannel. Second, the modulation is possible at high ionic concentration, too. Third, in contrast to bulk regimes, the increase of the gate effectiveness is not a linear function of the average temperature inside the nanochannel. This implies that the surface charge is a polynomial function of the temperature that agrees

[1] The gate effectiveness was defined in 2.2.2

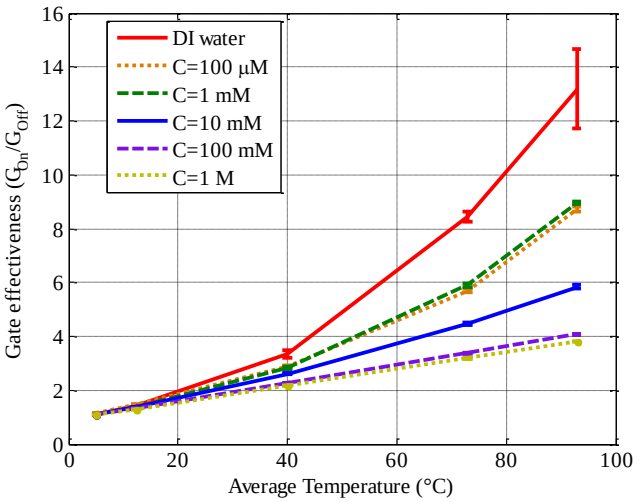

Figure 6-4. Evolution of gate effectiveness versus the average temperature at different ionic concentrations. The results clearly illustrate the major difference between low and high salinity.

with the variation of the equilibrium constant of the surface reactions depicted in Figure 5-1.

In order to clarify the effect of the wall surface charge, the gating effectiveness of 1 mM potassium chloride solutions at two different *pH* values has been investigated. As the point of zero charge (PZC) for a silicon dioxide surface is at *pH=3*[1], the surface charge of the nanochannel wall is very low at *pH=4*, while a much higher negative charge is expected at *pH=7*. Therefore, the dependence of the conductance of the nanochannel on the wall surface charge should be lower at *pH=4*. Consequently, at this *pH*, the sensitivity of the wall surface charge to temperature is low and the increase of the electric conductance can only be related to the bulk effects. Figure 6-5 illustrates the contribution of the enhancement of the surface charge effect due to the temperature increase for both solutions. A 1 M potassium chloride solution is used as a bulk control to demonstrate only the ionic mobility dependence of the electric conductance to the temperature. As shown in the Figure 6-5, the gate effectiveness of the solution at *pH=4* is close to the bulk while there is a major increase at *pH=7*. This difference emphasizes that the effectiveness of the thermal gate is mainly caused by the unique nanofluidic effect due to the charged wall. However, the effectiveness at the bulk regime is still comparable to the ones of other gating methods.

[1] See 4.5.

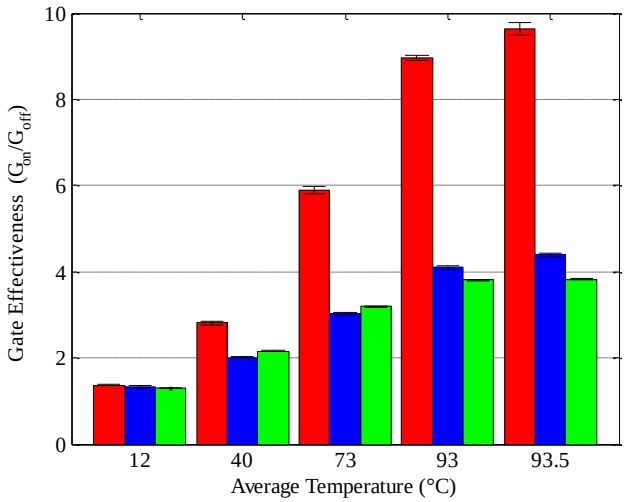

Figure 6-5. Effect of wall surface charge on the gate effectiveness. The figure compares the gate effectiveness for a 1 mM potassium chloride solution at pH=7 (red) to a solution of the same concentration at pH=4 (blue) while the solution at 1 M (green) shows the bulk behavior. At *pH=4*, the wall surface charge is low and consequently the sensitivity of the conductance of the nanochannel to temperature is low. At this condition, the increase of the nanochannel conductance is close to the one of the bulk. The nanochannel length is 110 μm while the width of the gate is only 72 μm. The error bars show the 95% confidence interval for 5 measurements.

6.5 Thermal gate v*ersus* other gating methods

Recalling Table 2-1 that compared the effectiveness of different gating method helps to evaluate the thermal gate in terms of its effectiveness. The last column of the table represented the values of the reported gate effectiveness for various nanofluidic transport gating methods. The reported values were the maximum achieved performances in the mentioned publications. For the case of the electrostatic gating, the ratio of maximum to minimum electric conductance was defined as the gate effectiveness.

Figure 6-6 compares the effectiveness of the mentioned gating mechanisms with the thermal gate. The gate effectiveness is less than 5 for most of the cases while the thermal gate achieved an effectiveness of more than 13. A small value of the gate effectiveness implies that the ionic transport can neither be stopped completely nor be enhanced considerably. The presented gating methods are only successful to modulate the ionic transport.

For the thermal gate, the effectiveness of the gating method exceeds one order of magnitude at low ionic concentrations while other gating methods have a considerably lower effectiveness. Heating the nanochannel does not need complicated microfabrication processing whereas other methods need complicated implementation. Moreover, the thermal gate does not suffer from the limitations in device manufacturing such as dielectric breakdown limitations for the field effect gating method. The thermal gate can easily be combined with other mechanisms in order to enhance the gating resolution and effectiveness.

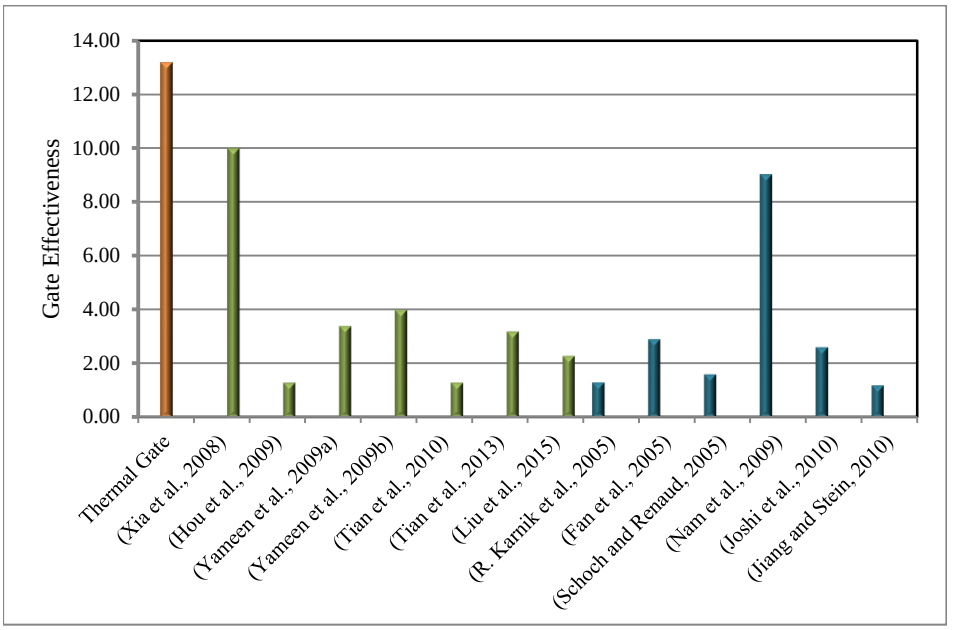

Figure 6-6. Comparison of the effectiveness of thermal gate with other reported results. The thermal gate is more effective than all the published works. The green bars used steric effect while the blue bars employed the field effect in order for gating the nanofluidic transport.

6.6 The effect of the gate width

The effectiveness of the thermal gate can be increased by using wider electrodes over the nanochannel. Using a wider electrode results in a uniform temperature inside the nanochannel, which leads to a larger highly conductive region inside the nanochannel and a higher gate effectiveness. Figure 6-7 demonstrates the maximum achieved gate effectiveness for three gates of different widths at different ionic concentrations. The wider gate has a higher effectiveness. At high ionic concentrations, in absence of the wall effects, the gate effectiveness can represent the average temperature inside the nanochannel. According to Figure 6-7, the average achieved temperature inside the nanochannel increases by increasing the gate width, which is in line with the numerical simulation presented in ure 6-2.d. Nevertheless, the trend is not similar at low ionic concentration where the wall effects are dominant.

The effect of the thermophoretic migration of ions toward or away from the nanochannel may influence the ionic transport inside the nanochannel. At first glance, the ionic concentration dependence of the thermophoresis can be suspected as the reason of considerable differences between nanofluidic and bulk regimes at low and high ionic concentrations. However, inspecting the properties of thermophoretic migration allows to reject this hypothesis. First, the thermophoretic depletion on ions from the hot region is time dependent while the result shows a negligible time dependency of the open-state electric conductance. Second, the concentration change due to thermophoresis is negligible relative to the nanofluidic effects present at low concentration.

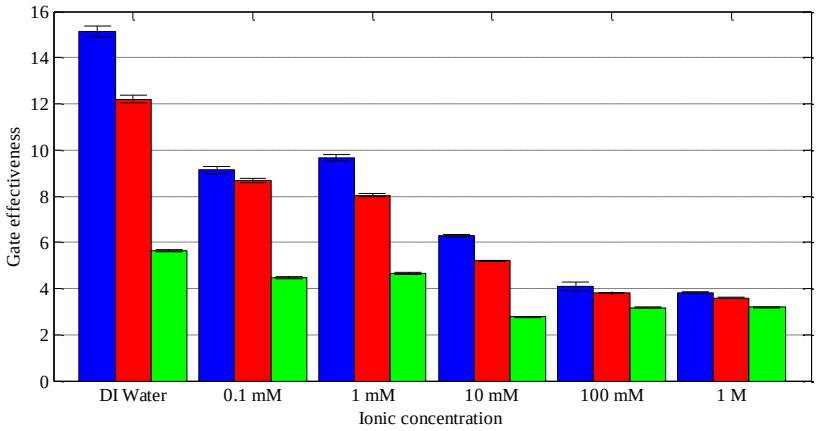

Figure 6-7. Comparison of the gate effectiveness for 72 μm (blue), 20μm (red) and 10 μm (green) in width electrodes at different ionic concentrations. The wider the gate electrode, the higher the gate effectiveness. Wider gate heats up a larger region of the nanochannel. The error bars show the 95% confidence interval for 5 measurements.

6.7 Response time of the thermal gate

Figure 6-8 shows the temperature distribution inside the nanochannel at different times after switching the gate on. The response time of the thermal gate to reach its maximum effectiveness is less than a second. Nevertheless, it does not mean that the gate is not working, before reaching this point. Moreover, considering that the time constant for the diffusion of an H^+ ion into the nanochannel is more than one second, which implies that the thermal gate is faster than other influential physiochemical processes to modulate the nanofluidic transport.

The response time of thermal gate is determined, on one hand, by the thermal diffusivity of the materials, which determines the dynamical temperature profile, and on the other hand, by the ion diffusion and the reaction rate of surface reactions,

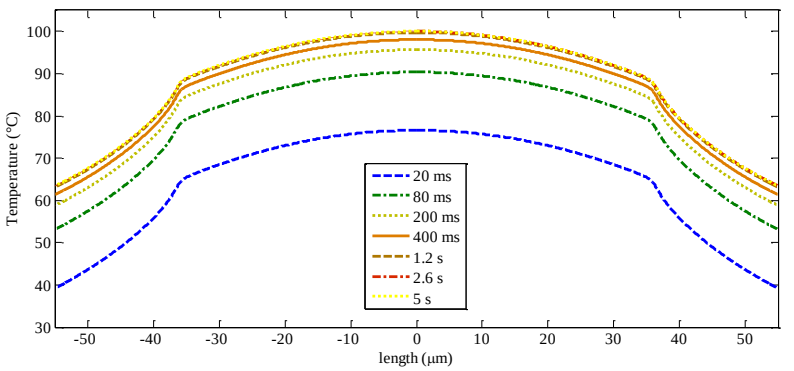

Figure 6-8. Temperature distribution inside the nanochannel at different time steps after truing on the gate of 72 in width. In less than one second the nanochannel reaches its maximum temperature.

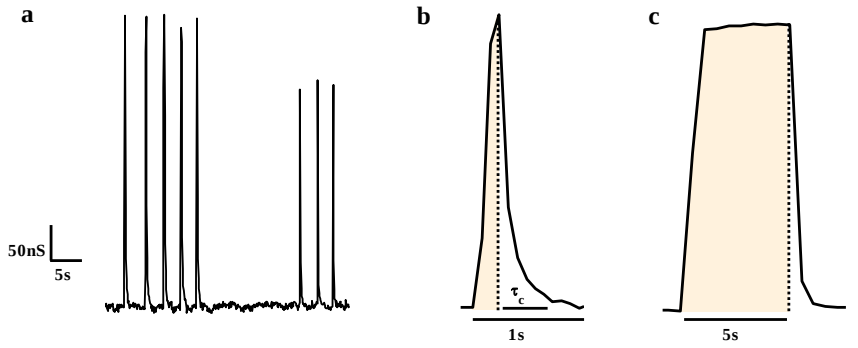

Figure 6-9. **a**) Short time pulses can be applied for thermal gating. The signal shows five 200 ms (left) and three 50 ms (right) on-state pulses at 1M ionic concentration. **b**) A zoomed view of a 200 ms pulse. Both opening and closing occur in a relatively short period of time. **c**) A single 5 s pulse. The closing process is still quick, even if the gate is kept open for a longer time.

which determine the dynamical ion concentration profile in the case of change of surface charge. In Figure 6-9, some examples of the applied thermal pulses are depicted. 200 ms pulses (left side of Figure 6-9**.a**) have higher effectiveness than 50 ms pulses (right side), which is correct according to Figure 6-8. Figure 6-9.b shows the opening and closing process of a single 200 ms pulse. The closing process needs more time than the opening one. In our particular design, the typical closing time is about $\tau_c \cong 400\ ms$ whereas the opening is much faster. The closing time is indicated by τ_c in the figure. As depicted in Figure 6-9.**c**, for longer pulses, we clearly see the thermal time constant on both opening and closing transitions.

For the case of pure thermal diffusion, the opening and closing time should be equal when the temperature reaches its steady state level. Therefore, the difference in opening and closing times is caused by another factor such as thermophoresis.

The pulses Figure 6-9.a-c correspond to a 1 M ionic concentration, which is considered as bulk regime ionic transport. Therefore, the result can represent the average temperature inside the nanochannel at any ionic concentration using the calibration that was performed before[1]. Alternatively, it can represent the proportion of the ionic mobility in enhancement of the ionic transport. At lower ionic concentrations, the additional effect of the surface charge appears.

Figure 6-10 depicts 5 s pulses at different ionic concentrations. First, it emphasizes the additional increase of the gate effectiveness at low ionic concentrations that occurs only in the EDL overlapping regime. Secondly, it shows that the gating dynamics at low ionic concentration is different from the one of the bulk regime. As represented in Figure 6-10, the electric conductance does not settle down instantly to its off-state value. By switching the gate off, the electric conductance decreases to a value higher than the normal off-state. This decrease occurs in a time in the order of τ_c. Then, it decreases to the normal value of the off-state with

[1] See 6.3.

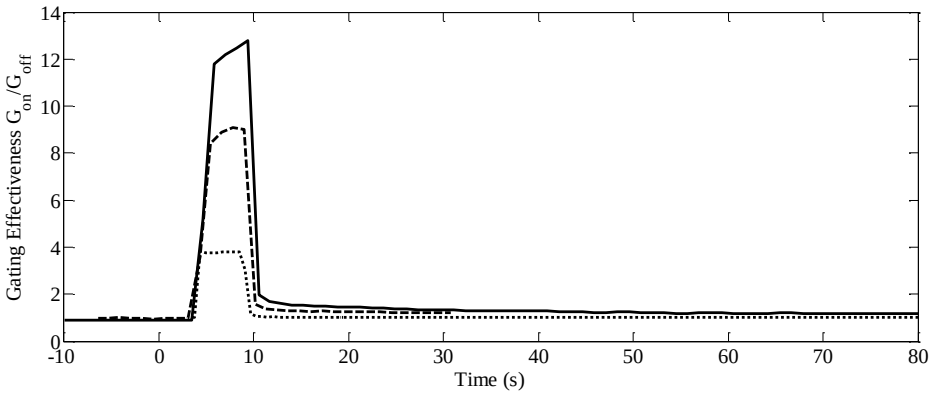

Figure 6-10. Comparison of 5 s pulses at 1 M (dotted line), 1 mM (dashed line) ionic concentrations and DI water (solid line). The vertical axis shows the ratio of on- to off-states conductance. At low ionic concentration, the conductance needs an excess time to stabilize which results from the dynamical ion concentration profile.

a slower rate. Thus, the slower rate of settling down cannot be justified by the temperature. Beside, this effect appears only at low ionic concentrations where the nanofluidic regime occurs. In other words, it is dependent on the surface charge of the nanochannel.

6.8 Highlights

The most important properties of Thermal gate are as follows:

- Temperature can be exploited as an external stimulus to modulate the ionic transport inside the nanochannel.
- The thermal gate has a higher effectiveness and requires less technological implementations compared to other gating mechanisms
- The thermal gate can modulate the ionic transport in both the bulk and EDL overlapping regime.
- The higher the gate width, the higher the achievable average temperature and gate effectiveness.
- The thermal gate is fast enough to be used for the manipulation of small molecules inside nanofluidic channels.

Chapter 7
Conclusions and Outlook

Nanofluidic transport through solid-state nanometer-size channels can be controlled using an external stimulus. In the previous chapters, different mechanisms for controlling the nanofluidic transport were studied, a new mechanism was introduced and the theoretical background that supports the new gating mechanism was discussed. This chapter summarizes the findings of the present thesis and suggestions for future investigations and development.

7.1 State of the art

The recent advances in the fabrication of nanofluidic features, the nanofluidic apertures platforms and their applications were surveyed. Particularly, the possibility of controlling the ionic and fluidic transport at the nanoscale was evaluated. Different reported gating mechanisms were investigated and their properties were compared. Using the steric volume exclusion effect of macro-molecules to occlude the channel, employing the effect of the electrostatic field to influence the fluidic transport and modulating the surface wettability, have been reported as gating mechanisms in nanofluidic studies.

Most of the research groups used the nanopore platform for gating studies. The nanochannel and nanotube platforms were only used for field effect gating. The size of the conduits varies from less than 10 nm up to 35 nm, which is much larger than the 2-3 nm size of cell-membranes ion channels. In terms of gating effectiveness, although the reported devices can modulate the ionic transport, the range of modulation is not large enough to be able to open or close the channel completely. This level of sensitivity allows the nanofluidic devices to be used for sensing applications. Nevertheless, compared to ion channels, that allows only a specific ion of interest to pass, the solid-state counterparts still need improvements.

It is expected to have combinations of different gating mechanisms in order to enhance the resolution and selectivity of the gating. New gating methods might also be introduced as far as the fluid transport at the nanoscale is better understood and the related technologies are developed. The thermal gate is an example of new possible gating methods.

The integration of a highly effective gating mechanism to nanopipets will have a great impact on the technological side of the nanofluidics. The unique characteristics of nanopipets such as simple fabrication, cost effective and easy integration to macroscale would make it an ideal platform for single molecule manipulation and detection if gating could be implemented in such devices.

7.2 Microfabrication

Standard microfabrication techniques were utilized and nanofluidic channels of 30-45 nm in height, 2-5 μm in width and 20-110 μm in length were fabricated in silicon dioxide using a ‘‘sacrificial layer’’ method. Platinum electrodes were embedded close to the entrance of the nanochannels for electrical measurements. Some other electrodes were placed over the nanochannels for the purpose of sensing and gating. The microfabrication process was simple since it didn’t need further steps for microscale integration.

7.3 Analytical modeling

A new model was developed for the nanochannel electric conductance based on the surface reactions and taking in account contribution of dissociated H^+ and OH^- ions. In this model, the surface charge density cannot be considered constant for all ionic concentrations. It decreases for more dilute solutions, which leads to a

lower conductance of the nanochannel. However, considering the role of H^+ ions in the nanochannel conductance results in an increase of electric conductance at low ionic concentrations, due to the high ionic mobility of H^+ ions.
The model was validated by the experimental measurements. The electrical conductance of nanochannels was measured using an AC impedance analysis at different ionic concentrations. There was a good agreement between both analytical and experimental results.
Our model is capable of estimating the nanochannel conductance for different physiochemical conditions of symmetric electrolytes.
In terms of future developments, the model should be improved to consider the EOF in the measurements. Moreover, improving the accuracy of the electric potential distribution inside the nanochannel for the case of the EDL overlapping regime is necessary.
Modifying the model to consider the unique properties of nanopores such as the small length to diameter ratio, will result in a better tool for estimating the electrical conductance in nanopores.
Measureing the electrical conductance of nanochannels with different surface chemistry will be useful in order to validate the model.

7.4 The influence of temperature on nanofluidic transport

The effect of temperature on the nanochannel electrical conductance was studied. The results showed that the response of the ionic transport at the nanoscale and in the bulk to a temperature variation are not similar. At the nanoscale, the ionic transport can be more sensitive to temperature.
The surface charge of the nanochannel walls depends on temperature, which causes the temperature sensitivity of the nanochannel conductance to be different from the bulk in the EDL overlapping regime. For a silicon dioxide nanochannel, the temperature sensitivity of the electrical conductance is higher at low ionic concentrations.
This implies that using the bulk values of the temperature sensitivity of the electric conductance in a nanochannel configuration leads to major errors at low ionic concentrations. An error of 8 percent was measured for only 2°C temperature difference at low ionic concentrations in a silicon dioxide nanochannel filled with 1 mM potassium chloride solution. This implies that different experiments that use the nanochannel electrical measurements should consider the temperature effect correctly.
The error is more considerable for temperature changes of more than tens of degrees. At this condition, neglecting the nanoscale effects may result in a measurement error of more than one order of magnitude at low ionic concentrations. In this situation, using equations that are valid for the bulk should be avoided for equivalent temperature estimations inside the nanochannel.
The analytical modeling predicted more than one order of magnitude increase in nanochannel conductance compared to bulk values for a 60°C temperature rise. This influence of temperature on nanochannel conductance suggests a new possibility of nanofluidic transport modulation, that was introduced in the present the-

sis with in the name ‘‘thermal gate’’. Furthermore, the temperature sensitivity of nanochannels is a strong function of the enthalpy change of surface reactions at low ionic concentrations, which leads to a new method for measuring the enthalpy change of different surface reactions.
This study can be improved by experimental investigations of the temperature sensitivity of the electrical conductance of the nanochannel at different pH values. Moreover, measuring the enthalpy of different surface types is useful. Specially, measuring the enthalpy of reactions of the functional groups of an immobilized molecule can offer new and valuable information.

7.5 Thermal gate

The possibility of controlling the ionic transport in nanochannels using the thermal gating was developed and introduced in this thesis for the first time. The thermal gate modulates the ionic transport by heating up the nanochannel. It increases the ionic transport *via* raising both the ionic mobility and the surface charge of the nanochannel wall.
According to the two mentioned mechanisms of increasing the ionic flux with temperature, summarized in the previous section, the effectiveness of the thermal gate is dependent on the ionic concentration. At low ionic concentration, a high effectiveness was achieved while it decreased by increasing the ionic concentration. In contrast to the field effect gating method, the thermal gating could still modulate the ionic transport at bulk regimes.
The thermal gate effectiveness was compared to other gating mechanisms. The thermal gate has a higher effectiveness and requires less technological restrictions compared to other gating mechanisms.
The response time of the thermal gate was also investigated. The thermal gate is fast enough to be used for the manipulation of small molecules inside nanofluidic channels. A time response in the order of tens of milliseconds was observed for the opening process. The closing process needed hundreds of milliseconds at the maximum achieved effectiveness.
The thermal gate can be used in applications that require controlling the ionic or fluidic transport at the small scale. The thermal gate has the possibility of being stimulated remotely, which is an advantage over the field effect gating method. It can remotely control the delivery process of sub-femtoliter volumes.
The thermal gate can be combined with other gating mechanisms in order to enhance the effectiveness of gating. For example, a combination of thermal gate and immobilized temperature sensitive polymer is a good option for gating.
The integration of the thermal gate in a solid state nonporous membrane can illustrate its potential as a practical gating mechanism. The heating process can be carried out either by joule heating or by plasmonic effects.
Optical observation of the fluid flow inside the thermally gated nanochannels using fluorescent nanoparticles like quantum dots can be used to investigate how the thermal gate influences the ionic transport.
One of the specifications of the thermal gate is its possibility to generate a high temperature gradient up to 5 $°C.\mu m^{-1}$. This large temperature gradient can cause a

considerable thermophoretic migration of the ions inside the nanochannel. This property can be employed to create an ionic pump by using a small number of electrodes working in a programmed manner.
A combination of the thermal effect and the electrostatic effect would lead to the fabrication of effective devices for trapping a single DNA molecule and observing a polymer chain reaction (PCR).

Bibliography

Ali, M., Nasir, S., Ramirez, P., Cervera, J., Mafe, S., Ensinger, W., 2013. Carbohydrate-Mediated Biomolecular Recognition and Gating of Synthetic Ion Channels. J. Phys. Chem. C 117, 18234–18242. doi:10.1021/jp4054555

Ali, M., Neumann, R., Ensinger, W., 2010. Sequence-Specific Recognition of DNA Oligomer Using Peptide Nucleic Acid (PNA)-Modified Synthetic Ion Channels: PNA/DNA Hybridization in Nanoconfined Environment. ACS Nano 4, 7267–7274. doi:10.1021/nn102119q

Alishahi, M., Kamali, R., Abouali, O., 2015. Molecular dynamics study of electric double layer in nanochannel. Russ. J. Electrochem. 51, 49–55. doi:10.1134/S1023193515010024

Atkins, P., de Paula, J., 2013. Elements of Physical Chemistry. OUP Oxford.

Baldessari, F., Santiago, J.G., 2009. Corrigendum to "Electrokinetics in nanochannels. Part I. Electric double layer overlap and channel-to-well equilibrium" [J. Colloid Interface Sci. 325 (2008) 526–538]. J. Colloid Interface Sci. 331, 539–546. doi:10.1016/j.jcis.2008.12.013

Baldessari, F., Santiago, J.G., 2006. Electrophoresis in nanochannels: brief review and speculation. J. Nanobiotechnology 4, 12. doi:10.1186/1477-3155-4-12

Banerjee, S., Wilson, J., Shim, J., Shankla, M., Corbin, E.A., Aksimentiev, A., Bashir, R., 2015. Slowing DNA Transport Using Graphene–DNA Interactions. Adv. Funct. Mater. 25, 936–946. doi:10.1002/adfm.201403719

Barry, P.H., Lynch, J.W., 1991. Liquid junction potentials and small cell effects in patch-clamp analysis. J. Membr. Biol. 121, 101–117. doi:10.1007/BF01870526

Belkin, M., Chao, S.-H., Giannetti, G., Aksimentiev, A., 2014. Modeling thermophoretic effects in solid-state nanopores. J. Comput. Electron. 13, 826–838. doi:10.1007/s10825-014-0594-8

Belkin, M., Maffeo, C., Wells, D.B., Aksimentiev, A., 2013. Stretching and Controlled Motion of Single-Stranded DNA in Locally Heated Solid-State Nanopores. ACS Nano 7, 6816–6824. doi:10.1021/nn403575n

Bérubé, Y.G., de Bruyn, P.L., 1968. Adsorption at the rutile-solution interface: I. Thermodynamic and Experimental Study. J. Colloid Interface Sci. 27, 305–318. doi:10.1016/0021-9797(68)90038-6

Bocquet, L., Charlaix, E., 2010. Nanofluidics, from bulk to interfaces. Chem. Soc. Rev. 39, 1073. doi:10.1039/b909366b

Braun, M., Cichos, F., 2013. Optically Controlled Thermophoretic Trapping of Single Nano-Objects. ACS Nano 7, 11200–11208. doi:10.1021/nn404980k

Buchsbaum, S.F., Nguyen, G., Howorka, S., Siwy, Z.S., 2014. DNA-Modified Polymer Pores Allow pH- and Voltage-Gated Control of Channel Flux. J. Am. Chem. Soc. 136, 9902–9905. doi:10.1021/ja505302q

Burgreen, D., Nakache, F.R., 1964. Electrokinetic Flow in Ultrafine Capillary Slits1. J. Phys. Chem. 68, 1084–1091. doi:10.1021/j100787a019

Cheng, L.-J., Guo, L.J., 2009. Ionic Current Rectification, Breakdown, and Switching in Heterogeneous Oxide Nanofluidic Devices. ACS Nano 3, 575–584. doi:10.1021/nn8007542

Daiguji, H., Oka, Y., Shirono, K., 2005. Nanofluidic Diode and Bipolar Transistor. Nano Lett. 5, 2274–2280. doi:10.1021/nl051646y

Daiguji, H., Yang, P.D., Majumdar, A., 2004. Ion transport in nanofluidic channels. Nano Lett. 4, 137–142. doi:10.1021/nl0348185

Davis, J.A., James, R.O., Leckie, J.O., 1978. Surface ionization and complexation at the oxide/water interface: I. Computation of electrical double layer properties in simple electrolytes. J. Colloid Interface Sci. 63, 480–499. doi:10.1016/S0021-9797(78)80009-5

De Keizer, A., Fokkink, L.G.J., Lyklema, J., 1990. Thermodynamics of proton charge formation on oxides. Microcalorimetry. Colloids Surf. 49, 149–163. doi:10.1016/0166-6622(90)80099-P

de Vreede, L.J., van den Berg, A., Eijkel, J.C.T., 2015. Nanopore Fabrication by Heating Au Particles on Ceramic Substrates. Nano Lett. 15, 727–731. doi:10.1021/nl5042676

Duan, C., Karnik, R., Lu, M.-C., Majumdar, A., 2012. Evaporation-induced cavitation in nanofluidic channels. Proc. Natl. Acad. Sci. 109, 3688–3693. doi:10.1073/pnas.1014075109

Duan, C., Majumdar, A., 2010. Anomalous ion transport in 2-nm hydrophilic nanochannels. Nat. Nanotechnol. 5, 848–852. doi:10.1038/nnano.2010.233

Duan, C., Wang, W., Xie, Q., 2013. Review article: Fabrication of nanofluidic devices. Biomicrofluidics 7. doi:10.1063/1.4794973

Durand, N., 2010. Biomolecular Diffusion in Nanofluidics. EPFL, Lausanne.

Durand, N.F.Y., Saveriades, E., Renaud, P., 2008. Detecting proteins complex formation using steady-state diffusion in a nanochannel. Anal. Bioanal. Chem. 394, 421–425. doi:10.1007/s00216-008-2550-6

Eijkel, J.C.T., Berg, A. van den, 2010. Nanofluidics and the chemical potential applied to solvent and solute transport. Chem. Soc. Rev. 39, 957. doi:10.1039/b913776a

Eijkel, J.C.T., Berg, A. van den, 2005. Nanofluidics: what is it and what can we expect from it? Microfluid. Nanofluidics 1, 249–267. doi:10.1007/s10404-004-0012-9

Eijkel, J.C.T., van den Berg, A., 2010. Nanofluidics: Tiny electrostatic traps. Nature 467, 666–667. doi:10.1038/467666a

Fan, R., Yue, M., Karnik, R., Majumdar, A., Yang, P., 2005. Polarity Switching and Transient Responses in Single Nanotube Nanofluidic Transistors. Phys. Rev. Lett. 95, 086607. doi:10.1103/PhysRevLett.95.086607

Freedman, K.J., Jürgens, M., Prabhu, A., Ahn, C.W., Jemth, P., Edel, J.B., Kim, M.J., 2011. Chemical, Thermal, and Electric Field Induced Unfolding of Single Protein Molecules Studied Using Nanopores. Anal. Chem. 83, 5137–5144. doi:10.1021/ac2001725

Gajar, S.A., Geis, M.W., 1992. An Ionic Liquid-Channel Field-Effect Transistor. J. Electrochem. Soc. 139, 2833–2840. doi:10.1149/1.2068989

Girault, H.H., 2004. Analytical and Physical Electrochemistry, Fundamental sciences: Chemistry. EPFL Press.

Glover, P.W.J., Meredith, P.G., Sammonds, P.R., Murrell, S.A.F., 1994. Ionic surface electrical conductivity in sandstone. J. Geophys. Res. Solid Earth 99, 21635–21650. doi:10.1029/94JB01474

Goldberger, J., Fan, R., Yang, P., 2006. Inorganic Nanotubes: A Novel Platform for Nanofluidics. Acc. Chem. Res. 39, 239–248. doi:10.1021/ar040274h

Grahame, D.C., 1947. The Electrical Double Layer and the Theory of Electrocapillarity. Chem. Rev. 41, 441–501. doi:10.1021/cr60130a002

Guan, W., Fan, R., Reed, M.A., 2011. Field-effect reconfigurable nanofluidic ionic diodes. Nat. Commun. 2, 506. doi:10.1038/ncomms1514

Guo, W., Cheng, C., Wu, Y., Jiang, Y., Gao, J., Li, D., Jiang, L., 2013. Bio-Inspired Two-Dimensional Nanofluidic Generators Based on a Layered Graphene Hydrogel Membrane. Adv. Mater. 25, 6064–6068. doi:10.1002/adma.201302441

Guo, W., Xia, H., Xia, F., Hou, X., Cao, L., Wang, L., Xue, J., Zhang, G., Song, Y., Zhu, D., Wang, Y., Jiang, L., 2010. Current Rectification in Temperature-Responsive Single Nanopores. ChemPhysChem 11, 859–864. doi:10.1002/cphc.200900989

Han, J., Craighead, H.G., 1999. Entropic trapping and sieving of long DNA molecules in a nanofluidic channel. J. Vac. Sci. Technol. A 17, 2142–2147. doi:10.1116/1.581740

Harms, Z.D., Mogensen, K.B., Nunes, P.S., Zhou, K., Hildenbrand, B.W., Mitra, I., Tan, Z., Zlotnick, A., Kutter, J.P., Jacobson, S.C., 2011. Nanofluidic Devices with Two Pores in Series for Resistive-Pulse Sensing of Single Virus Capsids. Anal. Chem. 83, 9573–9578. doi:10.1021/ac202358t

Harrell, C.C., Kohli, P., Siwy, Z., Martin, C.R., 2004. DNA - Nanotube artificial ion channels. J. Am. Chem. Soc. 126, 15646–15647. doi:10.1021/ja044948v

Haywood, D.G., Saha-Shah, A., Baker, L.A., Jacobson, S.C., 2015. Fundamental Studies of Nanofluidics: Nanopores, Nanochannels, and Nanopipets. Anal. Chem. 87, 172–187. doi:10.1021/ac504180h

Helmholtz, H., 1853. Ueber einige Gesetze der Vertheilung elektrischer Ströme in körperlichen Leitern mit Anwendung auf die thierisch-elektrischen Versuche. Ann. Phys. 165, 211–233. doi:10.1002/andp.18531650603

Heng, J.B., Aksimentiev, A., Ho, C., Marks, P., Grinkova, Y.V., Sligar, S., Schulten, K., Timp, G., 2005. Stretching DNA Using the Electric Field in a Synthetic Nanopore. Nano Lett. 5, 1883–1888. doi:10.1021/nl0510816

Hille, B., 1978. Ionic channels in excitable membranes. Current problems and biophysical approaches. Biophys. J. 22, 283–294. doi:10.1016/S0006-3495(78)85489-7

Hou, X., Guo, W., Jiang, L., 2011. Biomimetic smart nanopores and nanochannels. Chem. Soc. Rev. 40, 2385–2401. doi:10.1039/C0CS00053A

Hou, X., Guo, W., Xia, F., Nie, F.-Q., Dong, H., Tian, Y., Wen, L., Wang, L., Cao, L., Yang, Y., Xue, J., Song, Y., Wang, Y., Liu, D., Jiang, L., 2009. A Biomimetic Potassium Responsive Nanochannel: G-Quadruplex DNA Conformational Switching in a Synthetic Nanopore. J. Am. Chem. Soc. 131, 7800–7805. doi:10.1021/ja901574c

Hou, X., Hu, Y., Grinthal, A., Khan, M., Aizenberg, J., 2015. Liquid-based gating mechanism with tunable multiphase selectivity and antifouling behaviour. Nature 519, 70–73. doi:10.1038/nature14253

Hsu, J.-P., Tai, Y.-H., Yeh, L.-H., Tseng, S., 2012. Importance of Temperature Effect on the Electrophoretic Behavior of Charge-Regulated Particles. Langmuir 28, 1013–1019. doi:10.1021/la203245n

Iler, R.K., 1979. The Chemistry of Silica: Solubility, Polymerization, Colloid and Surface Properties and Biochemistry of Silica. Wiley.

Ivanov, A.P., Instuli, E., McGilvery, C.M., Baldwin, G., McComb, D.W., Albrecht, T., Edel, J.B., 2011. DNA Tunneling Detector Embedded in a Nanopore. Nano Lett. 11, 279–285. doi:10.1021/nl103873a

Jensen, K., Kristensen, J., Crumrine, A., Andersen, M.B., Bruus, H., Pennathur, S., 2011. Hydronium-dominated ion transport in carbon-dioxide-saturated electrolytes at low salt concentrations in nanochannels. Phys. Rev. E 83, 056307. doi:10.1103/PhysRevE.83.056307

Jiang, Z., Stein, D., 2011. Charge regulation in nanopore ionic field-effect transistors. Phys. Rev. E 83. doi:10.1103/PhysRevE.83.031203

Jiang, Z., Stein, D., 2010. Electrofluidic Gating of a Chemically Reactive Surface. Langmuir 26, 8161–8173. doi:10.1021/la9044682

Jonsson, M.P., Dekker, C., 2013. Plasmonic Nanopore for Electrical Profiling of Optical Intensity Landscapes. Nano Lett. 13, 1029–1033. doi:10.1021/nl304213s

Joshi, P., Smolyanitsky, A., Petrossian, L., Goryll, M., Saraniti, M., Thornton, T.J., 2010. Field effect modulation of ionic conductance of cylindrical silicon-on-insulator nanopore array. J. Appl. Phys. 107. doi:10.1063/1.3298468

Kaatze, U., 1997. The dielectric properties of water in its different states of interaction. J. Solut. Chem. 26, 1049–1112. doi:10.1007/BF02768829

Kallay, N., Preočanin, T., Žalac, S., Lewandowski, H., Narres, H.D., 1999. Electrostatic Contribution to the Enthalpy of Charging at Hematite/Electrolyte Interface. J. Colloid Interface Sci. 211, 401–407. doi:10.1006/jcis.1998.6003

Kalman, E.B., Sudre, O., Vlassiouk, I., Siwy, Z.S., 2009. Control of ionic transport through gated single conical nanopores. Anal. Bioanal. Chem. 394, 413–419. doi:10.1007/s00216-008-2545-3

Karnik, R., Castelino, K., Fan, R., Yang, P., Majumdar, A., 2005. Effects of Biological Reactions and Modifications on Conductance of Nanofluidic Channels. Nano Lett. 5, 1638–1642. doi:10.1021/nl050966e

Karnik, R., Castelino, K., Majumdar, A., 2006. Field-effect control of protein transport in a nanofluidic transistor circuit. Appl. Phys. Lett. 88. doi:10.1063/1.2186967

Karnik, R., Duan, C., Castelino, K., Daiguji, H., Majumdar, A., 2007. Rectification of Ionic Current in a Nanofluidic Diode. Nano Lett. 7, 547–551. doi:10.1021/nl062806o

Karnik, R., Fan, R., Yue, M., Li, D.Y., Yang, P.D., Majumdar, A., 2005. Electrostatic control of ions and molecules in nanofluidic transistors. Nano Lett. 5, 943–948. doi:10.1021/nl050493b

Kasianowicz, J.J., Brandin, E., Branton, D., Deamer, D.W., 1996. Characterization of individual polynucleotide molecules using a membrane channel. Proc. Natl. Acad. Sci. 93, 13770–13773.

Katayama, S., 1976. Conductimetric determination of ion-association constants for calcium, cobalt, zinc, and cadmium sulfates in aqueous solutions at various temperatures between 0°C and 45°C. J. Solut. Chem. 5, 241–248. doi:10.1007/BF00645461

Keyser, U.F., 2011. Controlling molecular transport through nanopores. J. R. Soc. Interface 8, 1369–1378. doi:10.1098/rsif.2011.0222

Kim, S.J., Ko, S.H., Kang, K.H., Han, J., 2010. Direct seawater desalination by ion concentration polarization. Nat. Nanotechnol. 5, 297–301. doi:10.1038/nnano.2010.34

Kowalczyk, S.W., Wells, D.B., Aksimentiev, A., Dekker, C., 2012. Slowing down DNA translocation through a nanopore in lithium chloride. Nano Lett. 12, 1038–1044. doi:10.1021/nl204273h

Kozak, D., Anderson, W., Vogel, R., Chen, S., Antaw, F., Trau, M., 2012. Simultaneous Size and ζ-Potential Measurements of Individual Nanoparticles in Dispersion Using Size-Tunable Pore Sensors. ACS Nano 6, 6990–6997. doi:10.1021/nn3020322

Laohakunakorn, N., Gollnick, B., Moreno-Herrero, F., Aarts, D.G.A.L., Dullens, R.P.A., Ghosal, S., Keyser, U.F., 2013. A Landau–Squire Nanojet. Nano Lett. 13, 5141–5146. doi:10.1021/nl402350a

Levine, S., Marriott, J.R., Neale, G., Epstein, N., 1975a. Theory of electrokinetic flow in fine cylindrical capillaries at high zeta-potentials. J. Colloid Interface Sci. 52, 136–149. doi:10.1016/0021-9797(75)90310-0

Levine, S., Marriott, J.R., Neale, G., Epstein, N., 1975b. Theory of electrokinetic flow in fine cylindrical capillaries at high zeta-potentials. J. Colloid Interface Sci. 52, 136–149. doi:10.1016/0021-9797(75)90310-0

Levine, S., Marriott, J.R., Robinson, K., 1975. Theory of electrokinetic flow in a narrow parallel-plate channel. J. Chem. Soc. Faraday Trans. 2 Mol. Chem. Phys. 71, 1–11. doi:10.1039/F29757100001

Li, J., Stein, D., McMullan, C., Branton, D., Aziz, M.J., Golovchenko, J.A., 2001. Ion-beam sculpting at nanometre length scales. Nature 412, 166–169. doi:10.1038/35084037

Liu, M., Zhang, H., Li, K., Heng, L., Wang, S., Tian, Y., Jiang, L., 2015. A Bio-inspired Potassium and pH Responsive Double-gated Nanochannel. Adv. Funct. Mater. 25, 421–426. doi:10.1002/adfm.201401655

Machevsky, M.L., Anderson, M.A., 1986. Calorimetric acid-base titrations of aqueous goethite and rutile suspensions. Langmuir 2, 583–587. doi:10.1021/la00071a009

Majumder, M., Chopra, N., Hinds, B.J., 2011. Mass Transport through Carbon Nanotube Membranes in Three Different Regimes: Ionic Diffusion and Gas and Liquid Flow. ACS Nano 5, 3867–3877. doi:10.1021/nn200222g

Malmberg, C.G., Maryott, A.A., 1956. Dielectric constant of water from 0° to 100° C. Journal of research of the National Bureau of Standards.

Marie, R., Kristensen, A., 2012. Nanofluidic devices towards single DNA molecule sequence mapping. J. Biophotonics 5, 673–686. doi:10.1002/jbio.201200050

Martins, D.C., Chu, V., Conde, J.P., 2013. The effect of the surface functionalization and the electrolyte concentration on the electrical conductance of silica nanochannels. Biomicrofluidics 7. doi:10.1063/1.4811277

Ma, Y., Yeh, L.-H., Lin, C.-Y., Mei, L., Qian, S., 2015. pH-Regulated Ionic Conductance in a Nanochannel with Overlapped Electric Double Layers. Anal. Chem. doi:10.1021/acs.analchem.5b00536

Nam, S.-W., Rooks, M.J., Kim, K.-B., Rossnagel, S.M., 2009. Ionic Field Effect Transistors with Sub-10 nm Multiple Nanopores. Nano Lett. 9, 2044–2048. doi:10.1021/nl900309s

Nasir, S., Ali, M., Ensinger, W., 2012. Thermally controlled permeation of ionic molecules through synthetic nanopores functionalized with amine-terminated polymer brushes. Nanotechnology 23, 225502. doi:10.1088/0957-4484/23/22/225502

Nicoli, F., Verschueren, D., Klein, M., Dekker, C., Jonsson, M.P., 2014. DNA Translocations through Solid-State Plasmonic Nanopores. Nano Lett. 14, 6917–6925. doi:10.1021/nl503034j

O'Hern, S.C., Jang, D., Bose, S., Idrobo, J.-C., Song, Y., Laoui, T., Kong, J., Karnik, R., 2015. Nanofiltration across Defect-Sealed Nanoporous Monolayer Graphene. Nano Lett. 15, 3254–3260. doi:10.1021/acs.nanolett.5b00456

Oh, Y.-J., Bottenus, D., Ivory, C.F., Han, S.M., 2009. Impact of leakage current and electrolysis on FET flow control and pH changes in nanofluidic channels. Lab. Chip 9, 1609–1617. doi:10.1039/b816384g

Oh, Y.-J., Gamble, T.C., Leonhardt, D., Chung, C.-H., Brueck, S.R.J., Ivory, C.F., Lopez, G.P., Petsev, D.N., Han, S.M., 2008. Monitoring FET flow control and wall adsorption of charged fluorescent dye molecules in nanochannels integrated into a multiple internal reflection infrared waveguide. Lab. Chip 8, 251–258. doi:10.1039/b711682a

Pardon, G., van der Wijngaart, W., 2013. Modeling and simulation of electrostatically gated nanochannels. Adv. Colloid Interface Sci. 199–200, 78–94. doi:10.1016/j.cis.2013.06.006

Pennathur, S., Santiago, J.G., 2005. Electrokinetic Transport in Nanochannels. 1. Theory. Anal. Chem. 77, 6772–6781. doi:10.1021/ac050835y

Powell, M.R., Cleary, L., Davenport, M., Shea, K.J., Siwy, Z.S., 2011. Electric-field-induced wetting and dewetting in single hydrophobic nanopores. Nat. Nanotechnol. 6, 798–802. doi:10.1038/NNANO.2011.189

Raillon, C., Cousin, P., Traversi, F., Garcia-Cordero, E., Hernandez, N., Radenovic, A., 2012. Nanopore Detection of Single Molecule RNAP–DNA Transcription Complex. Nano Lett. 12, 1157–1164. doi:10.1021/nl3002827

Reppert, P.M., Morgan, F.D., 2003a. Temperature-dependent streaming potentials: 1. Theory. J. Geophys. Res. Solid Earth 108, 2546. doi:10.1029/2002JB001754

Reppert, P.M., Morgan, F.D., 2003b. Temperature-dependent streaming potentials: 2. Laboratory. J. Geophys. Res. Solid Earth 108, 2547. doi:10.1029/2002JB001755

Revil, A., Glover, P.W.J., 1997. Theory of ionic-surface electrical conduction in porous media. Phys. Rev. B 55, 1757–1773. doi:10.1103/PhysRevB.55.1757

Revil, A., Pezard, P.A., Glover, P.W.J., 1999. Streaming potential in porous media: 1. Theory of the zeta potential. J. Geophys. Res. Solid Earth 104, 20021–20031. doi:10.1029/1999JB900089

Sanz, R., Johansson, A., Skupinski, M., Jensen, J., Possnert, G., Boman, M., Vázquez, M., Hjort, K., 2006. Fabrication of Well-Ordered High-Aspect-Ratio Nanopore Arrays in TiO2 Single Crystals. Nano Lett. 6, 1065–1068. doi:10.1021/nl0602185

Scales, P.J., Grieser, F., Healy, T.W., White, L.R., Chan, D.Y.C., 1992. Electrokinetics of the silica-solution interface: a flat plate streaming potential study. Langmuir 8, 965–974. doi:10.1021/la00039a037

Schasfoort, R.B.M., Schlautmann, S., Hendrikse, J., Berg, A. van den, 1999. Field-Effect Flow Control for Microfabricated Fluidic Networks. Science 286, 942–945. doi:10.1126/science.286.5441.942

Schoch, R.B., 2006. Transport phenomena in nanofluidics. EPFL, Lausanne.

Schoch, R.B., Bertsch, A., Renaud, P., 2006. pH-Controlled Diffusion of Proteins with Different pI Values Across a Nanochannel on a Chip. Nano Lett. 6, 543–547. doi:10.1021/nl052372h

Schoch, R.B., Han, J., Renaud, P., 2008. Transport phenomena in nanofluidics. Rev. Mod. Phys. 80, 839–883. doi:10.1103/RevModPhys.80.839

Schoch, R.B., Renaud, P., 2005. Ion transport through nanoslits dominated by the effective surface charge. Appl. Phys. Lett. 86, 253111. doi:10.1063/1.1954899

Schoch, R.B., Renaud, P., 2005. Ion transport through nanoslits dominated by the effective surface charge. Appl. Phys. Lett. 86, 253111. doi:10.1063/1.1954899

Segerink, L.I., Eijkel, J.C.T., 2014. Nanofluidics in point of care applications. Lab. Chip 14, 3201–3205. doi:10.1039/C4LC00298A

Shin, S., Kim, B.S., Song, J., Lee, H., Cho, H.H., 2012. A facile route for the fabrication of large-scale gate-all-around nanofluidic field-effect transistors with low leakage current. Lab. Chip 12, 2568–2574. doi:10.1039/C2LC40112F

Singh, K.P., Kumari, K., Kumar, M., 2011. Field-effect control of electrokinetic ion transport in a nanofluidic channel. J. Appl. Phys. 110. doi:10.1063/1.3651634

Siria, A., Poncharal, P., Biance, A.-L., Fulcrand, R., Blase, X., Purcell, S.T., Bocquet, L., 2013. Giant osmotic energy conversion measured in a single transmembrane boron nitride nanotube. Nature 494, 455–458. doi:10.1038/nature11876

Siwy, Z., Trofin, L., Kohli, P., Baker, L.A., Trautmann, C., Martin, C.R., 2005. Protein Biosensors Based on Biofunctionalized Conical Gold Nanotubes. J. Am. Chem. Soc. 127, 5000–5001. doi:10.1021/ja043910f

Sluyters, J.H., Sluyters-Rehbach, M., 2013. Temperature Dependence of the Properties of Water and Its Solutes, Including the Supercooled Region. ChemPhysChem 14, 3788–3800. doi:10.1002/cphc.201300553

Smeets, R.M.M., Keyser, U.F., Krapf, D., Wu, M.-Y., Dekker, N.H., Dekker, C., 2006. Salt Dependence of Ion Transport and DNA Translocation through Solid-State Nanopores. Nano Lett. 6, 89–95. doi:10.1021/nl052107w

Smirnov, S.N., Vlassiouk, I.V., Lavrik, N.V., 2011. Voltage-Gated Hydrophobic Nanopores. Acs Nano 5, 7453–7461. doi:10.1021/nn202392d

Sparreboom, W., van den Berg, A., Eijkel, J.C.T., 2010. Transport in nanofluidic systems: a review of theory and applications. New J. Phys. 12, 015004. doi:10.1088/1367-2630/12/1/015004

Sparreboom, W., van den Berg, A., Eijkel, J.C.T., 2009. Principles and applications of nanofluidic transport. Nat. Nanotechnol. 4, 713–720. doi:10.1038/nnano.2009.332

Steinbock, L.J., Bulushev, R.D., Krishnan, S., Raillon, C., Radenovic, A., 2013. DNA Translocation through Low-Noise Glass Nanopores. ACS Nano 7, 11255–11262. doi:10.1021/nn405029j

Steinbock, L.J., Otto, O., Chimerel, C., Gornall, J., Keyser, U.F., 2010. Detecting DNA Folding with Nanocapillaries. Nano Lett. 10, 2493–2497. doi:10.1021/nl100997s

Steinbock, L.J., Steinbock, J.F., Radenovic, A., 2013. Controllable Shrinking and Shaping of Glass Nanocapillaries under Electron Irradiation. Nano Lett. 13, 1717–1723. doi:10.1021/nl400304y

Stein, D., Kruithof, M., Dekker, C., 2004. Surface-Charge-Governed Ion Transport in Nanofluidic Channels. Phys. Rev. Lett. 93, 035901. doi:10.1103/PhysRevLett.93.035901

Stern, M.B., Geis, M.W., Curtin, J.E., 1997. Nanochannel fabrication for chemical sensors. J. Vac. Sci. Technol. B 15, 2887–2891. doi:10.1116/1.589750

Storm, A.J., Chen, J.H., Zandbergen, H.W., Dekker, C., 2005. Translocation of double-strand DNA through a silicon oxide nanopore. Phys. Rev. E 71, 051903. doi:10.1103/PhysRevE.71.051903

Stumm, W., 1987. Aquatic Surface Chemistry: Chemical Processes at the Particle-Water Interface, Environmental Science and Technology: A Wiley-Interscience Series of Texts and Monographs. Wiley.

Taghipoor, M., Bertsch, A., Renaud, P., 2015. An improved model for predicting electrical conductance in nanochannels. Phys. Chem. Chem. Phys. 17, 4160–4167. doi:10.1039/C4CP05338A

Tian, Y., Hou, X., Wen, L., Guo, W., Song, Y., Sun, H., Wang, Y., Jiang, L., Zhu, D., 2010. A biomimetic zinc activated ion channel. Chem. Commun. 46, 1682–1684. doi:10.1039/B918006K

Tian, Y., Wen, L., Hou, X., Hou, G., Jiang, L., 2012. Bioinspired Ion-Transport Properties of Solid-State Single Nanochannels and Their Applications in Sensing. Chemphyschem 13, 2455–2470. doi:10.1002/cphc.201200057

Tian, Y., Zhang, Z., Wen, L., Ma, J., Zhang, Y., Liu, W., Zhai, J., Jiang, L., 2013. A biomimetic mercury(II)-gated single nanochannel. Chem. Commun. 49, 10679–10681. doi:10.1039/C3CC42748J

Traversi, F., Raillon, C., Benameur, S.M., Liu, K., Khlybov, S., Tosun, M., Krasnozhon, D., Kis, A., Radenovic, A., 2013. Detecting the translocation of DNA through a nanopore using graphene nanoribbons. Nat. Nanotechnol. 8, 939–945. doi:10.1038/nnano.2013.240

Turner, S.W., Craighead, H.G., 1998. Monolithic fabrication of nanofluidic artificial gel media for DNA electrophoresis. pp. 114–121. doi:10.1117/12.304369

van der Heyden, F.H.J., Bonthuis, D.J., Stein, D., Meyer, C., Dekker, C., 2007. Power Generation by Pressure-Driven Transport of Ions in Nanofluidic Channels. Nano Lett. 7, 1022–1025. doi:10.1021/nl070194h

van der Heyden, F.H.J., Stein, D., Dekker, C., 2005. Streaming Currents in a Single Nanofluidic Channel. Phys. Rev. Lett. 95, 116104. doi:10.1103/PhysRevLett.95.116104

van der Wouden, E.J., Heuser, T., Hermes, D.C., Oosterbroek, R.E., Gardeniers, J.G.E., van den Berg, A., 2005. Field-effect control of electro-osmotic flow in microfluidic networks. Colloids Surf. -Physicochem. Eng. Asp. 267, 110–116. doi:10.1016/j.colsurfa.2005.06.048

van Hal, R.E.G., Eijkel, J.C.T., Bergveld, P., 1996. A general model to describe the electrostatic potential at electrolyte oxide interfaces. Adv. Colloid Interface Sci. 69, 31–62. doi:10.1016/S0001-8686(96)00307-7

Venditti, R., Xuan, X., Li, D., 2006. Experimental characterization of the temperature dependence of zeta potential and its effect on electroosmotic flow velocity in microchannels. Microfluid. Nanofluidics 2, 493–499. doi:10.1007/s10404-006-0100-0

Vlassiouk, I., Siwy, Z.S., 2007. Nanofluidic Diode. Nano Lett. 7, 552–556. doi:10.1021/nl062924b

Wang, E.N., Karnik, R., 2012. Water desalination: Graphene cleans up water. Nat. Nanotechnol. 7, 552–554. doi:10.1038/nnano.2012.153

Wei, C., Bard, A.J., Feldberg, S.W., 1997. Current Rectification at Quartz Nanopipet Electrodes. Anal. Chem. 69, 4627–4633. doi:10.1021/ac970551g

Wells, D.B., Belkin, M., Comer, J., Aksimentiev, A., 2012. Assessing Graphene Nanopores for Sequencing DNA. Nano Lett. 12, 4117–4123. doi:10.1021/nl301655d

Wildhaber, F., 2014. Ionic and molecular transport through active nanoporous membranes. STI, Lausanne.

William M. Haynes, W.M.H., 2014. CRC Handbook of Chemistry and Physics, 95th Edition, 95, Revised. ed. Apple Academic Press Inc., Oakville.

Windbacher, T., 2010. Engineering Gate Stacks for Field-Effect Transistors. Vienna University of Technology, Vienna.

Wong, C.C., Agarwal, A., Balasubramanian, N., Kwong, D.L., 2007. Fabrication of self-sealed circular nano/microfluidic channels in glass substrates. Nanotechnology 18, 135304. doi:10.1088/0957-4484/18/13/135304

Wu, S., Wildhaber, F., Bertsch, A., Brugger, J., Renaud, P., 2013. Field effect modulated nanofluidic diode membrane based on Al2O3/W heterogeneous nanopore arrays. Appl. Phys. Lett. 102, 213108. doi:10.1063/1.4807781

Wu, S., Wildhaber, F., Vazquez-Mena, O., Bertsch, A., Brugger, J., Renaud, P., 2012. Facile fabrication of nanofluidic diode membranes using anodic aluminium oxide. Nanoscale 4, 5718–5723. doi:10.1039/C2NR31243C

Wu, S., Ye, W., Yang, M., Taghipoor, M., Meissner, R., Brugger, J., Renaud, P., 2015. Impedance sensing of DNA immobilization and hybridization by microfabricated alumina nanopore membranes. Sens. Actuators B Chem. 216, 105–112. doi:10.1016/j.snb.2015.03.094

Xia, F., Guo, W., Mao, Y., Hou, X., Xue, J., Xia, H., Wang, L., Song, Y., Ji, H., Ouyang, Q., Wang, Y., Jiang, L., 2008. Gating of single synthetic nanopores by proton-driven DNA molecular motors. J. Am. Chem. Soc. 130, 8345–8350.

Yameen, B., Ali, M., Neumann, R., Ensinger, W., Knoll, W., Azzaroni, O., 2009a. Single Conical Nanopores Displaying pH-Tunable Rectifying Characteristics. Manipulating Ionic Transport With Zwitterionic Polymer Brushes. J. Am. Chem. Soc. 131, 2070–+. doi:10.1021/ja8086104

Yameen, B., Ali, M., Neumann, R., Ensinger, W., Knoll, W., Azzaroni, O., 2009b. Ionic Transport Through Single Solid-State Nanopores Controlled with Thermally Nanoactuated Macromolecular Gates. Small 5, 1287–1291. doi:10.1002/smll.200801318

Yameen, B., Ali, M., Neumann, R., Ensinger, W., Knoll, W., Azzaroni, O., 2009c. Synthetic Proton-Gated Ion Channels via Single Solid-State Nanochannels Modified with Responsive Polymer Brushes. Nano Lett. 9, 2788–2793. doi:10.1021/nl901403u

Yates, D.E., Healy, T.W., 1975. Mechanism of anion adsorption at the ferric and chromic oxide/water interfaces. J. Colloid Interface Sci. 52, 222–228. doi:10.1016/0021-9797(75)90192-7

Yates, D.E., Levine, S., Healy, T.W., 1974. Site-binding model of the electrical double layer at the oxide/water interface. J. Chem. Soc. Faraday Trans. 1 Phys. Chem. Condens. Phases 70, 1807–1818. doi:10.1039/F19747001807

Yeh, L.-H., Xue, S., Joo, S.W., Qian, S., Hsu, J.-P., 2012. Field Effect Control of Surface Charge Property and Electroosmotic Flow in Nanofluidics. J. Phys. Chem. C 116, 4209–4216. doi:10.1021/jp211496b

Yellen, G., 2002. The voltage-gated potassium channels and their relatives. Nature 419, 35–42. doi:10.1038/nature00978

Mojtaba TAGHIPOOR

Education

PhD in Microsystems and microelectronics Nov 2011-Nov 2015
École Polytechnique Fédérale de Lausanne (EPFL)

MSc in Mechanical engineering Sep 2008-Sep 2010
Shiraz University, Iran
Ranked 1st in Energy conversion students

BSc in Mechanical engineering Sep 2003-Sep 2008
Shiraz University, Iran

Publications

- M. Taghipoor, A. Bertsch, and P. Renaud, "*Thermal control of ionic transport and fluid flow in nanofluidic channels*" Nanoscale, Sep 2015,
- M. Taghipoor, A. Bertsch, and P. Renaud, "*Temperature Sensitivity of Nanochannel Electrical Conductance*" ACS Nano, vol. 9, no. 4, pp. 4563–4571, Apr. 2015,
- M. Taghipoor, A. Bertsch, and P. Renaud, "*An improved model for predicting electrical conductance in nanochannels*" Phys. Chem. Chem. Phys., vol. 17, no. 6, pp. 4160–4167, Jan. 2015
- S. Wu, W. Ye, M. Yang, M. Taghipoor, R. Meissner, J. Brugger, and P. Renaud, "*Impedance sensing of DNA immobilization and hybridization by microfabricated alumina nanopore membranes*" Sensors and Actuators B: Chemical, vol. 216, pp. 105–112, Sep. 2015
- F. S. Majedi, M. M. Hasani-Sadrabadi, S. H. Emami, M. Taghipoor, E. Dashtimoghadam, A. Bertsch, H. Moaddel, and P. Renaud, "*Microfluidic synthesis of chitosan-based nanoparticles for fuel cell applications*" Chem. Commun., vol. 48, no. 62, pp. 7744–7746, Jul. 2012
- M. Taghipoor, A. Bertsch, and P. Renaud, "*A Surface Charge Dependent Model for Electrical Conductance of Nanochannels*" ISME2015, Tehran, Iran
- M. Taghipoor, A. Bertsch, and P. Renaud, "*Thermal gate, a new tool for ionic transport control inside nanochannels*" IEEENANO 2015, Rome, Italy

Technical Skills

Computer SolidWorks, COMSOL, MATLAB, Maple, ADMAS, Gambit, ANSYS/Fluent, C/C++, LabVIEW, Microsoft Office (Word, Excel, PowerPoint, Visio, OneNote, project)

Microfabrication
Photolithography, Dry (DRIE) and Wet Etching, Thin Films, Scanning Electron Microscope (SEM), Surface functionalization, PDMS, Laser ablation, Wafer Bonding

Laboratory Microfluidics, Fluorescence microscopy, Electrochemistry, Design of experiments, Machining, Welding